CHAPTER FOUR

RESULTS AND DISCUSSION

In this chapter, the results obtained on the process based on utilizing non-silylated and silylated Ti-MCM-41 which involves reaction on model feedstock (1-octene) are presented. The discussion will be centered on the structural features of the catalysts and their catalytic activities; taking into account the optimization parameters attained from 1-octene epoxidation. The effect of Si/Ti ratio, reaction temperature, reaction time and alkene:oxidant molar ratio towards catalytic performances are revealed. Based on the optimized conditions, the best epoxidation system for methyl oleate is proposed. On the other hand, characterization of catalysts is done to understand the structural, thermal, chemical and catalytic properties of Ti-MCM-41 catalysts, developed in this work.

4.1 Process Based on Utilizing Non-Silylated Ti-MCM-41

The main objective of this study is to find out the optimal reaction conditions for the epoxidation of Methyl Oleate maximizing both epoxide selectivity and yield.

4.1.1 Characterization of Non-Silylated Sample

Although a variety of techniques exist for the characterization of heterogeneous catalysts and support materials, MCM-41 is most frequently studied with x-ray diffraction for determination of structural properties, nitrogen physisorption, UV-Visible and FTIR to confirm the presence of titanium species. Therefore, these techniques will be dealt with here.

Due to the facts that titanium is very insensitive and has a large quadrupolar moment showing very broad lines, the attachment of titanium species could not be confirmed by MAS NMR technique. However, the UV-Vis spectra and FTIR spectra (inset) can confirm the presence of titanium species on the Ti- MCM-41 sample.

(a) Nitrogen Physisorption (BET)

Nitrogen physisorption probes the textural properties of materials, *i.e.* surface area, pore volume, pore size (distribution) and pore geometry. Moreover, the technique also discloses to some extent the measured surface area is associated with micro-, meso- and / or macropores. Adsorption isotherms have the advantage of producing a macroscopic average measurement for evaluating structural properties as compared to XRD.

A typical nitrogen isotherm for MCM-41 is shown in Figure 4.1. Both the adsorption (straight line) and desorption (dotted line) curves are shown below. Five distinct regions can be discerned in this graph.

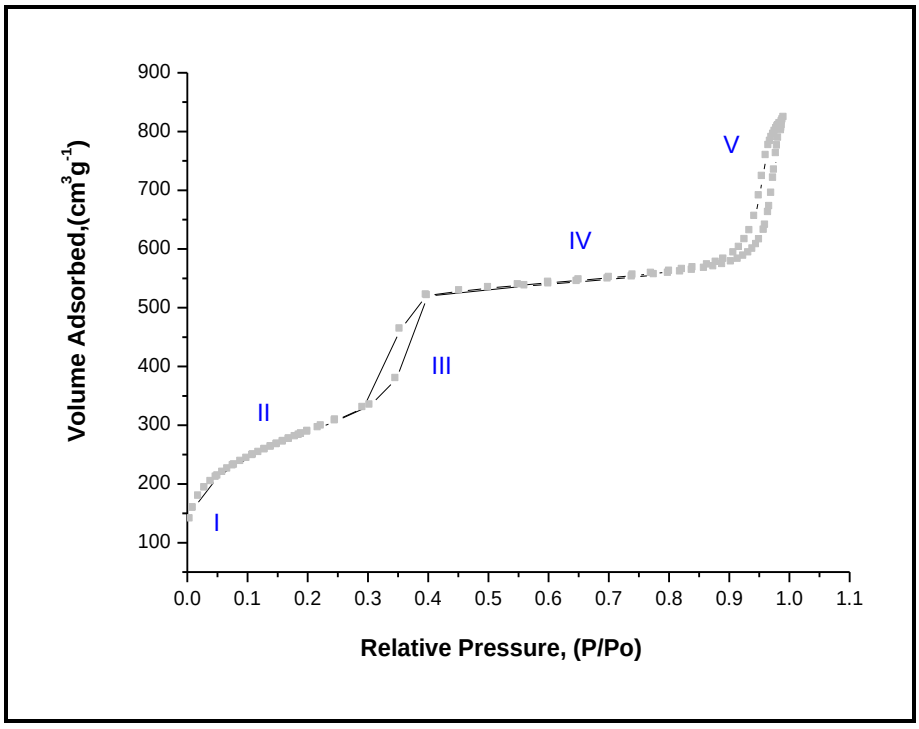

Figure 4.1: Nitrogen adsorption-desorption isotherms of MCM-41

At very low relative pressures (P/Po) a very large amount of nitrogen becomes physisorbed (region I). Nitrogen physisorption at these low pressures is usually assigned to condensation of nitrogen inside the micropores of a material. However, as outlined before, MCM-41 is a completely mesoporous material and does not contain any micropores. Therefore, the process taking place in region I is monolayer adsorption of nitrogen on the surface of MCM-41 (both on the external surface and inside the mesopores). Because the surface area is very high, the concomitant monolayer adsorption requires a large amount of nitrogen.

Upon monolayer adsorption, multilayer of nitrogen starts to develop at higher relative pressures of nitrogen (region II). Also in this case both the external surface area and the mesopores contribute to the physisorption process. Therefore, the data collected in this part of the isotherm are used for the calculation of the surface area of the material with the method developed by Brunauer, Emmett and Teller (BET-method). Thus calculated surface area amounts to approximately 883 to 1,185 m^2g^{-1} for all-silica MCM-41 materials used in the research described here.

At a relative nitrogen pressure of approximately 0.37, a sudden steep increase of the amount of adsorbed nitrogen is observed (region III). This steep increase is caused by capillary condensation of nitrogen inside the mesopores, *i.e.* the mesopores of MCM-41 become suddenly filled by liquid nitrogen, since the meniscus of the liquid nitrogen film inside the mesopores becomes thermodynamically unstable at this pressure.

MCM-41 is a type IV isotherm that shows two distinct features: a sharp capillary condensation step at low relative pressures and no or relatively little hysteresis between the adsorption and sorption branches. The adsorption at very low relative pressure P/Po, is due to monolayer adsorption of N_2 on the walls of the mesopores and does not represent the presence of any micropores. The lack of any appreciable hystersis in the region P/Po>0.4 indicates the lack of any appreciable textural mesoporosity.

Hysteresis loops are associated with capillary condensation in the multilayer region, pore filling and emptying mechanism of physisorption isotherm. The micropore filling effects occur at the low relative pressure up to a unity relative pressure. Thus, the meniscus begins to form and increases steadily toward the pore entrance with increasing relative pressure. The evaporation process involves the same series of steps in the reverse direction of condensation.

The Kelvin equation relates the pore diameter of a material with the relative pressure at which capillary condensation occurs. Because filling of the mesopores takes place over a relatively small range of relative pressures *(i.e.* P/Po ≈ 0.34-0.40) the pores associated with this process are nearly equal in size. A further indication for this statement is the fact that the desorption curve almost completely coincides with the adsorption isotherm in this pressure range, giving a very narrow hysteresis loop *(i.e.* the difference between the adsorption and desorption curves). Moreover, the shapes of the curves and the hysteresis loop are very characteristic for cylindrical mesopores, which indeed constitute the MCM-41 structure.

When the mesopores become completely filled with nitrogen, only the external surface of MCM-41 remains accessible for nitrogen adsorption. Therefore region IV is associated with multilayer adsorption of nitrogen at the external surface of MCM-41. The very shallow slope of this region indicates that the external surface area of MCM-41 is rather small. Finally, at relative pressures close to 1

the nitrogen uptake by the sample increases again and a small hysteresis loop evolves upon the subsequent desorption of nitrogen (region V). These features can be assigned to condensation of nitrogen within the interstitial voids between the MCM-41 particles. From the adsorption and desorption curves, pore size distributions can be calculated according to the method of Barrett, Joyner and Halenda (BJH-method).

The nitrogen adsorption-desorption isotherms of MCM-41 usually exhibit a sharp step at P/Po in the range 0.1-0.5, depending on the average pore size. Figure 4.2 shows the nitrogen isotherms of various Si/Ti samples, along with that of the parent MCM-41 sample. The BJH pore size distributions curves based on the isotherms are depicted in Figure 4.2.

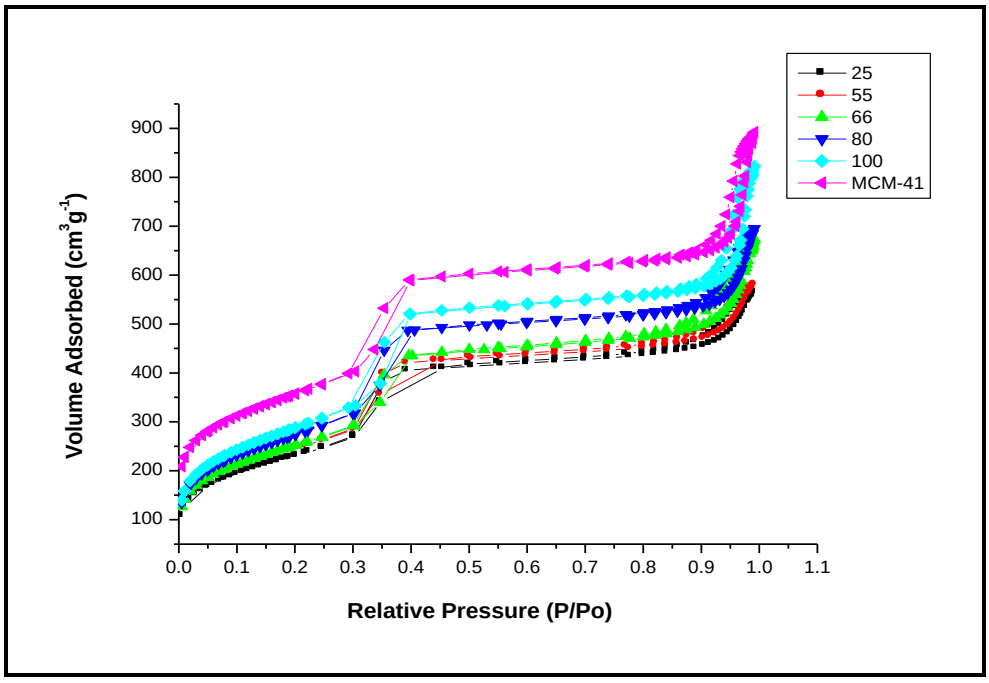

Figure 4.2: Nitrogen adsorption-desorption isotherms for parent MCM-41 sample and various Si/Ti ratio

It can be seen that all samples showed similar type IV isotherms having inflection around P/Po = 0.3-0.45, characteristic of MCM-41 type ordered mesoporous materials. The samples exhibited two separate well-expressed hysteresis loops *(i.e.* the difference between the adsorption and desorption curves) as defined by IUPAC [114] that is associated with solids with slit-shaped pores or plate-like particles.

One is in the P/Po = 0.3-0.45 region indicative of framework confined mesopores and have been further confirmed by a step increase of capillary condensation at P/Po = 0.85, expected for mesopores [115]. The position of inflection in the P/P_0 = 0.3-0.45 region, depends on the diameter of the mesopores and its sharpness indicates the uniformity of the narrow pore size distribution [116].

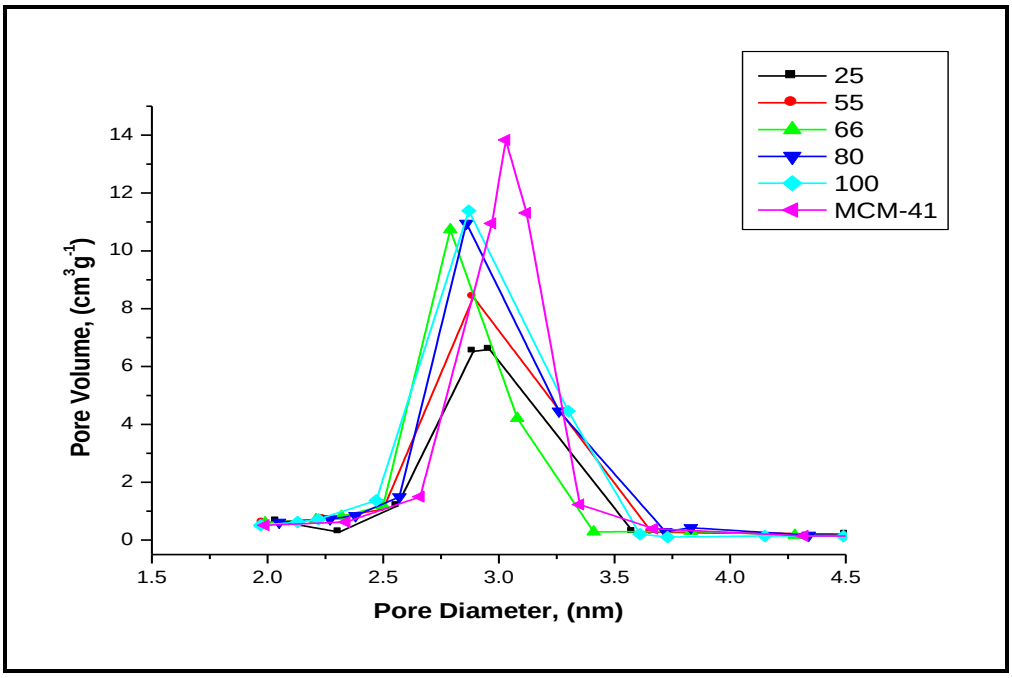

Figure 4.3: Pore size distribution for parent MCM-41 sample and various Si/Ti ratio.

The BJH calculation shows that pore diameters are in a narrow range between 2.5-3.5 nm. Since 25Ti-MCM-41 has a lower crystallinity, its pore size distribution was not as uniform as that of 100Ti-MCM-41 [117].

The specific BET surface area, average pore diameters (calculated from N_2 adsorption-desorption isotherm using BJH model) [118] and specific pore volume for the MCM-41 samples are presented in Table 4.1.

Table 4.1: Textural properties of the studied materials

PARAMETERS						
Si/Ti	25	55	66	80	100	MCM-41
% of Ti	2.85	2.29	1.68	1.24	1.13	0
Surface Area (m^2/g)	883.32	906.9	905.03	997.26	1075.16	1185.21
Pore Volume (cm^3/g)	0.58	0.59	0.65	0.68	0.71	0.79
Pore Diameter (nm)	2.85	2.85	2.84	2.86	2.89	2.95
Wall thickness (nm)	1.68	1.65	1.62	1.59	1.49	1.33
d_{100} (nm)	3.92	3.9	3.86	3.85	3.79	3.71

It has been observed that the BET surface area gradually decreases with an increase of titanium content, in agreement with those in the literature. Incorporation of titanium have caused a decrease in surface area possibly due to the loss in long-range ordering as clearly evidenced by the XRD pattern (Figure

4.5) in next section (b). The low surface area also indicates that the samples are not pure and contain amorphous silica. It should be noted that the samples in this study were synthesized at 100 ˚C for 48 hours. Most of the samples reported in the literature were synthesized at 150 ˚C for 6 days.

The data presented in Table 4.1 show that the framework wall thickness (FWT) between pores, calculated by subtracting pore diameter by a_0, of different Ti-containing MCM-41 and purely siliceous MCM-41 sample is comparable with the increase in Ti content. There is a very slight increase, in the range of 1.33-1.68 nm probably due to larger size of Ti^{4+} as compared to Si^{4+}. a_0 is the unit cell parameter calculated from *d*-spacing data from XRD patterns ($a_0 = 2d_{100}/\sqrt{3}$) [119] and *d* is pore diameter from N_2 sorption. The wall thickness can eventually become an important parameter in determining the catalytic behavior of Ti-MCM-41.

The unit cell parameter (a_0) also increases with the increasing incorporation of Ti, like other heterometal ions, which are larger than Si^{4+} ions [120-121]. However, the pore diameter was found to decrease slightly leading to comparable framework wall thickness of different Ti-MCM-41 as well as MCM-41 samples. The defect site may influence the a_0 or pore diameter or both, depending upon their density and nature. The increase in wall thickness and decrease in pore size may attribute by the deposition of titanium species onto the surface of cylindrical channels of MCM-41.

Although there is a reduction of pore size, pore volume and surface area with increasing Ti content, this reduction is considered small, indicating that thicker walls provide more stability. Ideally the thickness of the pore walls should be close to 1.5 nm, but values as low as 0.8 nm have been reported. Thus, the value obtained from this study which is within the range 1.33-1.68 nm is a good measure for the quality (stability) of the MCM-41 support material.

(b) XRD

First of all, the application of x-ray diffraction for the characterization of basically amorphous material appears to be rather useless, since x-ray diffraction is always used to attain information on crystalline materials.

The most dramatic difference among crystalline and amorphous materials is in how they scatter an X-ray beam. The crystalline forms produce sharp lines due to diffraction, whereas the amorphous usually produces a broad peak indicating only some short range order in the atomic arrangement. The so-called amorphous solids always exhibit a short-range order, for instance in silica gel. Small particles with sizes below 1.0-1.5 nm constitute a particular category of solids, which have no long-range order in that the inter-atomic distances are at most equal to the diameter of the particles.

Therefore, characterization of MCM-41 with x-ray diffraction yields a diffractogram with a limited number of reflections, all situated at low angles. A representative example can be seen in Figure 4.4.

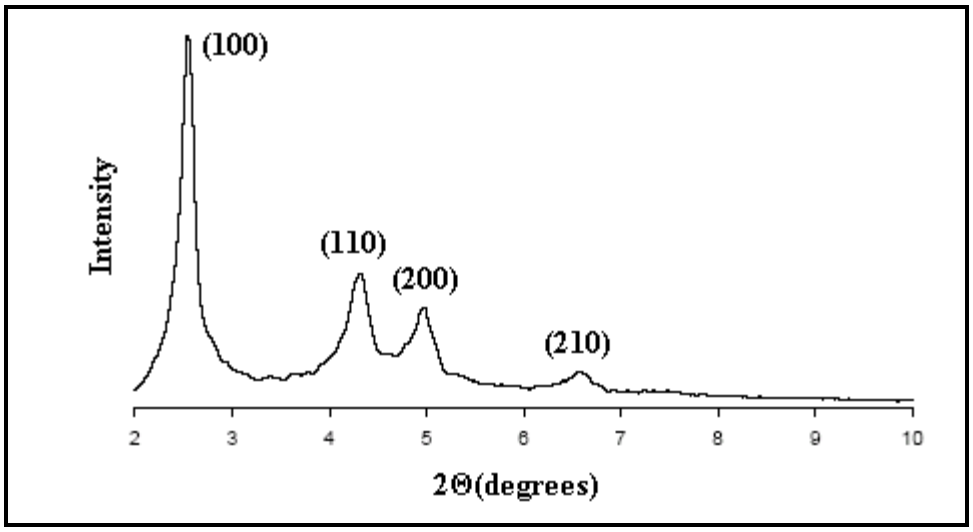

Figure 4.4: X-ray diffractogram of MCM-41 showing four reflections, which can be assigned to the hexagonal lattice of the mesoporous material. The (100), (110) and (200) reflections are well resolved. (Radiation used: Co K 1, with λ = 0.1788970 nm).

Generally only three diffractions are well resolved, corresponding to the (100), (110) and (200) reflections. A fourth diffraction petak with a notably lower intensity, corresponding to the (210) reflection, is sometimes also present. When an MCM-41 material of exceptionally good quality has been obtained, a fifth diffraction peak corresponding to the (300) reflection, is also observed. In this study, the hexagonal arrangement of the calcined and uncalcined Ti-MCM-41 samples is confirmed by the XRD pattern shown in Figure 4.5 and Figure 4.6.

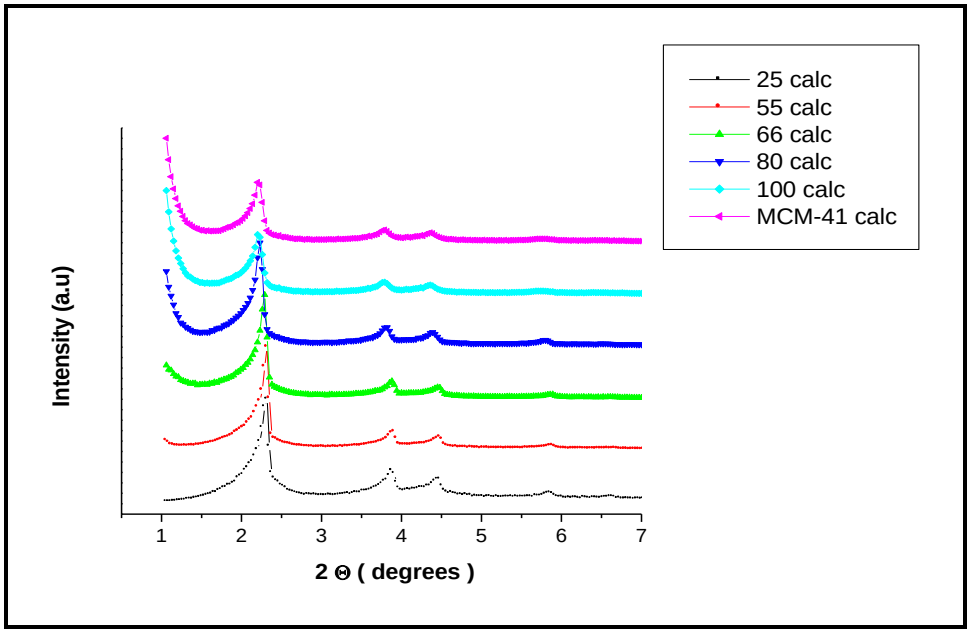

Figure 4.5: X-ray diffraction patterns of calcined Ti-MCM-41 samples; change of XRD pattern with Si/Ti

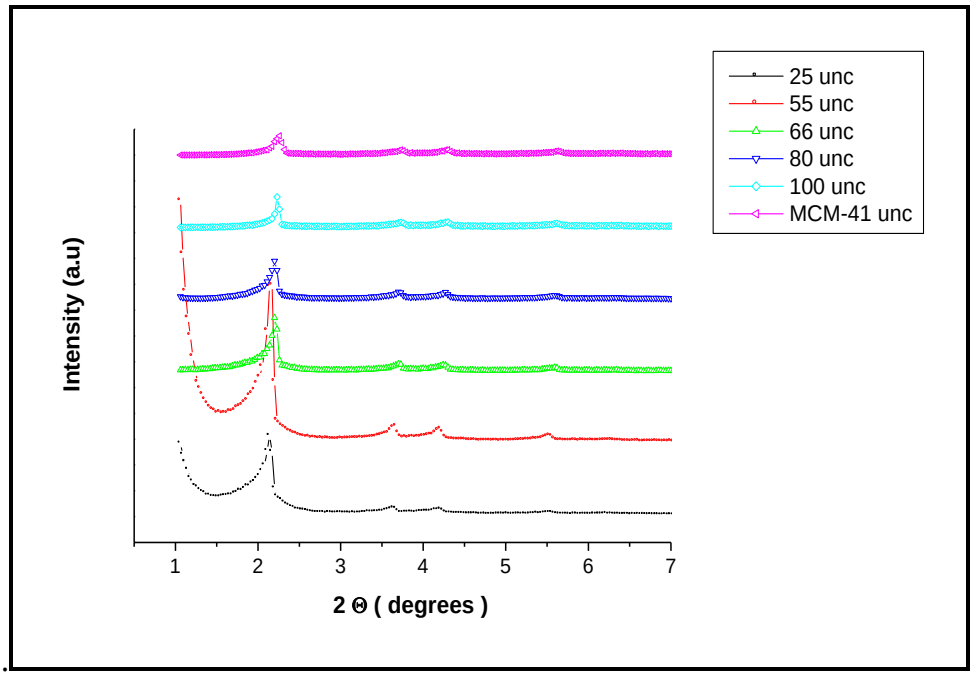

ratios.

Figure 4.6: X-ray diffraction patterns of uncalcined Ti-MCM-41 samples; change of XRD pattern with Si/Ti ratios.

For this research, the well-defined XRD patterns are indexed on the basis of four Bragg peaks, which can be distinguished in hexagonal lattice symmetry, characteristic of MCM-41 structure as reported by Beck [122]. All samples exhibit characteristic peaks in the low angle region in the range $1.5^{O} < 2\theta < 7^{O}$.

Both the diffractogram of calcined and uncalcined above (Fig. 4.5 and Fig. 4.6) show single intense peak in low angle region corresponding to (100) of MCM-41 structure at $2\theta = 2.1$, whereas two minor characteristic peaks in $2\theta = 3.6–4.4$ region are rather smeared out reflecting the diminished long range order caused by the presence of titanium [123].

A prominent peak for *hkl* = 100 as well as weaker peaks for *hkl* = 110, 200 and 210 were observed in the as-synthesized and in the calcined samples. The interplanar distance (d_{100}) values of different samples are given in Table 4.2 along with their corresponding unit cell parameter (a_0), calculated from the peak with *hkl* = 100 by the equation $a_0 = 2d_{100}/\sqrt{3}$ [124].

Table 4.2: Lattice contraction of Ti-MCM-41 at various Si/Ti ratios

Sample	As-synthesized		Calcined	
(Si/Ti)	$d_{10\,0}$ (nm)	a_0 (nm)	$d_{10\,0}$ (nm)	a_0 (nm)
25	4.23	4.88	3.92	4.53
55	4.2	4.85	3.9	4.5
66	4.11	4.75	3.86	4.46
80	4.11	4.75	3.85	4.45
100	4.03	4.65	3.79	4.38
MCM-41	3.96	4.57	3.71	4.28

A slight increase in the '*d*' and 'a_0' values is observed on increasing incorporation of titanium. The increase in unit-cell parameter (a_0) on Ti incorporation is due to the larger size of Ti^{4+} as compared to Si^{4+}. Similar observations were also reported by earlier workers with different metal ions incorporated MCM-41 [125,126].

However, as mentioned earlier, a gradual loss of long-range ordering is observed with increasing incorporation of Ti in the Ti-MCM-41 samples. This is probably due to increasing number of defect sites and bond strain in these materials as evidenced by the decreasing intensities of the [100] peak as well as the higher angle peaks.

With the incorporation of titanium atoms into the framework, these Bragg peaks move slightly to lower angle with different degrees and concurrently d_{100} spacing diminished, and lattice parameter, a_o increased as shown in Table 4.2. It demonstrates that introduction of Ti^{4+} influences the packing of the surfactant and the electrical double layer in the surfactant aggregate and the long-order structure to a certain degree at the same time.

The Ti-MCM-41 materials showed an average increase of 0.19 nm in the d_{100} spacing and 0.21 nm in the cell parameter a_0 for the as-synthesized Ti-MCM-41 while an average increase of 0.15 nm in the d_{100} spacing and 0.18 nm in the cell parameter a_0 for calcined samples as compared to the corresponding silica MCM-

41. For all the samples, a cell contraction of 0.1-0.3 nm upon calcination is observed in Ti-MCM-41. The data from the calcined material are in good agreement with those reported by Beck *et. al* [122].

The XRD patterns of both as-synthesized and calcined Ti-MCM-41 materials below (Fig. 4.7 – Fig. 4.11) show a sharp (100) peak and three higher order peaks of lesser intensity. It indicate the different intensities before and after calcination of 25-TiMCM-41, 55-TiMCM-41, 66-TiMCM-41, 80-TiMCM-41 and 100-TiMCM-41.

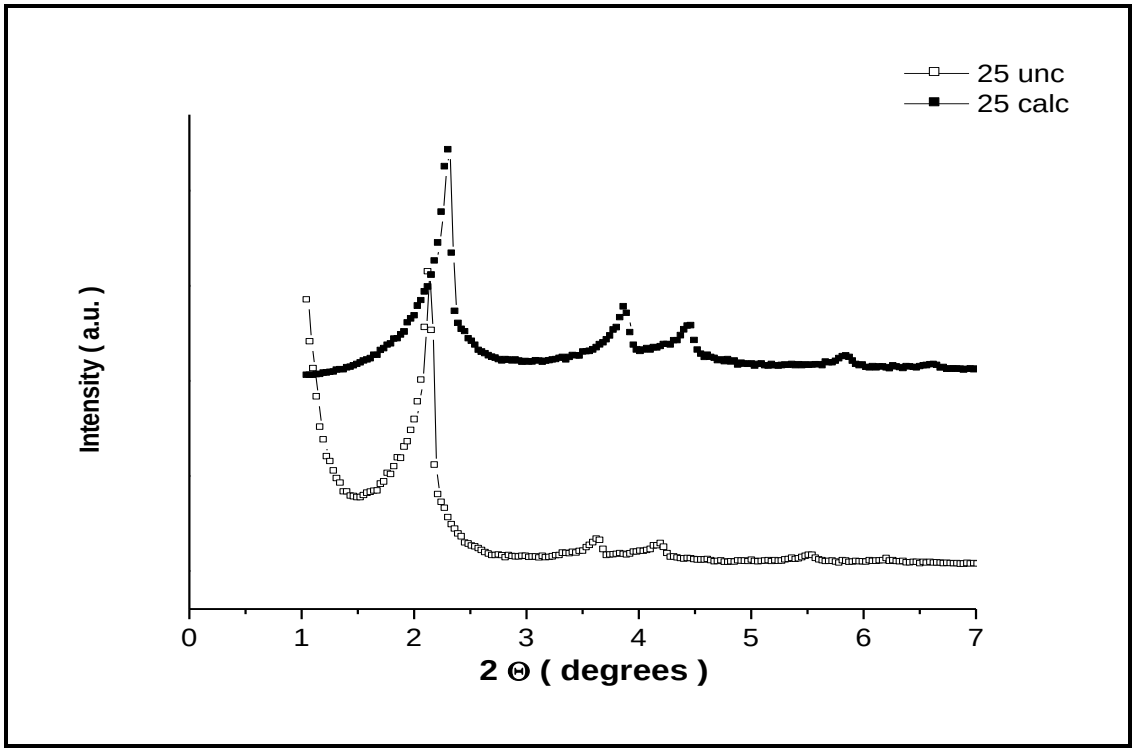

Figure 4.7: XRD patterns of 25Ti-MCM-41 (calcined & uncalcined).

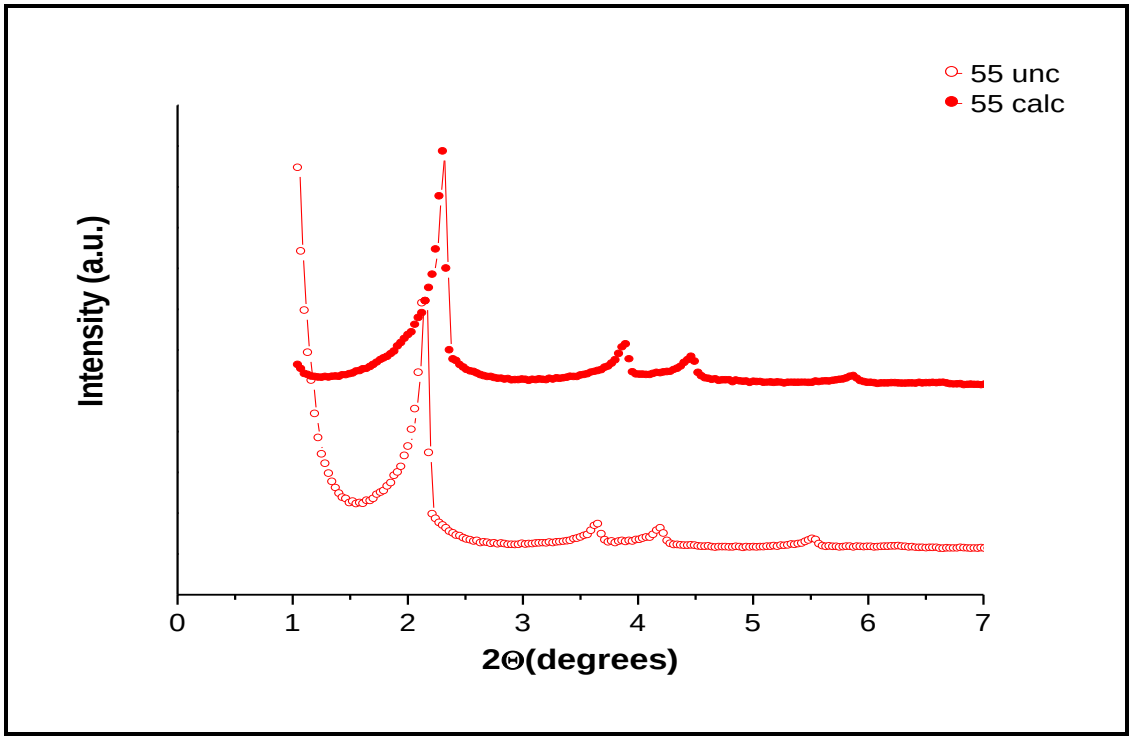

Figure 4.8: XRD patterns of 55Ti-MCM-41 (calcined & uncalcined).

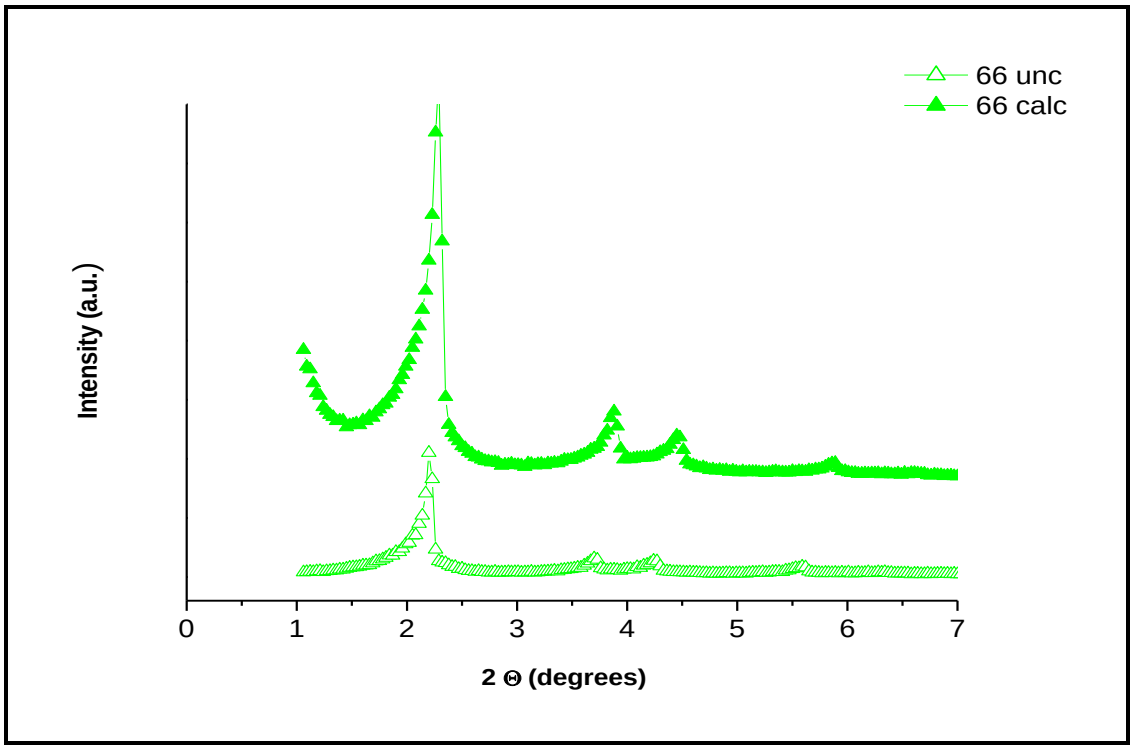

Figure 4.9: XRD patterns of 66Ti-MCM-41 (calcined & uncalcined).

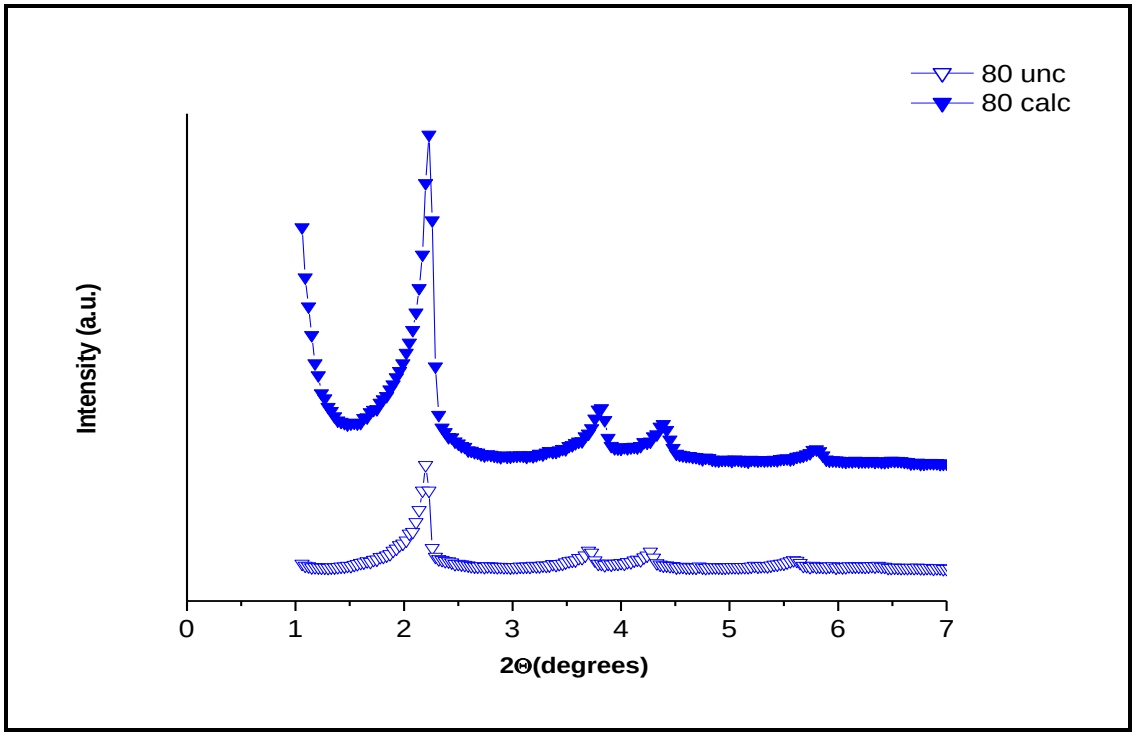

Figure 4.10: XRD patterns of 80Ti-MCM-41 (calcined & uncalcined).

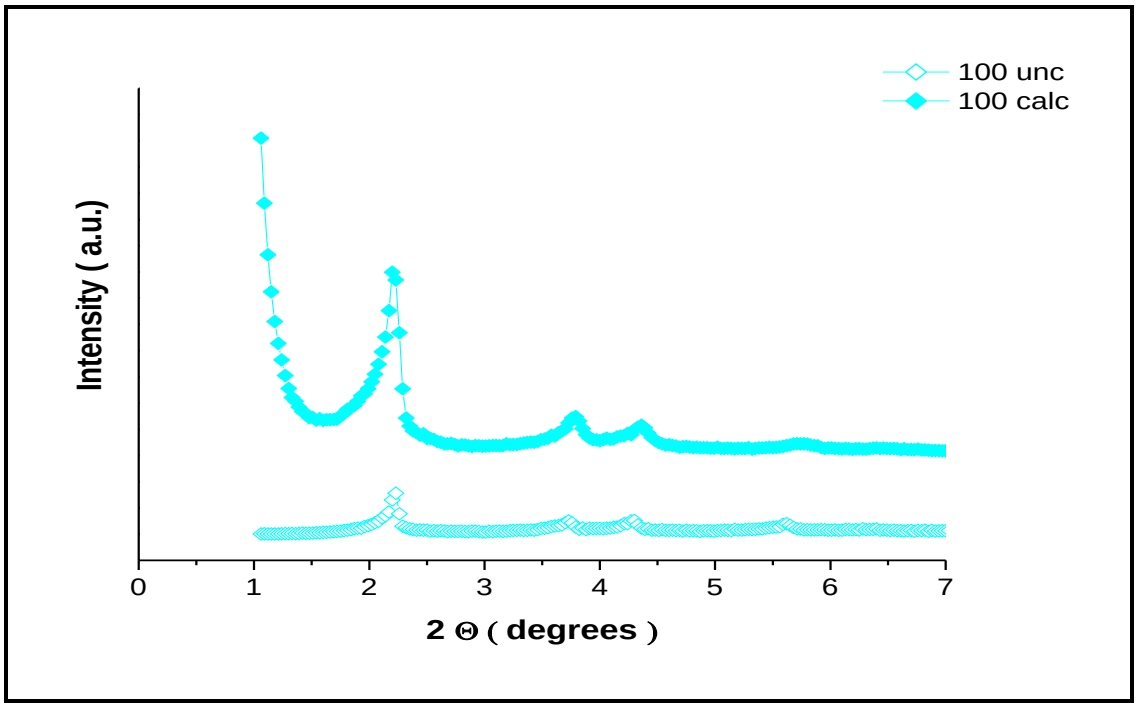

Figure 4.11: XRD patterns of 100Ti-MCM-41 (calcined & uncalcined).

The intensity of diffraction peak after calcination is almost two-fold greater than that before calcination. After calcination to decompose the surfactant, the XRD pattern of Ti-MCM-41 became better resolved. As it has been reported, MCM-41 framework contracts upon calcinations, as can be expected when organic cations were replaced by protons and adjacent silanol groups condense [127].

The removal of template which is up to 60 wt% of the as-synthesized Ti-MCM-41 is using calcinations at temperature of $540^{O}C$ for 7 hours. During the calcination, the cell diameter as found by XRD becomes smaller. Higher calcination temperatures and longer calcination times enhance this effect.

Upon calcination, some decrease in intensity of all peaks is also observed together with a shift towards higher 2θ values. It can be seen that the patterns of the Ti-MCM-41 samples are similar to that of the parent MCM-41 except the observation of slight differences both in terms of the positions and intensities of the (100) peak, showing that the pore structure integrity was maintained. It is known that the pore structure of MCM-41 materials is unstable in the presence of water because of the hydrolysis of Si-O-Si bonds [128].

In this work, the d_{100} spacing of the sample after calcination is narrower than that before calcination, the *d* spacing of 100 diffraction peak decreased from 4.23 nm to 3.92 nm, 4.2 nm to 3.9 nm, 4.11 nm to 3.86 nm, 4.11 nm to 3.85 nm, 4.03 nm

to 3.79 nm and 3.96 nm to 3.71 nm for 25-TiMCM-41, 55-TiMCM-41, 66-TiMCM-41, 80-TiMCM-41, 100-TiMCM-41 and MCM-41 respectively.

(c) SEM/EDX

The SEM photographs of Ti-MCM-41 sample, given in Figure 4.12, are typical of MCM-41 type materials. Two types of particle morphology were obtained. One is worm type may be formed due to stirred synthesis [129] in contrast to the synthesis in autoclaves under static conditions and the other one is hexagonal type [130].

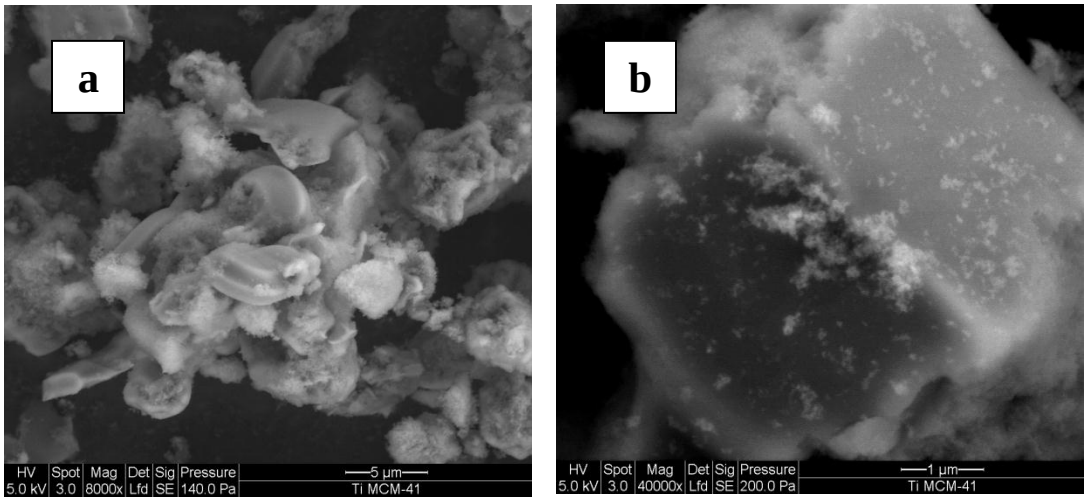

Figure 4.12: Scanning electron micrographs of calcined Ti-MCM-41 having different types of particle morphology: (a) worm type and (b) hexagonal type.

The particle size and morphology of different Ti-MCM-41 samples were determined by scanning electron microscopy. The SEM micrographs of Ti-MCM-41 samples, as shown in Figure 4.13, are typical of MCM-41 type materials

exhibiting two different kinds of particle morphology. One is winding worm type (Figure 4.13 a) and the other one is hexagonal (Figure 4.13 b). The hexagonal particles are of two types (i) well-formed relatively bigger particles of *ca.* 2 mm and (ii) smaller particles of *ca.* 0.5 mm size. The unique hexagonal rod type particle was also observed for the first time as shown in Figure 4.13, indicative of long-range ordering of Ti-MCM-41 samples. The worm type particles may be formed due to the stirred synthesis, in contrast to the conventional static autoclaves.

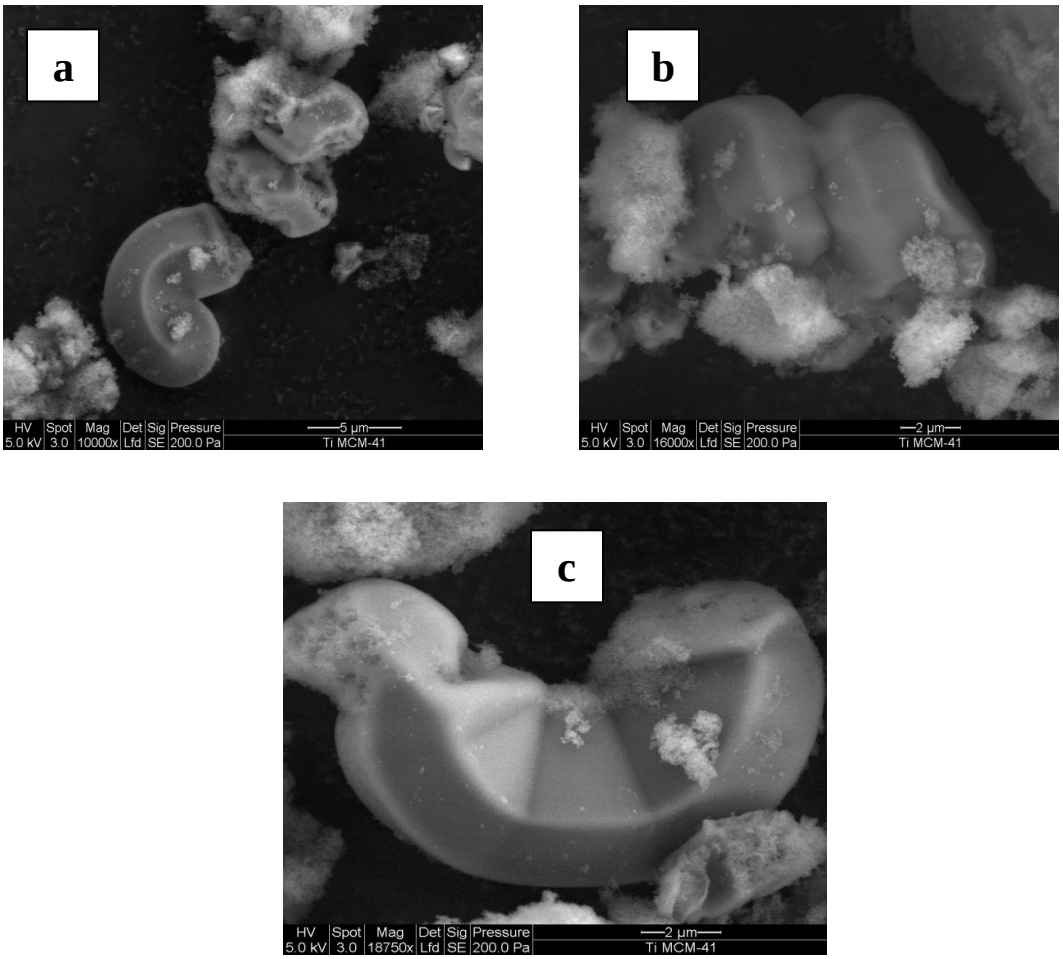

Figure 4.13: Scanning electron micrographs of calcined Ti-MCM-41 samples having different types of particle morphology: (a) winding worm type, (b) hexagonal type and (c) unique hexagonal rod type.

The SEM micrographs for samples 25Ti-MCM-41, 55Ti-MCM-41, 66Ti-MCM-41, 80Ti-MCM-41 and 100Ti-MCM-41 are shown in Figure 4.14 to Figure 4.18 below.

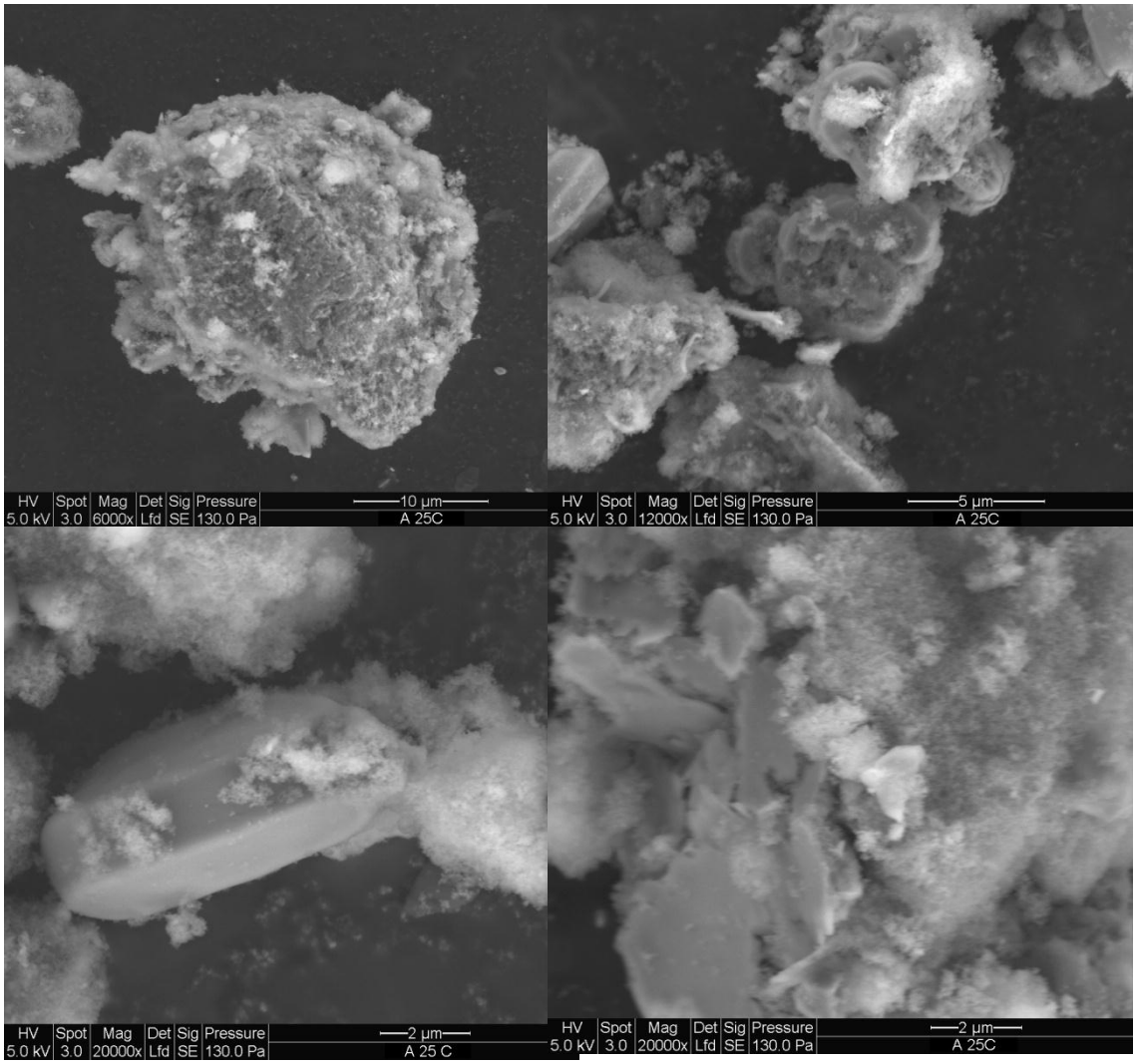

Figure 4.14: SEM images of sample 25Ti-MCM-41.

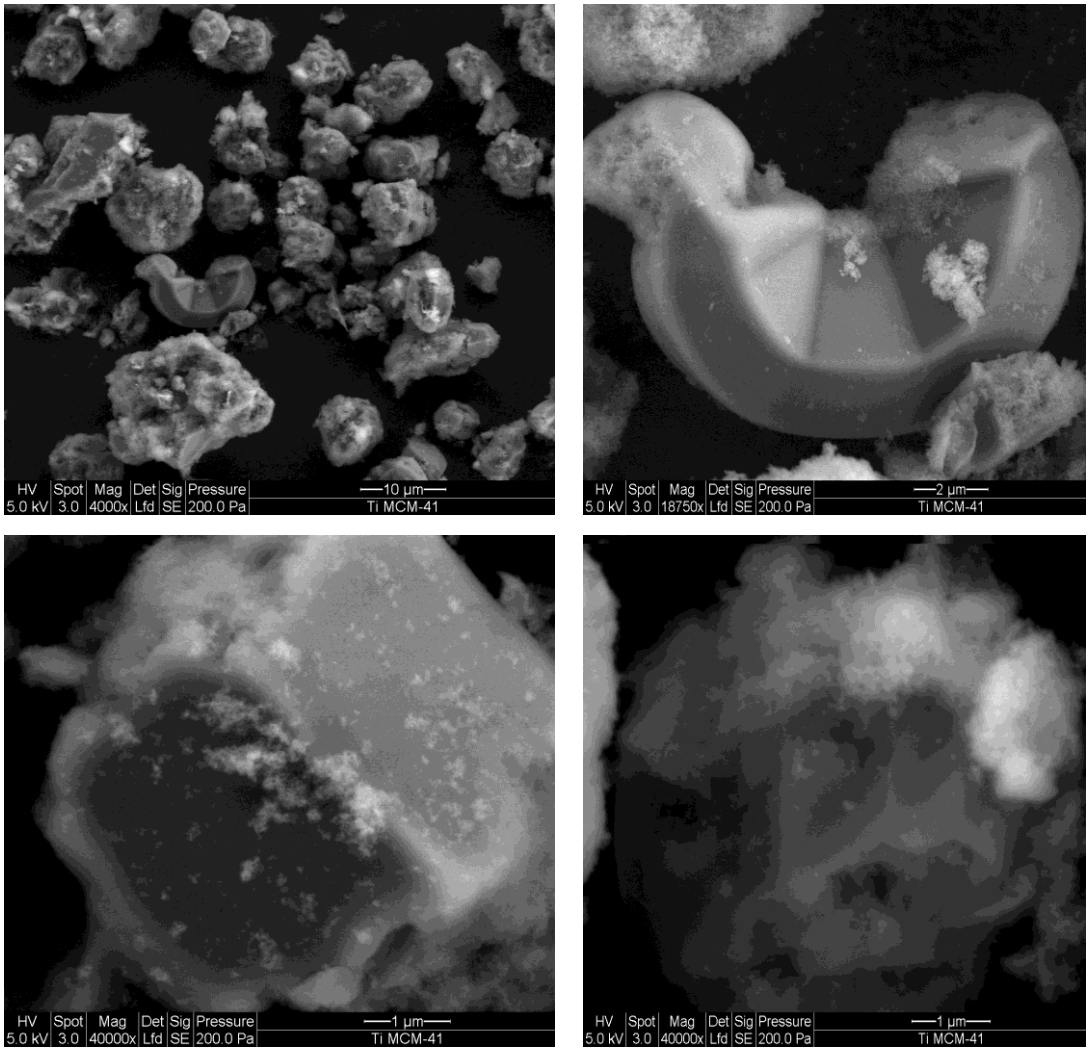

Figure 4.15: SEM images of sample 55Ti-MCM-41.

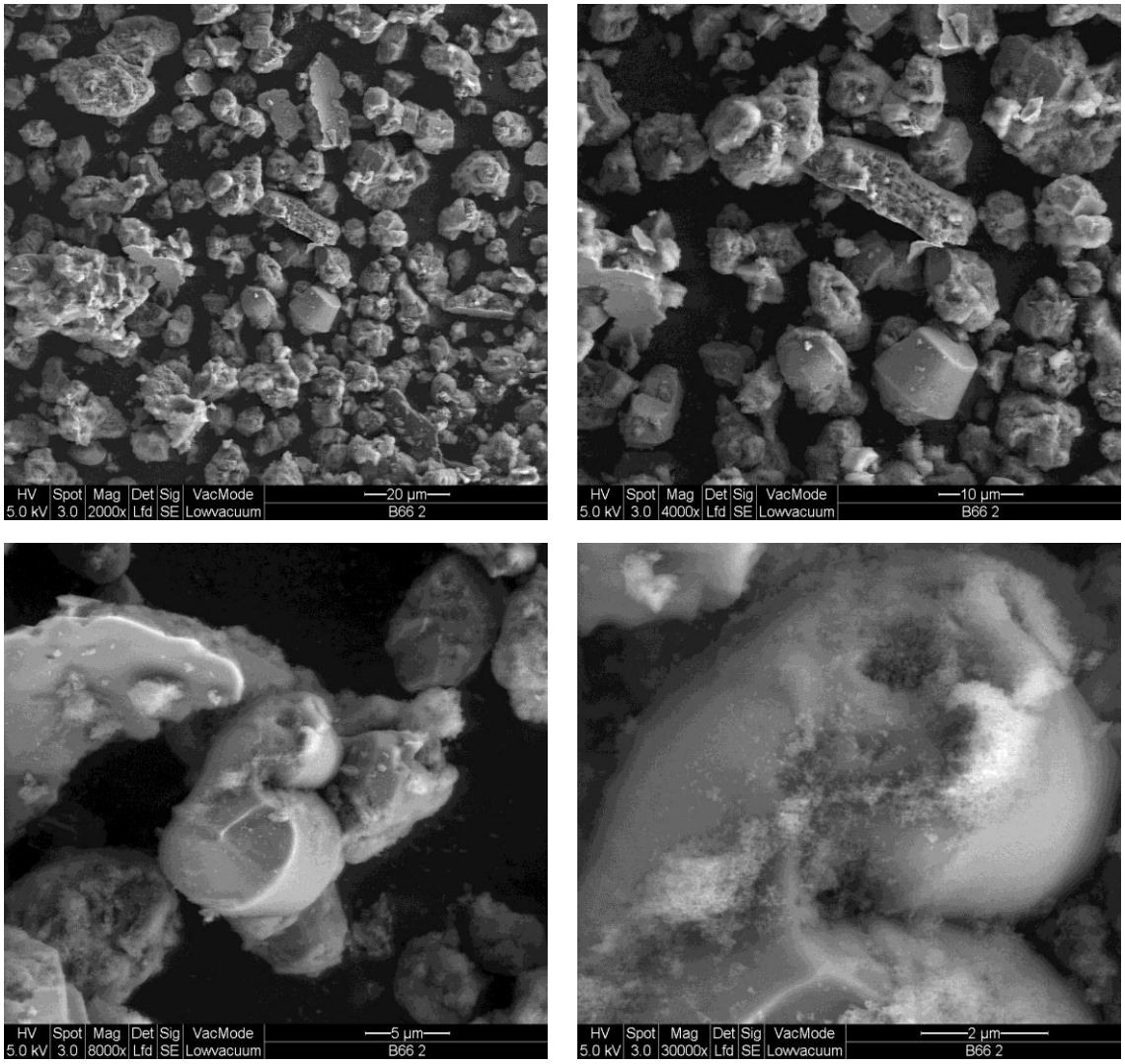

Figure 4.16: SEM images of sample 66Ti-MCM-41.

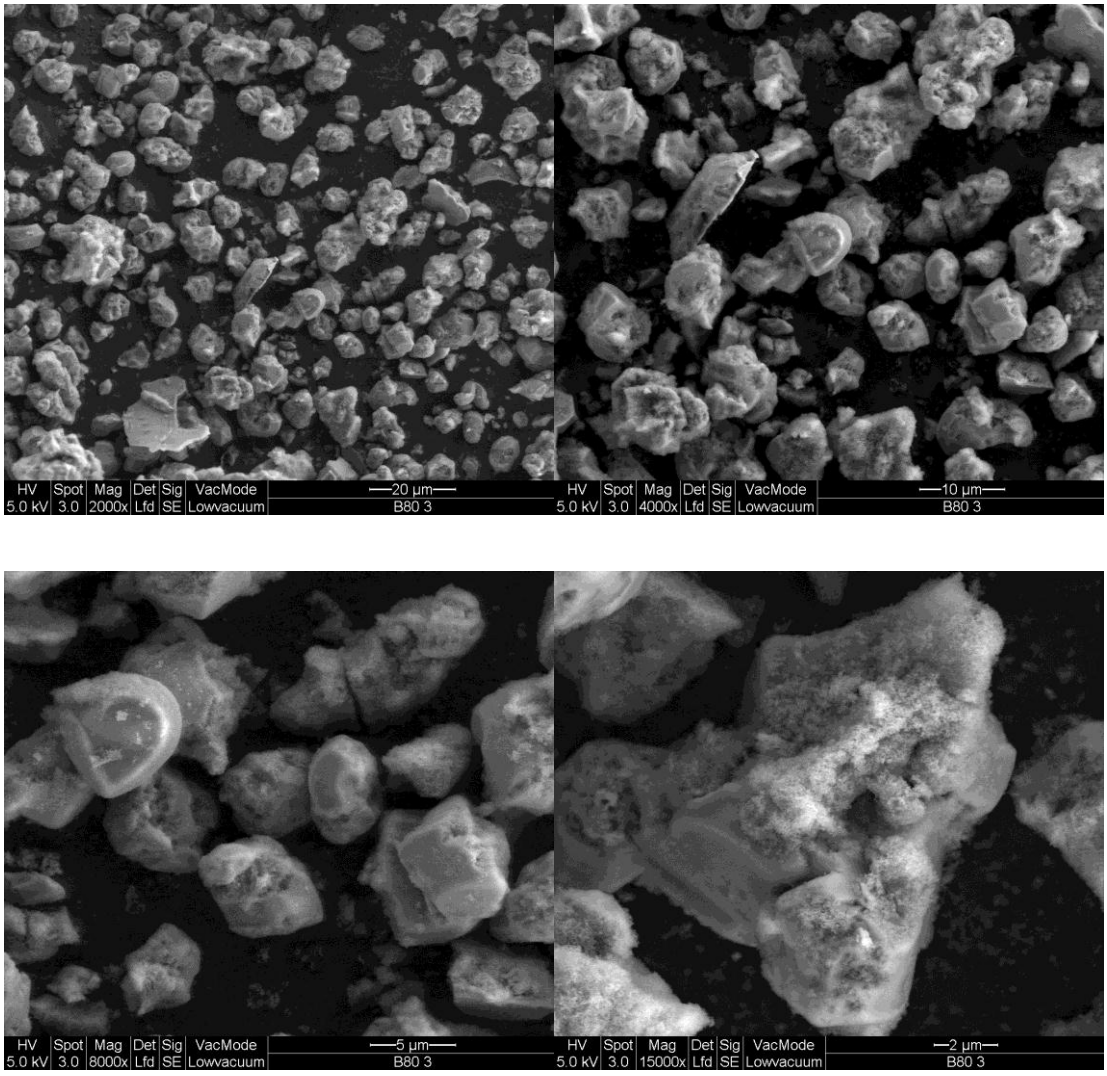

Figure 4.17: SEM images of sample 80Ti-MCM-41.

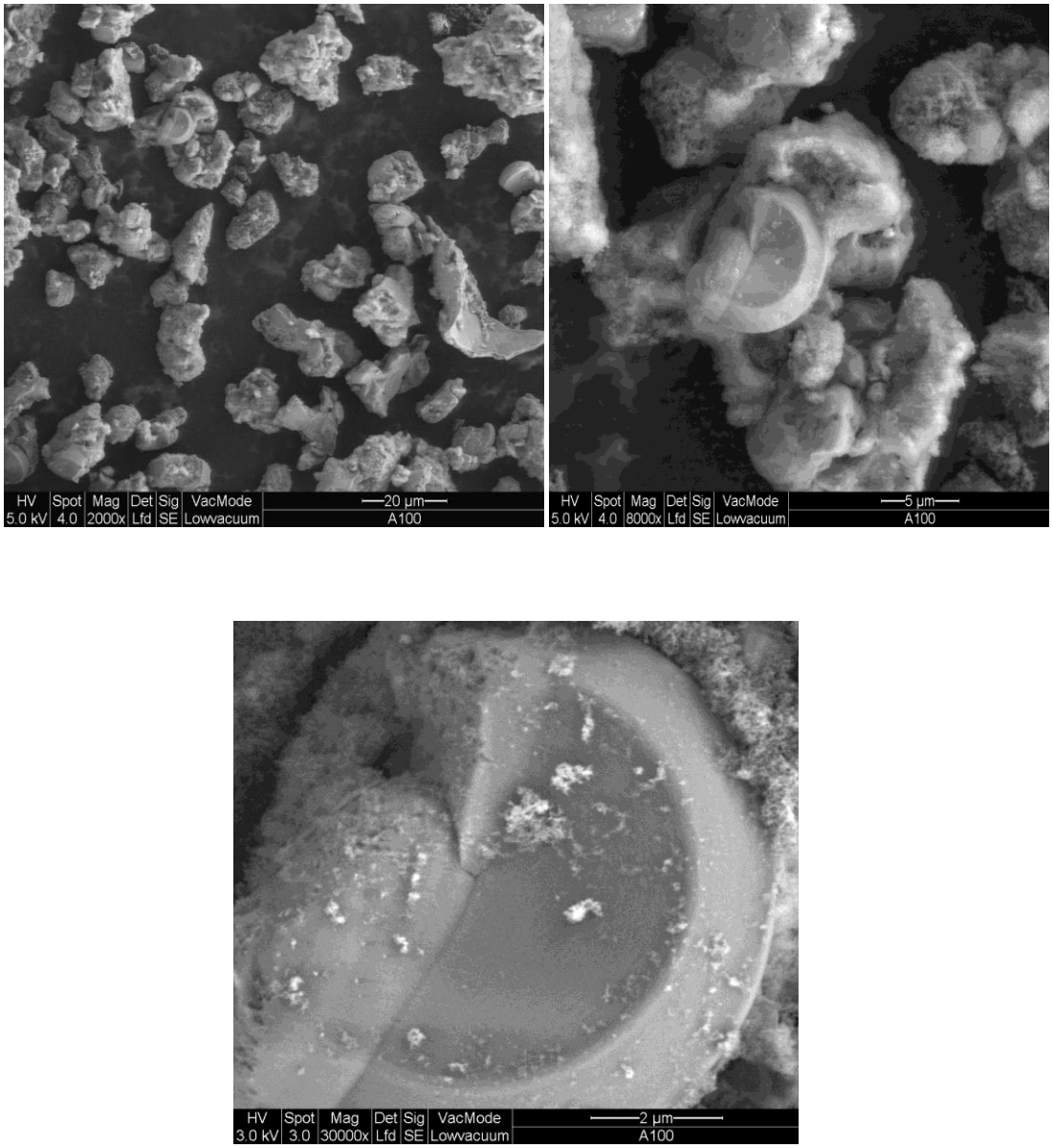

Figure 4.18: SEM images of sample 100Ti-MCM-41.

Ti-MCM-41 materials are having micellar rod-like shape hexagonal or spherical edges, as shown from scanning electron micrographs above. In materials synthesized using cetyltrimethylammonium bromide (CTMABr) as surfactant, Steel *et. al.* postulated that CTMABr surfactant molecules assembled directly into the liquid phase upon addition of the silicate species[131].

The energy dispersive X-ray analysis (EDX) for samples 25Ti-MCM-41, 55Ti-MCM-41, 66Ti-MCM-41, 80Ti-MCM-41 and 100Ti-MCM-41 are shown in Figure 4.19 to Figure 4.23. The Si/Ti ratios of the gels and the calcined Ti-MCM-41 samples do not differ significantly, which indicate quite high efficiency for the incorporation of well dispersed titanium into the framework and/or walls of silica matrix of MCM-41.

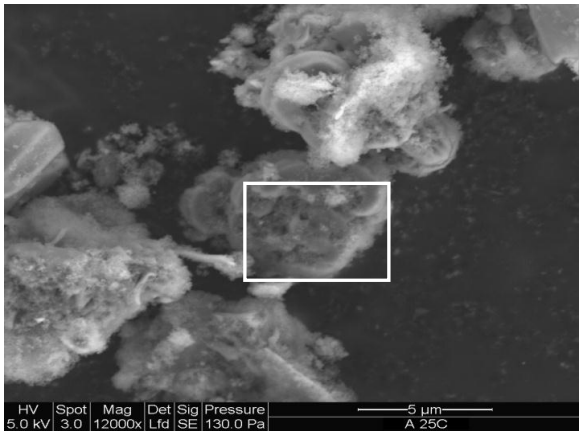

Element	Weight%	Atomic%
C K	35.88	46.26
O K	44.52	43.09
Si K	18.9	10.42
Ti K	0.7	0.22
Totals	100	

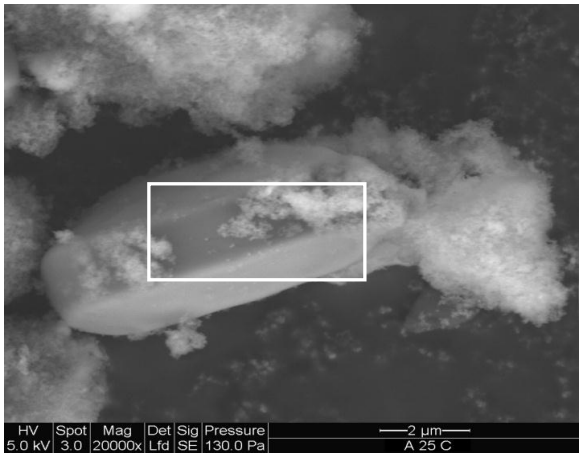

Element	Weight%	Atomic%
C K	22.71	31.12
O K	53.64	55.19
Si K	22.96	13.46
Ti K	0.68	0.23
Totals	100	

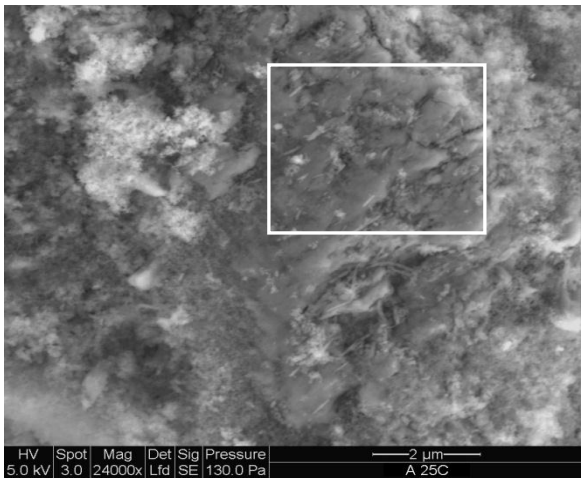

Element	Weight%	Atomic%
C K	23.05	32.39
O K	49.98	52.74
Si K	21.57	12.96
Ti K	5.41	1
Totals	100	

Figure 4.19: EDX analysis of sample 25Ti-MCM-41.

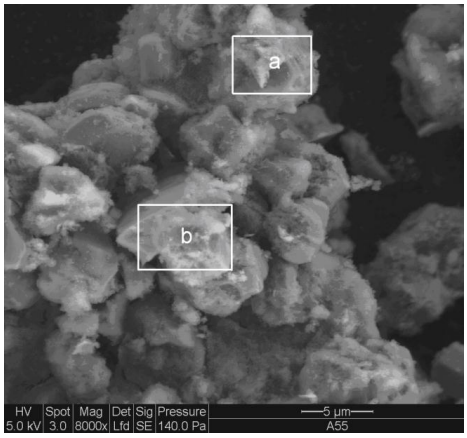

a		
Element	**Weight%**	**Atomic%**
C K	6.02	9.71
O K	62.31	73.39
Si K	30.80	16.48
Ti K	0.87	0.41
Totals	100	

b		
Element	**Weight%**	**Atomic%**
C K	7.19	9.67
O K	58.68	65.84
Si K	33.48	24.13
Ti K	0.66	0.36
Totals	100	

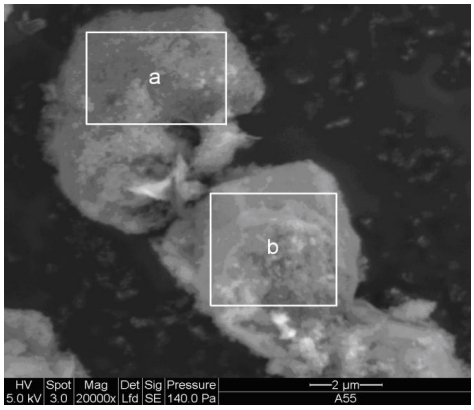

a		
Element	**Weight%**	**Atomic%**
C K	5.69	7.67
O K	62.05	71.25
Si K	31.40	20.63
Ti K	0.86	0.45
Totals	100	

b		
Element	**Weight%**	**Atomic%**
C K	7.23	11.58
O K	56.84	66.97
Si K	35.37	21.15
Ti K	0.56	0.30
Totals	100	

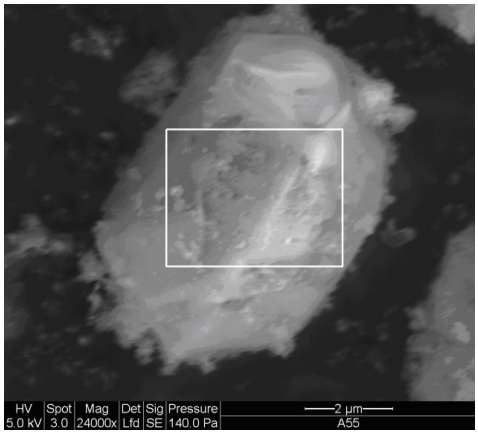

Element	**Weight%**	**Atomic%**
C K	11.31	16.81
O K	51.74	55.66
Si K	36.08	27.28
Ti K	0.87	0.25
Totals	100	

Figure 4.20: EDX analysis of sample 55TiMCM-41.

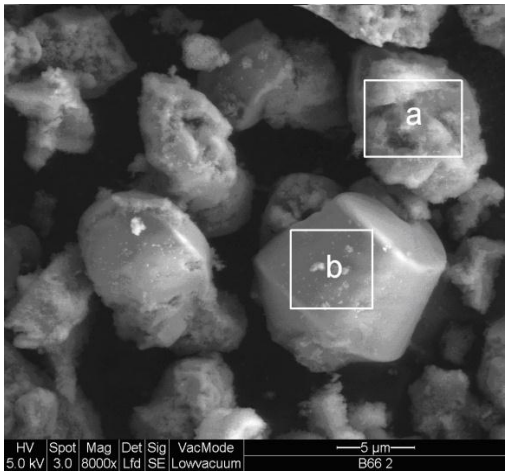

a		
Element	**Weight%**	**Atomic%**
C K	5.72	8.78
O K	59.58	68.65
Si K	33.93	22.27
Ti K	0.77	0.3
Totals	100	

b		
Element	**Weight%**	**Atomic%**
C K	6.98	10.88
O K	54.18	63.39
Si K	38.3	25.53
Ti K	0.53	0.21
Totals	100	

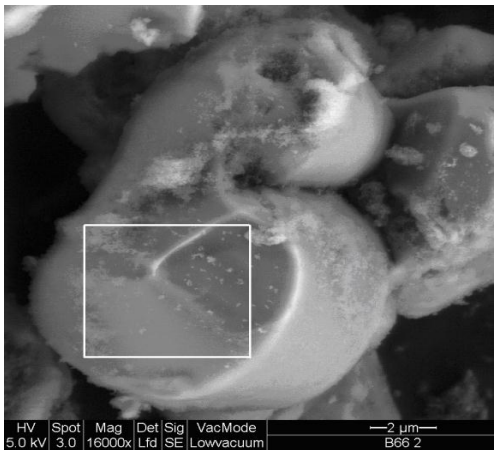

Element	**Weight%**	**Atomic%**
C K	6.92	10.8
O K	54.18	63.49
Si K	37.97	25.35
Ti K	0.93	0.36
Totals	100	

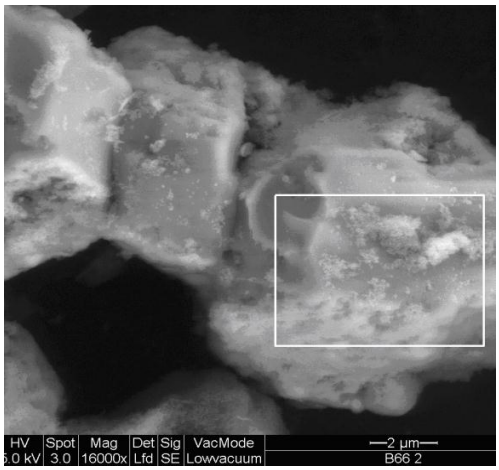

Element	**Weight%**	**Atomic%**
C K	11.43	17.33
O K	51.90	59.06
Si K	36.08	23.39
Ti K	0.60	0.23
Totals	100	

Figure 4.21: EDX analysis of sample 66Ti-MCM-41.

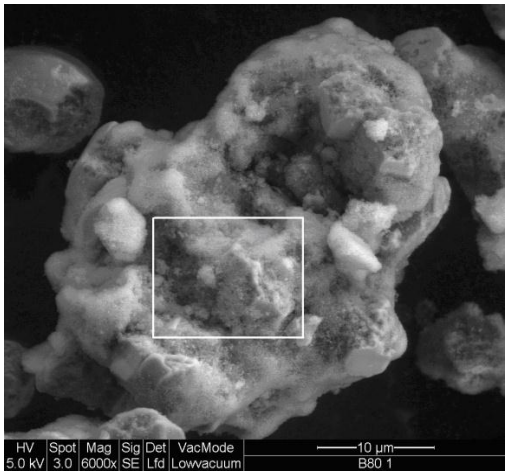

Element	Weight%	Atomic%
C K	12.83	18.9
O K	55.41	61.27
Si K	31.07	19.57
Ti K	0.69	0.26
Totals	100	

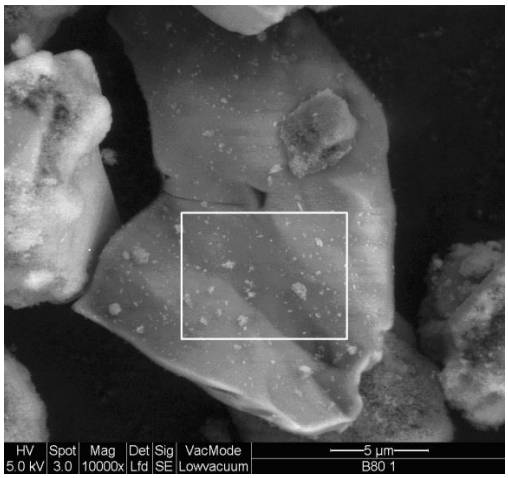

Element	Weight%	Atomic%
C K	14.51	22.29
O K	44.03	50.77
Si K	40.37	26.52
Ti K	1.09	0.42
Totals	100	

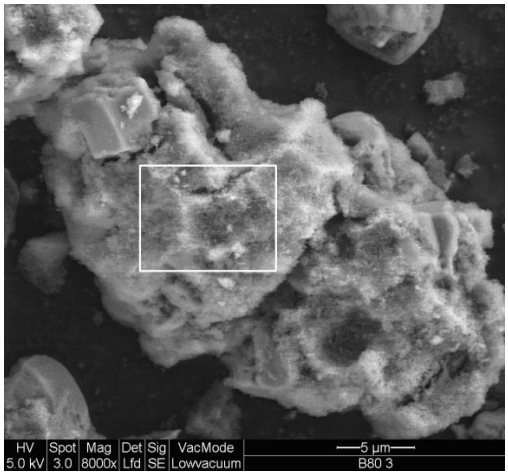

Element	Weight%	Atomic%
C K	6.11	9.49
O K	56.53	65.89
Si K	36.71	24.37
Ti K	0.64	0.25
Totals	100	

Figure 4.22 (i): EDX analysis of sample 80Ti-MCM-41.

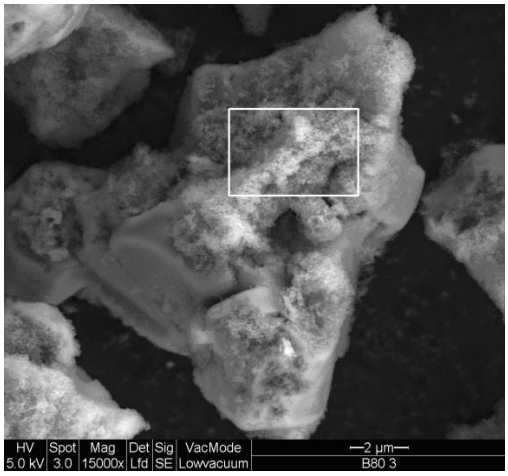

Element	Weight%	Atomic%
C K	6.49	10.09
O K	55.9	65.19
Si K	36.63	24.34
Ti K	0.99	0.38
Totals	100	

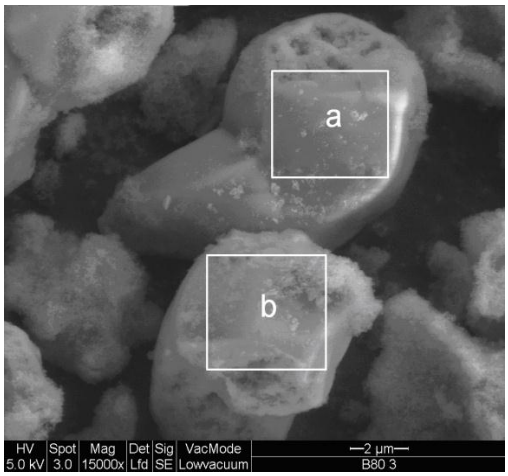

a		
Element	Weight%	Atomic%
C K	5.22	8.04
O K	59.57	68.89
Si K	34.73	22.88
Ti K	0.48	0.19
Totals	100	

b		
Element	Weight%	Atomic%
C K	5.29	8.1
O K	60.48	69.59
Si K	33.75	22.12
Ti K	0.48	0.19
Totals	100	

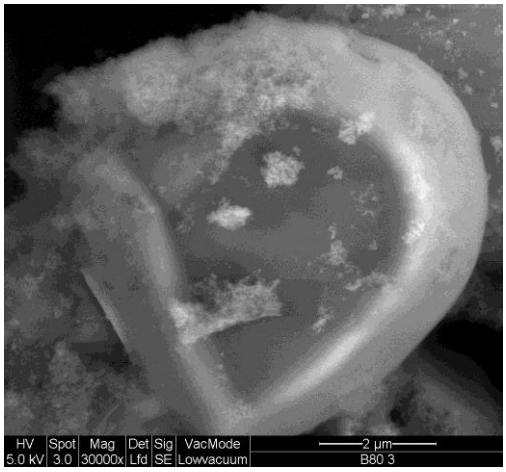

Element	Weight%	Atomic%
C K	7.16	11.02
O K	56.62	65.35
Si K	35.58	23.39
Ti K	0.64	0.25
Totals	100	

Figure 4.22 (ii): EDX analysis of sample 80Ti-MCM-41.

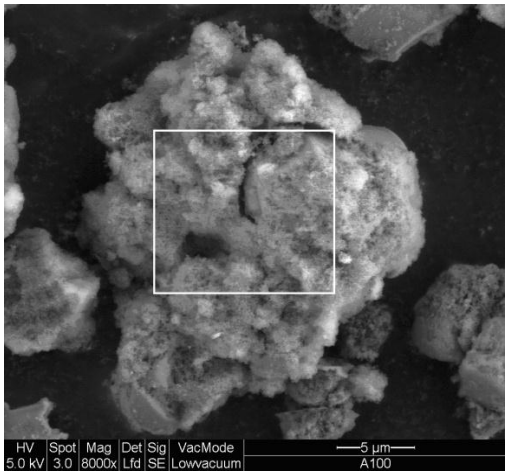

Element	Weight%	Atomic%
C K	24.86	34.11
O K	49.52	51.01
Si K	25.01	14.67
Ti K	0.61	0.21
Totals	100	

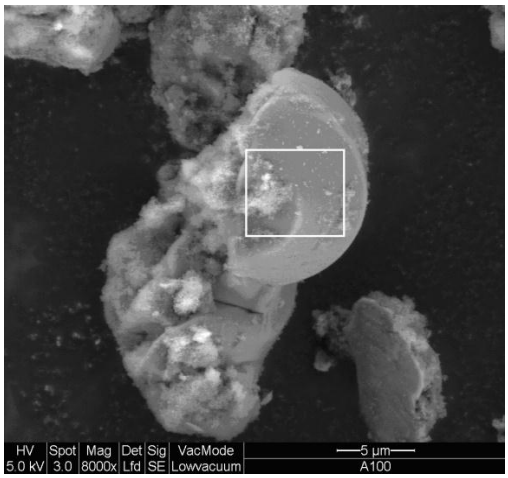

Element	Weight%	Atomic%
C K	20.04	27.96
O K	54.19	56.77
Si K	25.31	15.11
Ti K	0.46	0.16
Totals	100	

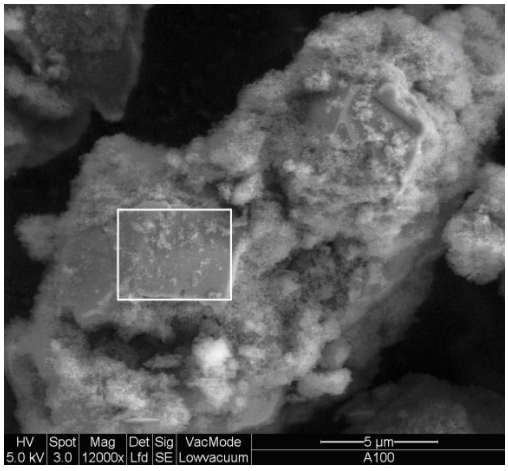

Element	Weight%	Atomic%
C K	22.35	30.41
O K	55.89	57.08
Si K	21.14	12.30
Ti K	0.62	0.21
Totals	100	

Figure 4.23 (i): EDX analysis of sample 100Ti-MCM-41.

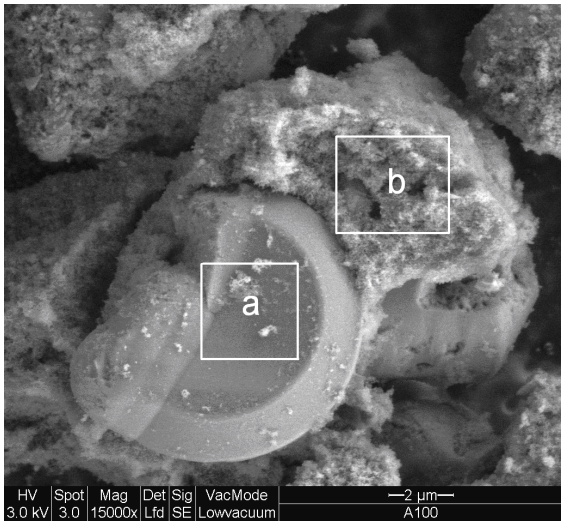

a		
Element	**Weight%**	**Atomic%**
C K	21.24	29.12
O K	55.93	57.57
Si K	22.52	13.20
Ti K	0.31	0.11
Totals	100	

b		
Element	**Weight%**	**Atomic%**
C K	24.86	34.11
O K	49.52	51.01
Si K	25.01	14.67
Ti K	0.61	0.21
Totals	100	

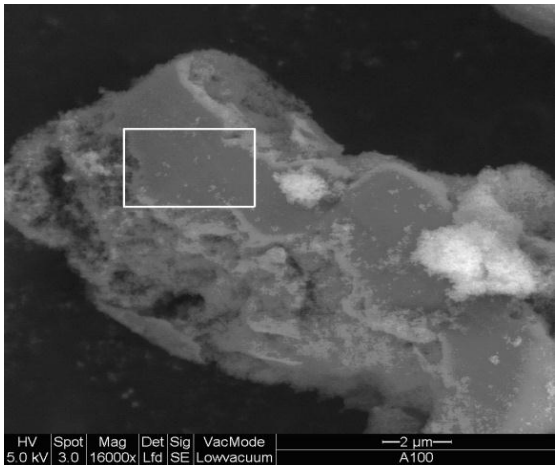

Element	**Weight%**	**Atomic%**
C K	21.80	29.90
O K	54.99	56.61
Si K	22.72	13.32
Ti K	0.49	0.17
Totals	100	

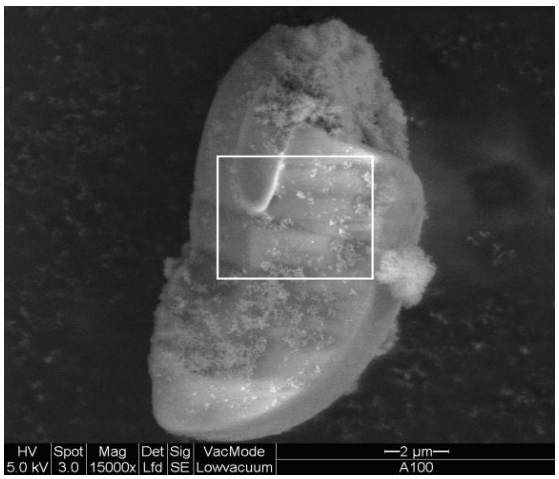

Element	**Weight%**	**Atomic%**
C K	22.21	30.38
O K	54.72	56.20
Si K	22.77	13.32
Ti K	0.30	0.10
Totals	100	

Figure 4.23 (ii): EDX analysis of sample 100Ti-MCM-41.

EDX of Ti -MCM-41 samples above confirm the presence of highly ordered needle-like titanium particles within the framework; the pores are seen to be arranged in patches composed of regular rows approximately 800 Å long. After hydrothermal treatment at 550 °C, the hexagonal pore array becomes more irregular and less geometric.

(d) TGA/DSC

The thermogravimetry (TG) and differential thermal analyses (DTA) temperature profile is shown in Figure 4.24 below.

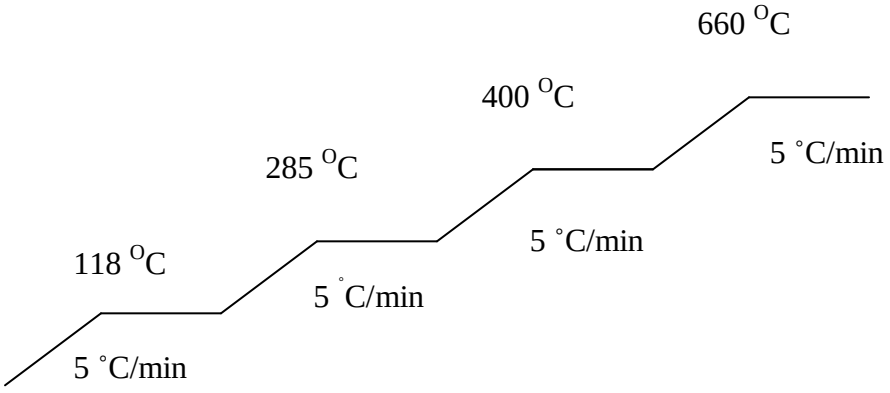

Figure 4.24: DTG-DTA-TGA temperature profile

Thermogravimetric analysis (TGA) shows distinct weight losses that depend on the framework composition (Table 4.3). As can be seen from Table 4.3, the as-synthesized Ti-MCM-41 consists of 55.0-65.0 wt% of water and organic templates. The removal of water and template can be divided into three stages of weight loss.

Table 4.3 : Thermogravimetric results for Ti-MCM-41 samples

Samples (Si/Ti)	Weight loss (wt %)			
	Total	25-150 ^{o}C	150-350 ^{o}C	350-700 ^{o}C
25	55.00	6.92	40.09	7.99
55	58.32	6.41	43.86	8.05
66	61.80	6.34	44.21	11.25
80	62.55	8.15	44.14	10.26
100	65.75	10.60	44.53	10.62

The first stage occurs between 25^{o}C until 150^{o}C and is due to the desorption of physisorbed water in the mesopores. The second stage of weight loss in the range of 150^{o}C to 350^{o}C are the result of decomposition and combustion of organic species, *i.e.* tetramethylammonium and cetyltrimethylammonium (TMA and CTMA). Weight losses in this temperature range are not as large as in the parent silicate because of stronger sorbate-sorbent interactions at the aluminosilicate surface. In the range of 280^{o}C to 340^{o}C, the oxidative decomposition of residual organic compounds occur which is accompanied by weak exotherms.

The third stage between 350^{o}C to 700^{o}C is the region of surfactant. DTA-TGA techniques are used to follow the development of surfactant decomposition-elimination process up. Weight losses in this temperature range are attributed to combustion of coke that has been deposited during the incomplete combustion of organic species in the former stage.

The last stage of weight loss occurs at temperatures above 550^{o}C and is related to water losses via condensation of silanol groups that are present on the pore walls of the Ti-MCM-41 materials to form siloxane bonds. However, there is almost no exothermal peak after 550^{o}C, which indicate the surfactant had been removed completely. The total weight losses at 800 ^{o}C for all ratios of Ti-MCM-41 samples are 55.00, 58.32, 61.80, 62.55 and 65.75 wt% for samples 25Ti-MCM-41, 55Ti-MCM-41, 66Ti-MCM-41, 80Ti-MCM-41 and 100Ti-MCM-41 respectively. The as-synthesized sample contains about 50 wt. % of organic species. The details of thermogravimetric results for 100Ti-MCM-41 sample are tabulated in Table 4.4 below.

Table 4.4: Thermogravimetric results for 100Ti-MCM-41 sample

onditions	Expected	Observed	Interpretation
i) Sample : Ti-MCM-41 (as-synthesized 100-TiMCM-41; Si/Ti = 100) ii) Sample weight : 20.1190 mg iii) Method : 30.0-800.0^{O}C/ 5^{O}C/min, N_2 50.0 ml/min, Alox	Three distinct steps; i) 25 – 130 ^{O}C ii) 130 – 300 ^{O}C iii) above 300 ^{O}C	Five distinct steps; i) 0 – 118 ^{O}C Wt. loss (%) = 10.5951 ii) 118 – 285 ^{O}C Wt. loss (%) = 33.2601 iii) 285 – 400 ^{O}C Wt. loss (%) = 11.2743 iv) 400 – 660 ^{O}C Wt. loss (%) = 9.8025 v) above 660 ^{O}C Wt. loss (%) = 0.8177	i) desorption of water exothermic processes related to combustion of organic species v) dehydroxylation of Si-OH from surface of Ti-MCM-41
	TOTAL WT. LOSS = 59.40 wt. %	TOTAL WT. LOSS = 65.75 wt. %	

The representive thermogram of sample 100Ti-MCM-41 is given in Figure 4.25.

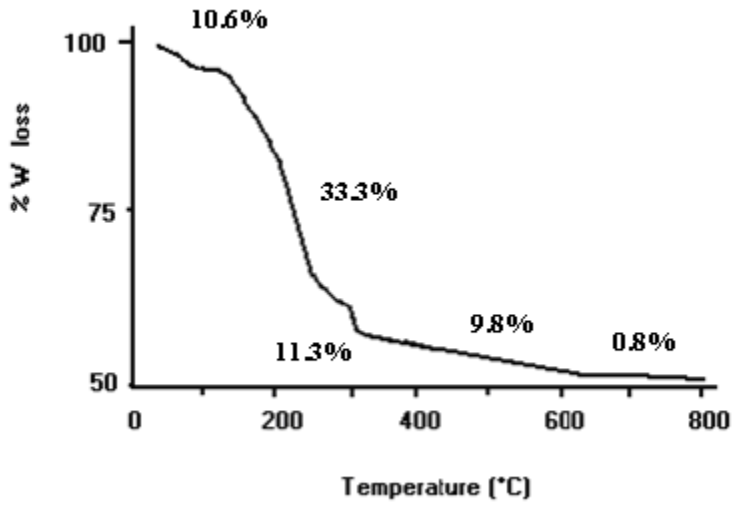

Figure 4.25: Thermogram of sample 100Ti-MCM-41

The TGA curves of three selected samples, 25Ti-MCM-41, 66Ti-MCM-41 and 100Ti-MCM-41 are shown in Figure 4.26, Figure 4.27 and Figure 4.28 below. The curves are showing five steps of weight loss.

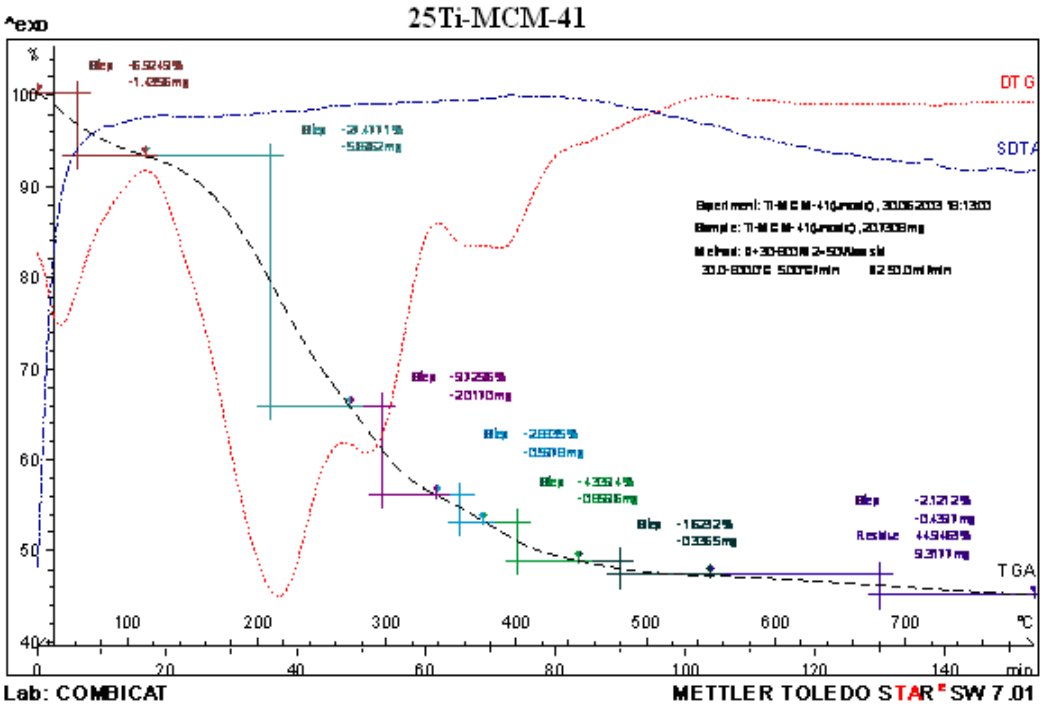

Figure 4.26: The TGA-DTA traces of as-synthesized 25Ti-MCM-41.

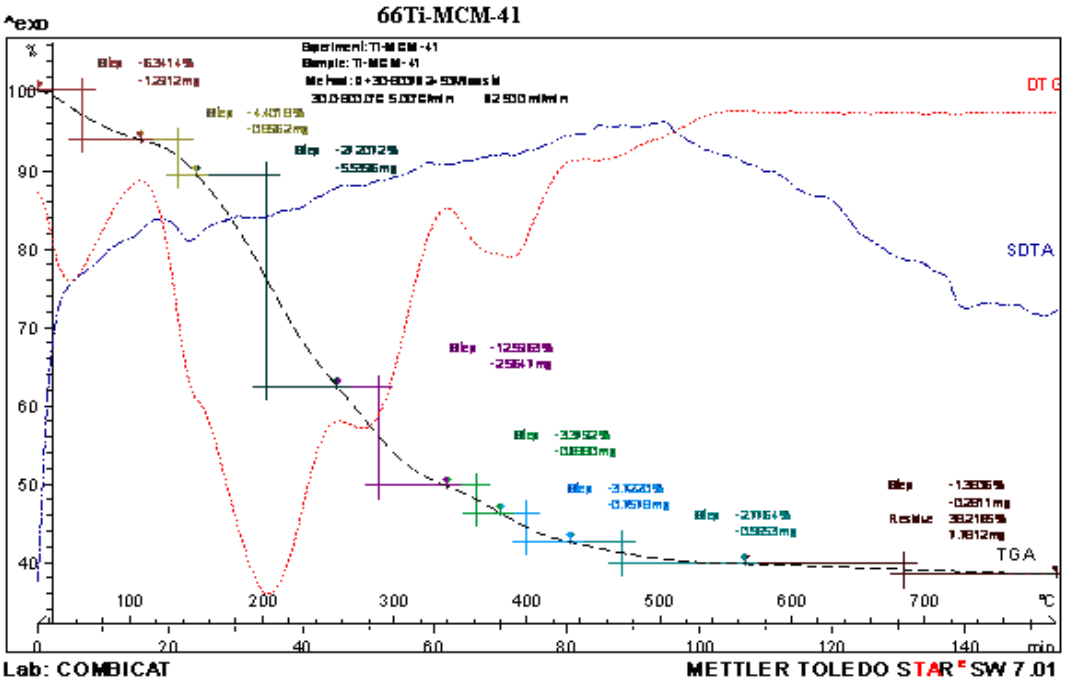

Figure 4.27: The TGA-DTA traces of as-synthesized 66Ti-MCM-41.

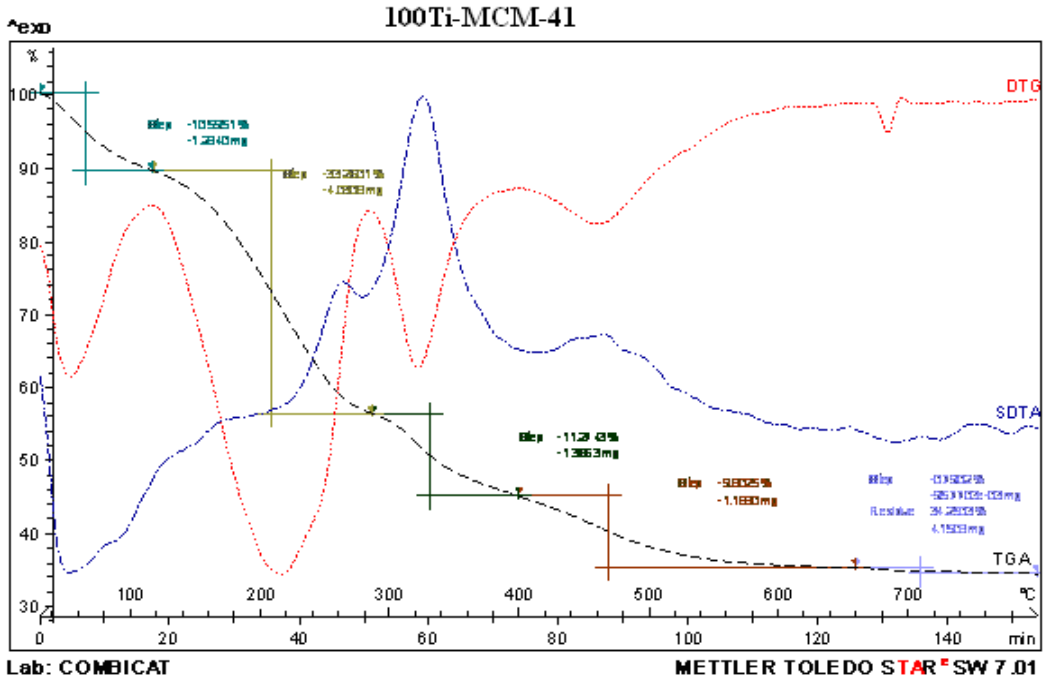

Figure 4.28: The TGA-DTA traces of as-synthesized 100Ti-MCM-41.

From the three curves above, the steps can be distinguished as 35-130 ºC, 130-300 ºC, 300-380 ºC, 380-480 ºC and 480-600 ºC. The weight loss for the three samples is ~ 8.0% to 11.0% in the first step due to desorption of physisorbed water held in the pores. The weight losses in the second (~ 33.0% to 38.0%) and third (~ 9.0% to 12.0%) steps are mainly associated with oxidative decomposition of templates. In the fourth step, the weight loss (~ 8.0% to 10.0%) is probably due to removal of coke formed in the previous steps by the decomposition of templates. Whereas, in the last step, the weight loss (~ 1.0 to 2.0%) is mainly due to water loss formed by the condensation of silanol groups. It can be noticed that the weight losses for the three samples are similar indicative of similar pore filling of MCM-41 samples.

TGA was also performed in a nitrogen flow of 50 cm^3min^{-1}. Essentially no difference between the TGA patterns obtained in air and nitrogen (N_2) flow were observed except that the sample after TGA in N_2 flow was light brown –coloured (related to the coke deposits). These results reveal that most of the organic template species can be removed upon decomposition and/or desorption in inert gas below 400 ^oC.

Calcination of the as-synthesized MCM-41 materials was performed in a temperature controlled plug flow reactor. About 1.0 g of the as-synthesized material was heated up to the calcination temperature at a rate of 3 ˚C per minute under a continuous N_2 gas flow. Calcination up to 350°C results in a brown/black solid still containing around 16 wt% of organics, which are removed by calcination at temperatures higher than 540 ˚C. Based on these results, we decided to use calcination at 540 ˚C for seven hours as the method for template removal throughout this study. It was confirmed by thermogravimetric analysis (TGA) that template had been totally removed upon such a treatment.

TGA analysis on calcined MCM-41 samples was also performed in order to get information about the hydrophobicity of the MCM-41 materials. In this case, samples were allowed to equilibrate with moisture from air over a period of several days prior to analysis. The weight loss than observed by TGA in the temperature range from 25 ˚C until 150 ˚C is caused by the loss of water that is adsorbed inside the pores. The amount of water and the temperature at which it

leaves the pores is indicative of the hydrophilic nature of the sample being analyzed.

Thermogravimetry (TG) and differential thermal analyses (DTA) of as-synthesized (uncalcined) and calcined Ti-MCM-41 samples are given in Figure 4.29 to 4.32. The thermal patterns of all samples are qualitatively very similar. The TG-DTA curves of all samples reveal that nearly all the template including the water formed due to condensation of silanol groups is lost from the pore system at a temperature of ~ 600 ºC.

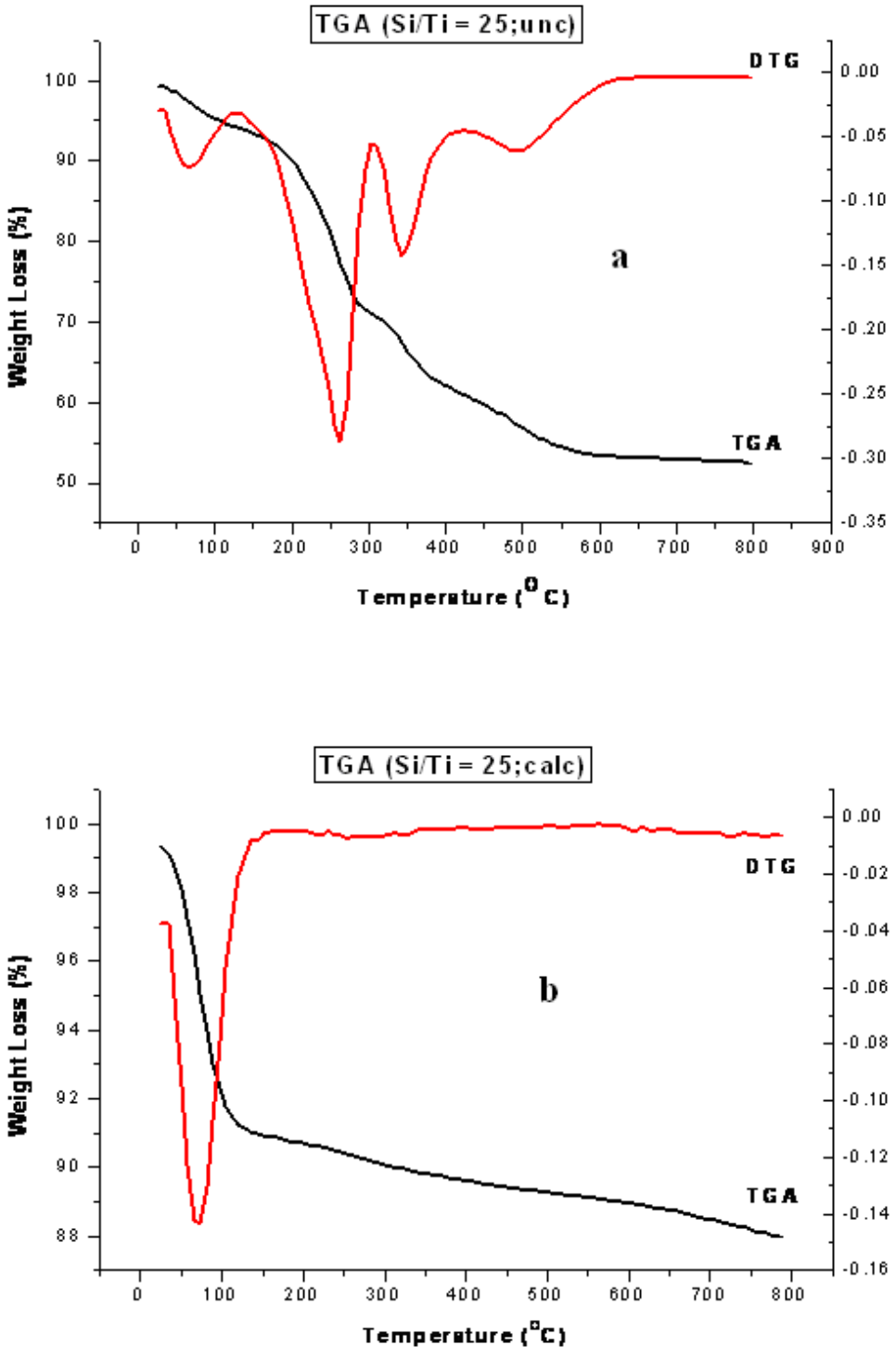

Figure 4.29: TGA-DTG curves of (a) as-synthesized (uncalcined) 25Ti-MCM-41 and (b) calcined 25Ti-MCM-41.

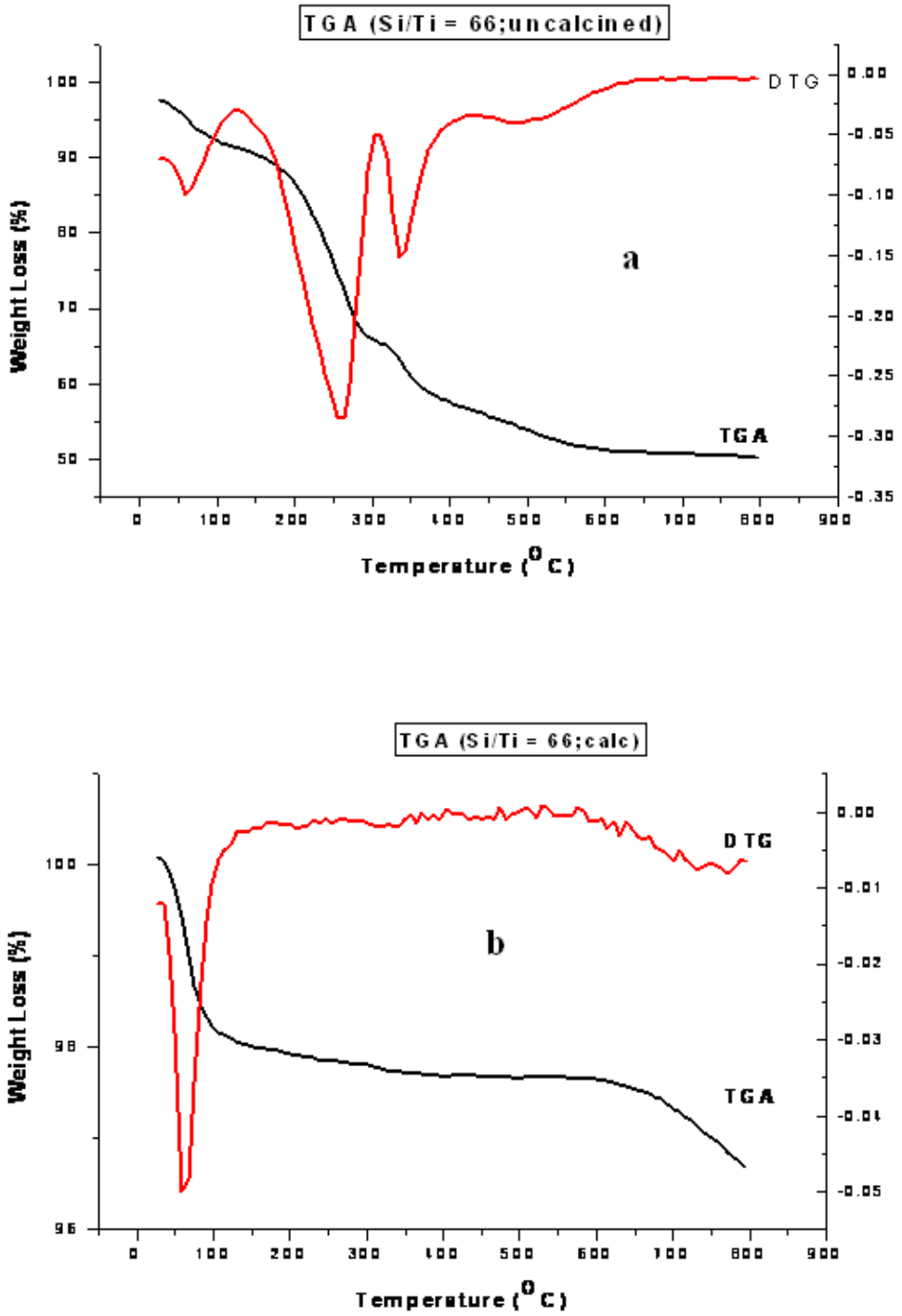

Figure 4.30: TGA-DTG curves of (a) as-synthesized (uncalcined) 66Ti-MCM-41 and (b) calcined 66Ti-MCM-41.

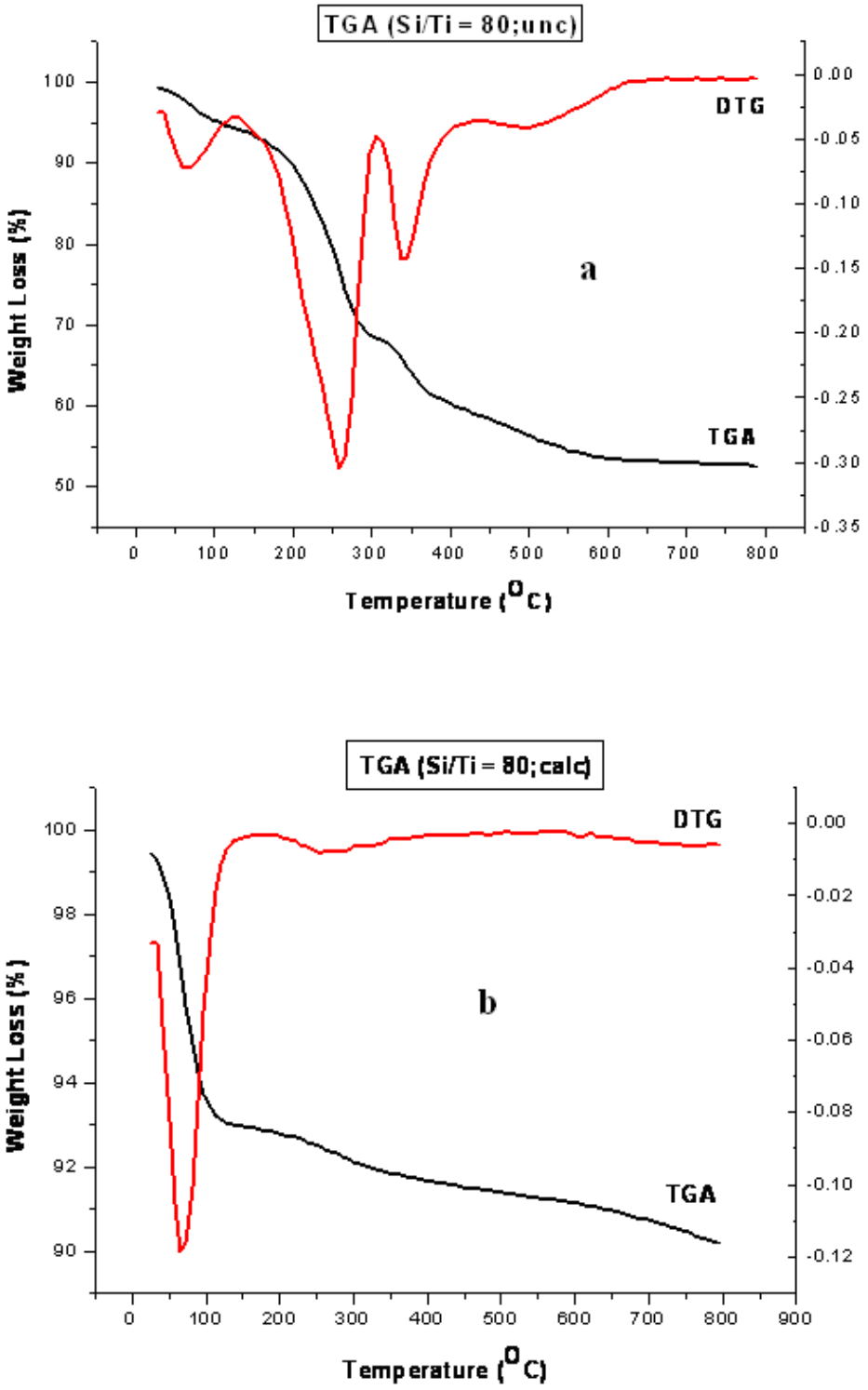

Figure 4.31: TGA-DTG curves of (a) as-synthesized (uncalcined) 80Ti-MCM-41 and (b) calcined 80Ti-MCM-41.

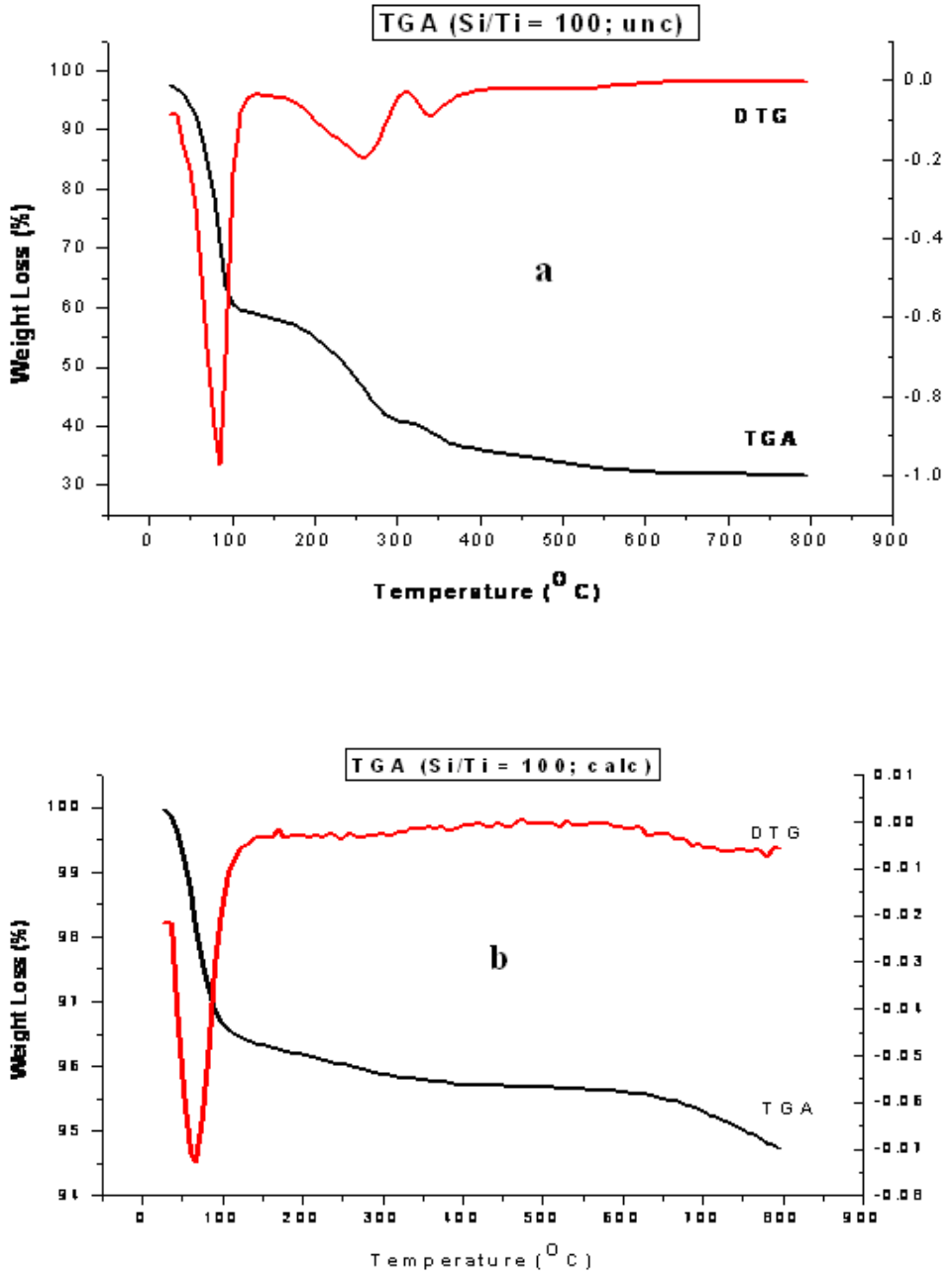

Figure 4.32: TGA-DTG curves of (a) as-synthesized (uncalcined) 100Ti-MCM-41 and (b) calcined 100Ti-MCM-41.

When an amorphous compound is "melted", there is no sharp change in structural characteristics, but rather a gradual loosing of interactions. There may only be a small change in the heat capacity as liquefaction occurs, shown by a shallow step in the baseline.

On the other hand, if crystallization of the amorphous solid occurs, which is quite likely, there will be a sharp exotherm. Enthalpy is released from the system as it goes to a lower free energy. Polymorphic changes may be either endothermic or exothermic, although exotherms are more commonly seen. Losses of surface or crystal water are both endothermic and can be correlated with the temperature (or temperatures) of mass losses in TGA experiments.

(e) UV-Visible

Diffuse Reflectance UV-visible spectroscopy (DRUV-vis) is a widely available technique and is very useful tool for characterizing Ti-MCM-41 sample. Besides its low detector limit (0.03 wt %), it provides valuable information on the coordination of titanium and hence, a very sensitive probe to detect the presence of framework and extra-framework titanium in MCM-41. The chemistry of the silica structure and active sites can also be determined using DRUV-vis spectroscopy. The reflection mode of UV-vis spectroscopy proved to be the simplest but powerful method for characterizing transition metal ions such as titanium.

Figure 4.33 shows the spectrograms of uncalcined and calcined Ti-MCM-41 samples; 25Ti-MCM-41, 55Ti-MCM-41, 66Ti-MCM-41, 80Ti-MCM-41 and 100Ti-MCM-41 prepared in the presence of promoter with several Si/Ti ratios. A sample containing only framework titanium should give an optical transition at 210 nm, which is assigned to a charge transfer (CT) in [TiO_4] and [O_3Ti-OH] moieties. Studies with UV-visible spectroscopy allow to check the coordination state of titanium, since if the titanium is in a monomeric tetrahedral species the maximum off the band appears at a wavelength near to 220 nm, while if it forms polymeric species, the maximum move up to higher wavelength.

In this study, all Ti-MCM-41 samples prepared revealed a narrow absorption at 220 nm, indicating titanium is in tetrahedral coordination. Isolated extraframework hexacoordinated titanium shows a charge transfer transition at about 225 nm [132-133]. The uncalcined samples exhibit two bands at around 280 and 340 nm. These transitions are probably due to the tetrahedrally coordinated V^{5+} ions.

The UV-visible spectra for calcined Ti-MCM-41 samples are shown in Figure 4.34. Upon calcinations (burning the template off), these bands became more intense. In the spectrum of calcined sample, the most intense UV absorption bands appeared due to higher titanium content in the sample compared to the uncalcined ones. There is around 50% template (CTMABr) in the pore of uncalcined samples and left with 50% of silica and titanium, while in calcined sample, 100% of the content is silica and titanium.

A shoulder at ~ 270 nm (Figure 4.33) can be seen in uncalcined samples, which is absent in calcined samples. Sample of uncalcined 55-Ti-MCM-41 (Si/Ti = 55) exhibits the lowest UV absorption bands compared to other ratios due to the low amount of titanium in the sample, which is around 2.29%. The shoulder at 270 nm as shown in Figure 4.35 for uncalcined samples probably corresponds to partially polymerized titanium species (five- and six-coordinate) in small titanium nanodomains. The presence of penta- or hexa-coordinated titanium-sites in Ti-

MCM-41 may be associated with the less crystallographic order in the pore walls and much higher accessible surface area [134-136].

In addition, it shows that the intensity of the band shoulder around 270 nm increased with titanium content as shown in Figure 4.36. 25Ti-MCM-41 sample has the highest titanium content whereas 100Ti-MCM-41 has the lowest titanium amount. This suggests that the probability to get polymeric species of titanium increases when the amount of titanium in the samples increases.

The absence of any absorption band at 330 nm indicates that no anatase (bulk titanium) is formed in the Ti-MCM-41 samples. The above results suggest that most of the titanium atoms occupy a site-isolated position in the silica framework of Ti-MCM-41.

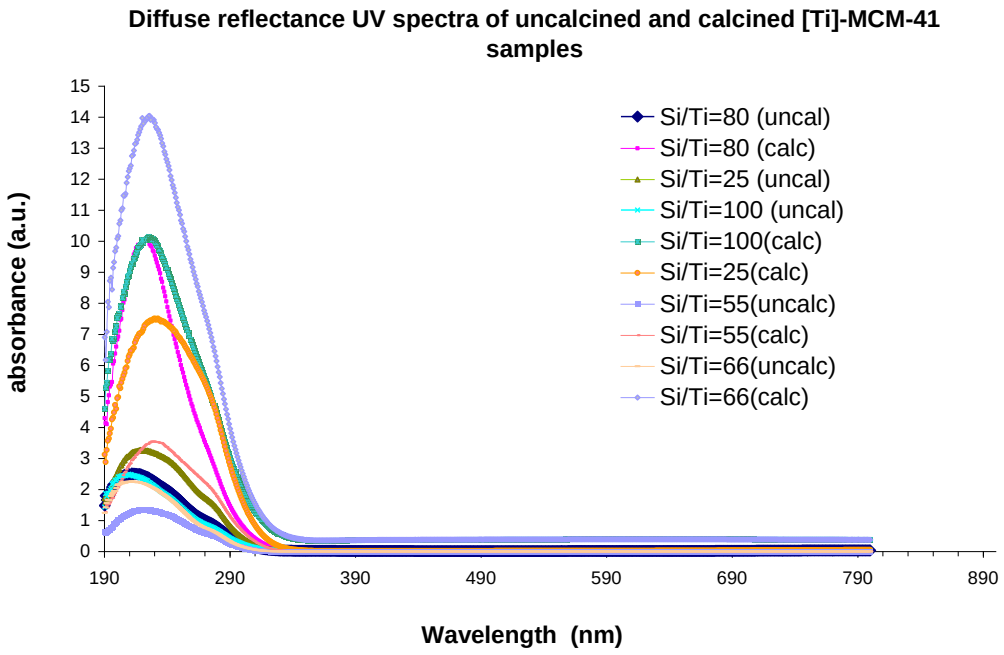

Figure 4.33: Diffuse reflectance UV-Vis spectra of calcined and uncalcined Ti-MCM-41 samples.

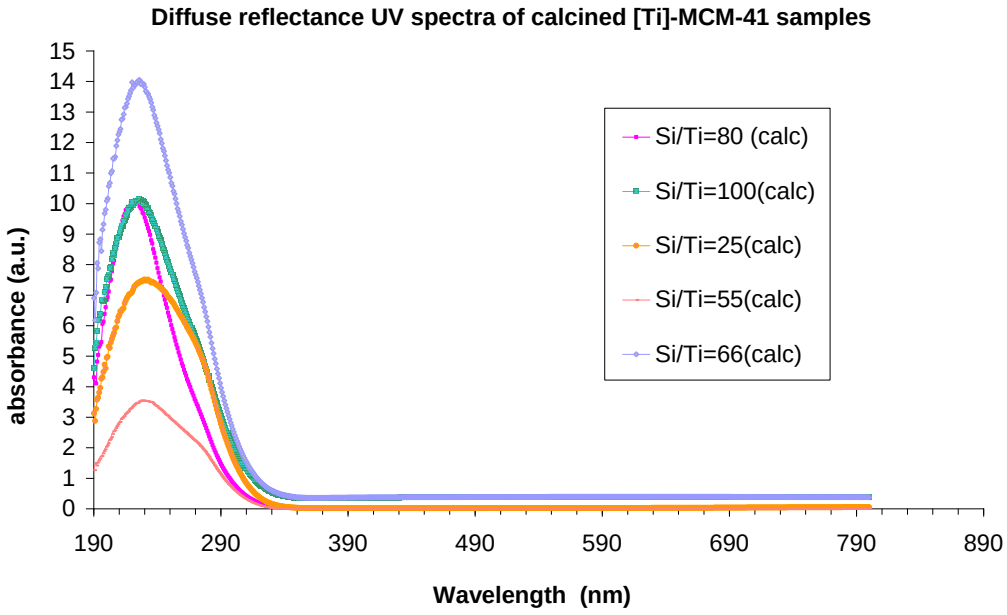

Figure 4.34: Diffuse reflectance UV-Vis spectra of calcined Ti-MCM-41 samples.

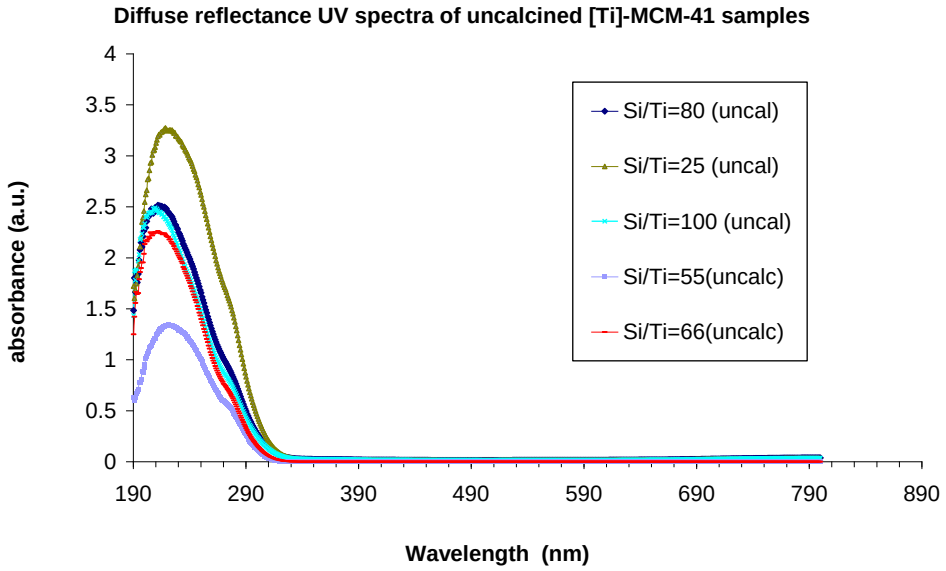

Figure 4.35: Diffuse reflectance UV-Vis spectra of uncalcined Ti-MCM-41 samples.

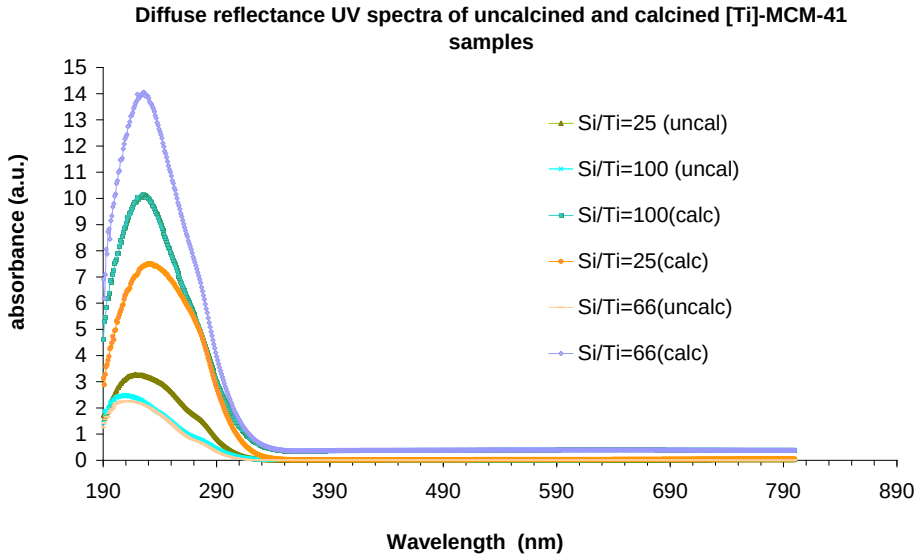

Figure 4.36**:** Diffuse reflectance UV-Vis spectra of the highest intensity of calcined and uncalcined (66Ti-MCM-41), medium intensity (100Ti-MCM-41) of calcined and uncalcined and the lowest intensity (25Ti-MCM-41) of calcined and uncalcined Ti-MCM-41 samples.

In summary, it can be stated that in all the Ti-MCM-41 samples studied, the major amount of titanium atom is mononuclearly dispersed in the pores of the MCM-41 support and largely tetrahedrally coordinated with oxygen.

(f) FTIR

The FTIR spectroscopy in the framework region (400-1300 cm^{-1}) provides additional information about the structural details including isomorphous substitution in molecular sieves, whereas the hydroxyl region (3000-4000 cm^{-1}) contributes for the determination of different (Brönsted and Lewis) acid sites [137] and silanol groups [138]. The band at 960 cm^{-1} in the framework region is very important and generally attributed to the incorporation of metal ions in the framework of silica matrix particularly for Ti-containing molecular sieves [139]. Acidic and basic properties as well as its strength in molecular sieves can also be determined by FTIR spectroscopy using CO_2, ammonia, pyridine and triphenylphosphine as the probe molecules [140].

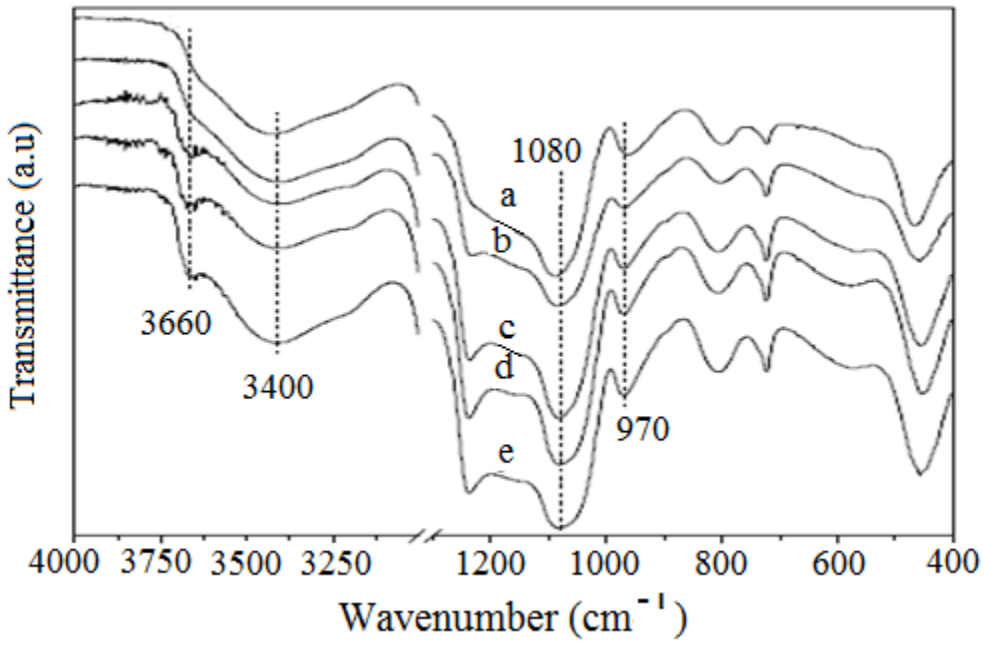

Figure 4.37: IR spectra in the framework and the hydroxyl vibration region of calcined (a) MCM-41 (b) 100Ti-MCM-41 (c) 80Ti-MCM-41 (d) 66Ti-MCM-41 and (e) 25Ti-MCM-41.

Figure 4.37 depicts the FTIR spectra of Transmittance against Wavenumber, cm^{-1} for Ti-MCM-41 catalysts. Previous work on the characterization of titanium-zeolites has been used as a guide for characterizing Ti-MCM-41 sample. Four characteristic absorption bands are observed.

The parent MCM-41 sample shows two main peaks, a broad one at about 810 cm^{-1} is attributed to the symmetrical Si-O-Si stretching vibration while the other one at about 980 cm^{-1} is assigned to symmetric stretching vibration of Si-OH groups. The Ti-MCM-41 sample also shows the absorption peak at 810 cm^{-1}, whereas the

980 cm^{-1} peak disappeared and a new peak at about 946 cm^{-1} appeared. The absorption band at 946 cm^{-1} is explained to be due to the formation of Ti-O-Si bridges [141] while the disappearance of the peak at 980 cm^{-1} is explained to be due to the replacement of Si-OH groups by titanium ligands.

The representative IR spectra in the framework region of MCM-41 and Ti-MCM-41 samples show characteristic band at 970 cm^{-1} attributed to Si-O-Ti vibration [142]. However, a band at 962 cm^{-1} for MCM-41 sample is attributed to Si-OH vibration [143]. So, 970 cm^{-1} band cannot be taken as proof for the incorporation of Ti in the framework of Ti-MCM-41 samples. But, the shift of this band (~ 10 cm^{-1}) to higher wavenumber [144] as well as the shift of the Si-O-Si band from 1090 cm^{-1} for MCM-41 to 1080 cm^{-1} for Ti-MCM-41 samples [145] are generally taken as an indication for the incorporation of Ti in the framework of respective MCM-41 samples. Its wavenumber decreases with increasing incorporation of titanium in the structure.

It may be demonstrated that the absorption at 970 cm^{-1} is essentially due to the increased degeneracy of the elongation vibration in the tetrahedral structure of SiO_4 induced by the change in the polarity of the Ti-O bond when Si is linked to Ti. The SiOH group formed by the hydrolysis of the Ti-O-Si bonds and the sharing of OH with Ti is then responsible for the absorption at higher wavenumbers compared to ordinary Si-OH groups [146].

In the hydroxyl region (3000-4000 cm^{-1}), a broad band centered at 3422 cm^{-1} is observed for MCM-41. However, in Ti-MCM-41 this band is shifted towards the lower wavenumber (15 cm^{-1}) and is observed at 3407 cm^{-1} for all the Ti-MCM-41 samples. A weak band at 3661 cm^{-1} is also observed for all the Ti-MCM-41 samples. However, this band is not observed in the MCM-41 sample. Both the bands were assigned to silanol group vibrations situated inside the channels of MCM-41.

The bands at 3422 and 3407 cm^{-1} results from silanol groups interacting via hydrogen bonding, whereas the other band at 3661 cm^{-1} is due to isolated silanol groups not interacting with each other via hydrogen bonding. The band shift from 3422 to 3407 cm^{-1} for Ti-MCM-41 samples compared to MCM-41 may be assumed to have more hydrogen bonding in Ti-MCM-41 samples due to presence of more defect sites (SiOH groups). The band assignments for the IR spectra of MCM-41 and Ti-MCM-41 are given in Table 4.5.

Table 4.5: Band assignments in the IR spectra of MCM-41 and Ti-MCM-41 (for all wt % Ti)

Wavenumber (cm^{-1})	Bond assignment for MCM-41	Wavenumber (cm^{-1})	Bond assignment for Ti-MCM-41
3400	ν_{OH}(Si-O-H)	3660, 3400	ν_{OH}(Si-O-H
1080	ν_{asym}(Si-O-Si)	1080, 1234	ν_{asym}(Si-O-Si)
960	ν_{asym}(Si-O-Si) and/or ν (Si-O-H)	970	ν_{asym}(Si-O-Ti) and/or ν (Si-O-H)
802, 721	ν_{sym}(Si-O-Si)	804, 721	ν_{sym}(Si-O-Si)
464	δ(Si-O-Si)	457	δ(Si-O-Si)

By correlating the intensity of 970 cm^{-1} with the catalytic activity, I found that sample 66Ti-MCM-41 with the strongest adsorption show the highest activity and conversion of 1-Octene and Methyl Oleate which is 18.1 % and 57.3 % respectively. Sample 100Ti-MCM-41 with weaker adsorption in 970 cm^{-1} show relatively lower activity and the conversion of 1-octene and methyl oleate is 10.9 % and 33.4 % respectively.

In summary, FTIR is not enough to prove the incorporation of titanium. The absence of the band at 970 cm^{-1} would indicate, without any doubt, the no-incorporation of titanium, but its presence is not conclusive enough to prove incorporation of titanium. Another important issue is that the catalysts do not show absorption bands in the region 700-400 cm^{-1}, which is the range where TiO_2 as separated phase absorbs.

4.1.2 Reactions of Model Compound: 1-octene

After having discussed in more or less detail in the characterization section of Ti-MCM-41 catalysts, the activity of these materials on the epoxidation of olefins will be described. Again, special focus is directed towards catalysts that have resulted from this research, with an emphasis on practical parameters such as catalyst productivity, turnover numbers and epoxide selectivity.

The strategy followed for this research is first to analyze the effect of Si/Ti ratio of the silylated and non-silylated Ti-MCM-41 catalysts towards epoxidation of model compound (1-octene), followed by the effect of temperature ($50^{o}C$–$75^{o}C$) and reactants concentration (C=C / TBHP) on the reaction rate and product distribution. Finally, the effect of reaction time (0-7 hr) is studied. One important considered element is to establish reaction systems, *i.e.* catalyst type and reaction conditions, that lead to the increment of olefin conversion, epoxide selectivity and product yields under as mild as possible working conditions in order to apply these approach for the epoxidation of bulky oleate molecule. Final part reveals the influence of degree of silylation towards epoxidation of the actual compound.

It has been shown above that the different physicochemical techniques indicate that in the Ti-MCM-41 samples prepared, the Ti is in framework positions, and

therefore it could be active for carrying out catalytic epoxidations of olefins using TBHP as oxidants.

The results obtained with the model catalysts in the epoxidation of 1-octene show that epoxidation activity increases with increasing dispersion of the titanium. This is logical, since the Lewis acidity of the Ti (IV) sites is responsible for the activation of the alkylhydroperoxide, coordination of the peroxide enhancing the electrophilicity of the oxygen atoms and thereby rendering the peroxo group more susceptible to nucleophillic attack by the olefin.

Isolated, coordinatively and electronically unsaturated Ti (IV) centres would, therefore, be anticipated to be the most active sites for epoxidation catalysis. It is now generally accepted that a four-coordinate-lattice titanium sites is the catalytically active species in titanium silicates. The epoxidation of 1-octene is proposed to proceed via the following transformation as shown in Figure 4.38.

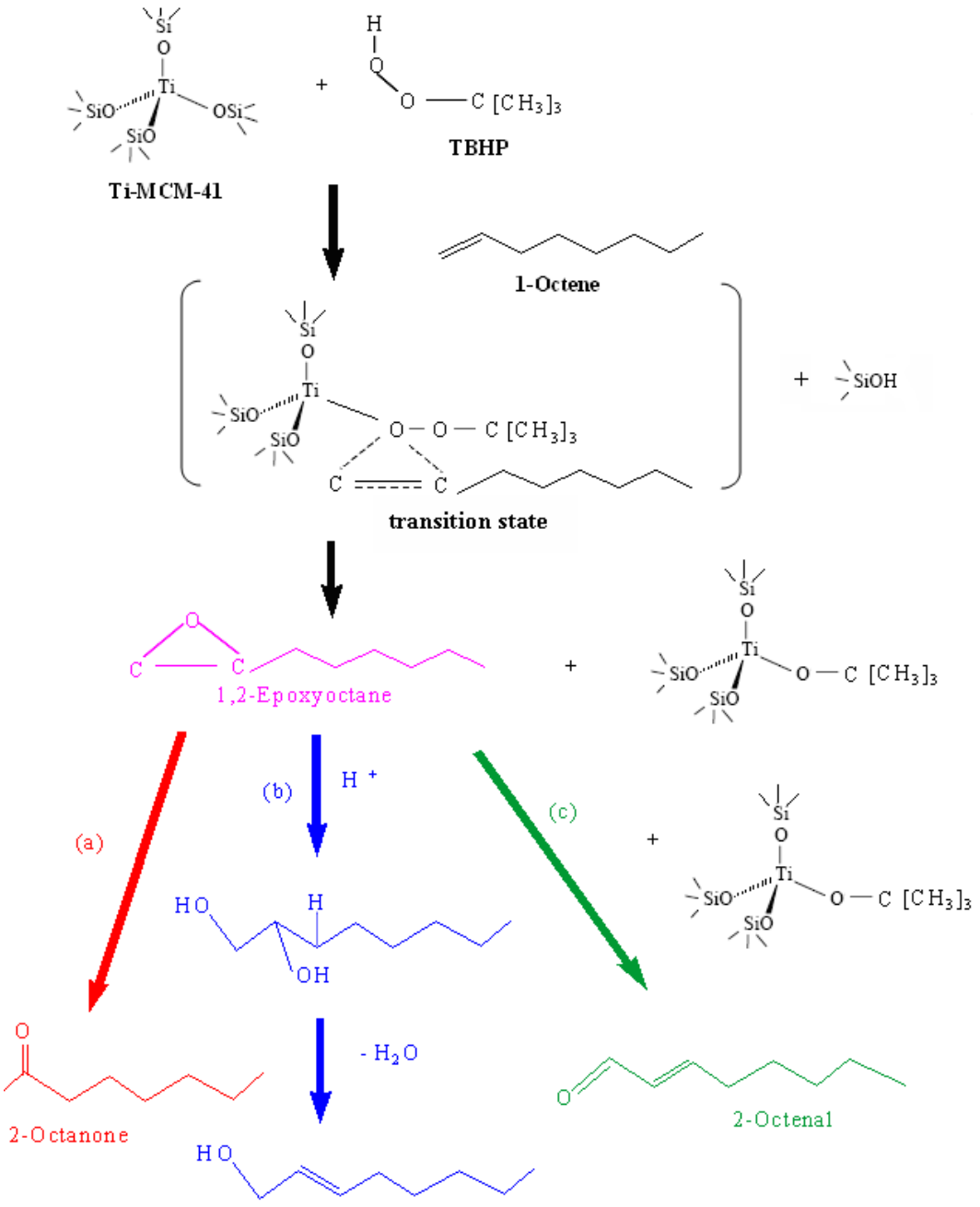

Figure 4.38: Possible mechanism of 1-octene epoxidation with *tert*-butyl hydroperoxide (TBHP) as oxidant by Ti-MCM-41. The desired product is 1,2-epoxyoctane, and the potential side products are 1,2-octanediol, 2-octene-1-ol and 2-octanone.

The desired product is 1,2-epoxyoctane generated by the heterolytic epoxidation of the 1-octene double bond. The acidic Ti-centers of Ti-MCM-41 lead to the formation of corresponding isomerized and hydrolyzed secondary products particularly 1,2-octanediol and 2-octanone. Although 2-octen-1-ol is theoretically predicted as one of the side products, 1-octen-3-ol is identified in the sample by GC-MS.

When using aqueous hydrogen peroxide as the oxidant in alkene epoxidations, two problems are encountered. Both these problems are related to the presence of water during the reaction. The first and most important problem consists of the irreversible hydrolysis of all the siloxy-titanium units in the active sites. This generally results in catalyst deactivation through leaching of catalytically inactive titanium derivatives.

The second problem is caused by the presence of water, which obstructs the active sites of the catalyst and thereby sterically prevents the alkene to react with this site. While the latter problem only gives rise to a decreased activity of the titanium catalyst, the former severely limits the applicability of the catalyst to processes involving rigorously dried media. Thus, it would be interesting to replace the processes based on peracids by a more desirable catalytic one.

The choice of oxidant in this reaction studies are based on the fact that *tert*-butyl hydroperoxide (TBHP) contains much lesser amount of water (~ 8%) compared to

hydrogen peroxide (~ 70%). In this case, no solvent is needed to perform the epoxidation, with corresponding savings in reactor volume and separation costs. Under such reactions conditions, Ti-MCM-41 is a highly effective catalyst with high conversions and selectivities to the epoxide and TBHP for sample 66Ti-MCM-41 (X= 57.3 % and S= 95.2 % respectively).

Conversely, the hydrophilic nature of titanium-on-silica prohibits the use of hydrogen peroxide as oxidant. Presence of water inhibits catalytic activity of Ti-MCM-41. Water competes with TBHP for active sites resulting in a decrease of epoxidation activity though the epoxide selectivity remains high.

The Ti-OOH species formed by the interaction between framework Ti atom and TBHP molecule, is able to form a stable five membered cyclic structure with a donor hydroxyl moiety coordinated on titanium (species I) as shown in Figure 4.39. The enhanced acid strength may be generated in charge-separated species (species II) due to greater hydrogen bonding. The acid centers (species I and II) are able to catalyze the epoxide ring opening.

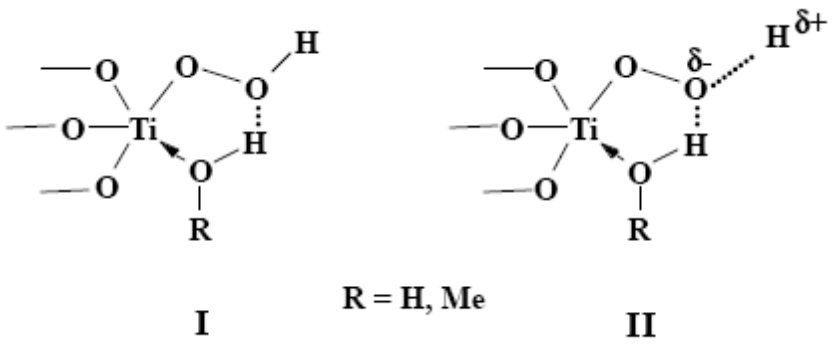

Figure 4.39: Different cyclic Ti-species active for epoxidation reactions.

In this study, a series of mesoporous titanosilicate Ti-MCM-41 molecular sieves with various Si/Ti ratios have been hydrothermally synthesized at $100^{O}C$ for 48 hours, using surfactant like hexadecyl-trimethylammonium bromide as template and tetramethylammonium hydroxide as mineralizer. These materials were characterized with powder X-ray diffraction (XRD), framework FTIR, diffuse reflectance Uv-visible spectroscopy, nitrogen sorption measurements, differential thermal analysis (DTA), and scanning electron microscopy (SEM).

The catalytic activities of Ti-MCM-41 are tested in the epoxidation of 1-octene, as a model compound and methyl oleate using *tert*-butyl hydroperoxide (TBHP) in a batch reactor. Epoxide (1,2-epoxyoctane) is produced by the process and consecutive formation of glycol (1,2-octanediol) as by-product is observed through rearrangement of alkene. Ketone (2-octanone) produced via the epoxide ring opening reaction is also observed as second by-product but in a lower concentration than the glycol. These types of reactions are responsible for the decrease in selectivity to the desired epoxide [147].

In order to make sure that the reaction temperature is constant at $60^{O}C$, the condenser is filled with ethylene glycol or any alcohol – base solution. Another crucial factor to ensure that the results from gas chromatography are acceptable, it is very important to check the area % of DTBP (contain in TBHP). It has to be constant because DTBP does not involve in any reaction. It should also exhibit sharp peak.

Apart from that, it is also important to take note on total area counts for gas chromatography injection, the volume injected is 0.5µl, so the total area counts are very good within 400 000 – 500 000 counts but 300 000 – 600 000 counts are also acceptable.

The evolution of reaction was monitored by means of gas chromatography. Conversion of TBHP and selectivity of TBHP and epoxide were calculated as follows:

$$\%\,\text{Conversion (t)} = \frac{C_{TBHP}(0) - C_{TBHP}(t)}{C_{TBHP}(0)}.100$$

$$\%\,\text{Selectivity}_{TBHP}(t) = \frac{C_{epox}(t)}{C_{TBHP}(0) - C_{TBHP}(t)}.100$$

$$\%\,\text{Selectivity}_{epox}(t) = \frac{C_{epox}(t)}{\sum_{1}^{p} C_i(t)}.100$$

Each parameter has been calculated at different reaction times (**t**). Variable **C** represents the molar concentration of the component **i** at this time and **P** is the number of oxidation products obtained in the reaction (epoxide, ketone, alcohol and diol).

(a) Effect of Si/Ti Ratio

Figure 4.40 and Figure 4.41 below depicts the influence of the Si/Ti ratio in Ti-MCM-41 on epoxidation of 1-octene.

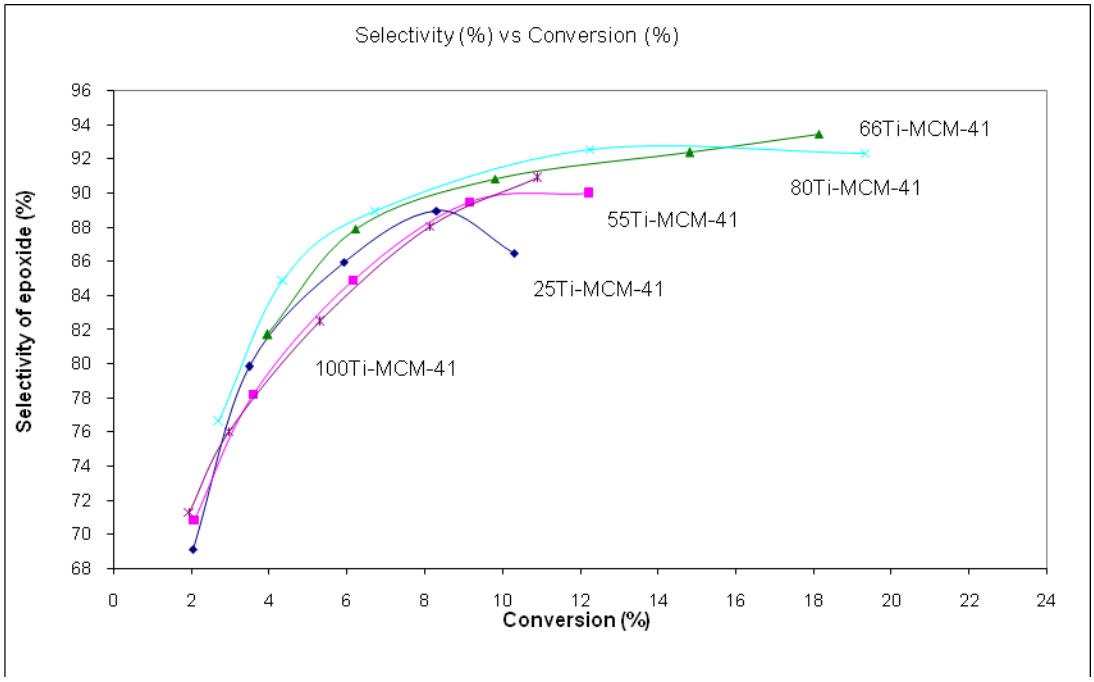

Figure 4.40: Catalytic performance of Ti-MCM-41 samples in the epoxidation reaction of 1-octene with TBHP at 60 ^{o}C with different Ti wt. % loadings.

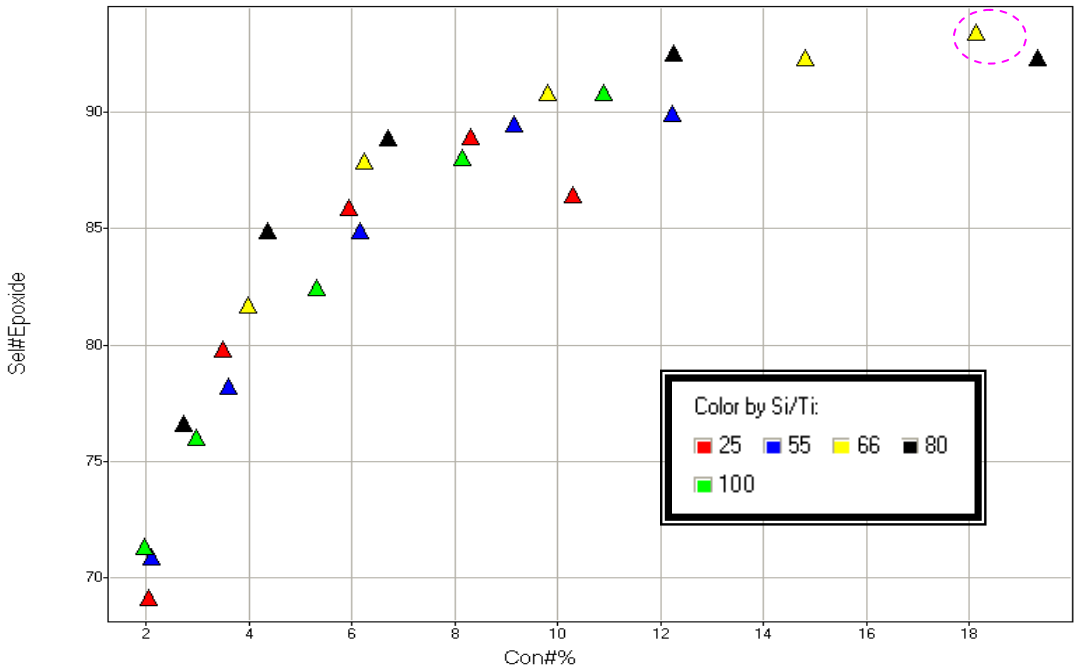

Figure 4.41: Selectivity to epoxide against 1-octene conversion at 60°C and a 1-octene: TBHP molar ratio of 4:1 on Ti-MCM-41.

In Figure above, the catalytic results for the series of Ti-MCM-41 samples are summarized. The most important finding is that the intrinsic catalytic activity (expressed as maximum conversion of 1-octene at the reported reaction conditions) does increase with titanium content. At the low conversion end, the most active catalyst is the one having titanium content of 1.68 wt. % that is 66Ti-MCM-41 sample followed by 1.24 wt. % (80Ti-MCM-41). However, this Ti-MCM-41 catalyst deactivates much more rapidly than the others, thereby yielding a lower total conversion when the reaction time increases. The data suggest that the overall conversion passes through a maximum near to 2 wt. % Ti content of the Ti-MCM-41 materials.

The selectivities to epoxide at different levels of conversion are given in Figure 4.40 and Figure 4.41. It is found that the selectivity to epoxide decreases as the conversion increases due to the production of glycols formed by the epoxide opening reaction. The formation of the undesired glycols is more important on the 2.85 wt. % sample (25Ti-MCM-41) at a high level of conversion, than on samples containing less than 2 wt. % titanium (66Ti-MCM-41 and 80Ti-MCM-41).

However, after 5 hours of reaction, the conversion for both catalysts is very similar. This indicates that, after prolonged reaction time, poisoning of the centres by the adsorption of glycols is stopping the reaction, a conclusion that is supported by the lower selectivity towards epoxides of sample 25Ti-MCM-41 and 100Ti-MCM-41 compared to the selectivity of 66Ti-MCM-41 and 80Ti-MCM-41. The lower selectivity maybe explained by the initially higher rate of conversion yielding correspondingly more glycols which are known to not only poison the active centres for epoxidation reactions, but also negatively affect their selectivity.

In the case of 66-TiMCM41 and 80-TiMCM41, it is clear that if taking into account the titanium loadings, one should expect similar intrinsic activity and selectivity for the epoxide in both samples, as it is observed experimentally. It is observed that the selectivity of 1,2-epoxyoctane for both samples are amongst the highest in comparison the rest titanium loadings.

From the results, the most active catalyst, 66Ti-MCM-41 (1-octene : TBHP = 4, 1.68 wt % Ti, 60^{o}C), followed by 80Ti-MCM41 (1-octene : TBHP = 4, 1.24 wt % Ti, 60^{o}C), a maximum epoxide yield of 20 %-30 % was reached. The results clearly show that the epoxide selectivity exhibited by five ratios decreases in the order: 66Ti-MCM41 > 80Ti-MCM41 > 25Ti-MCM41 > 55Ti-MCM41 > 100Ti-MCM41.

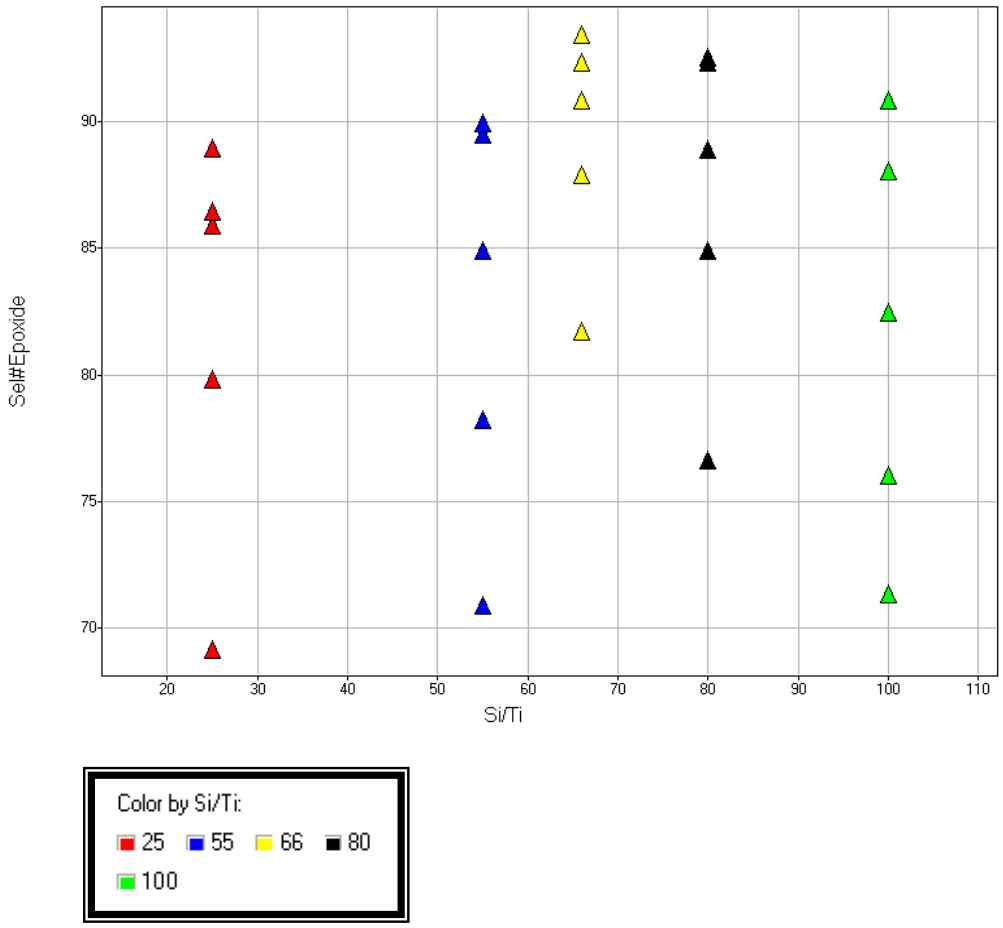

Figure 4.42: Effect of titanium contents towards selectivity to epoxide.

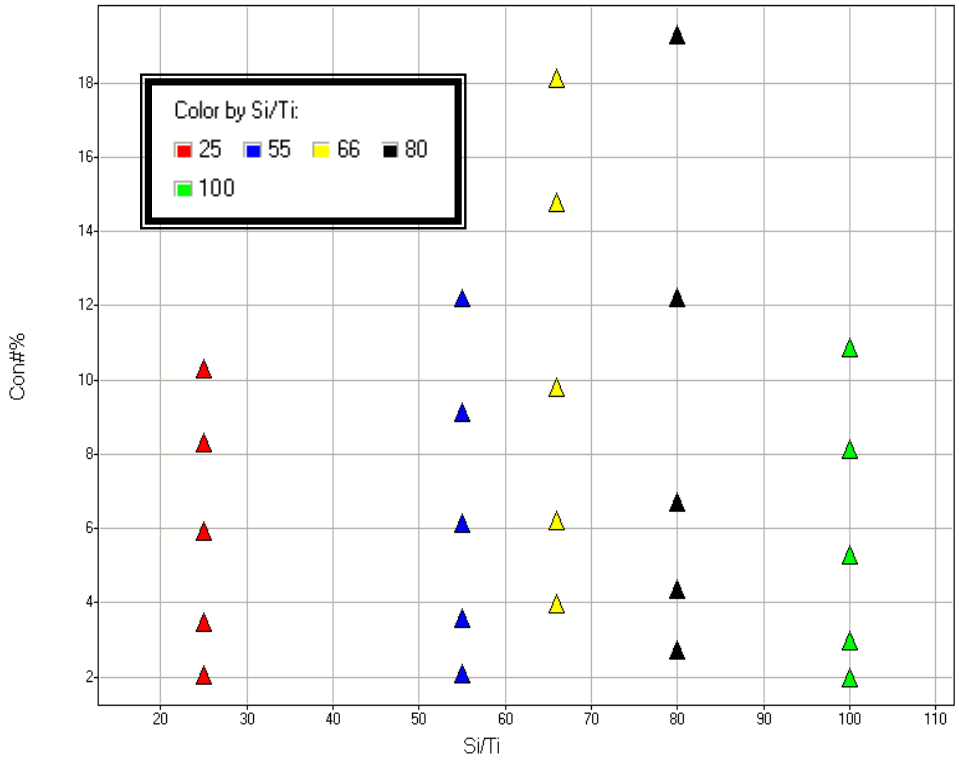

Figure 4.43: Effect of titanium contents towards conversion of 1-octene.

The selectivity of 1,2-epoxyoctane also increases with increase in catalyst concentration before reaching a limiting value of 90 ± 5 mol %. As expected, at low catalyst concentration, the concentration of Ti-superoxo complex is low and therefore, secondary reactions are facilitated. With the increase in the catalyst concentration, the concentration of Ti-superoxo complex also increases which facilitates the formation of desired epoxyoctane inside the mesoporous pore.

From the results, I can conclude that although conversion of 1-octene is rather low, it exhibits an increment with the increase of catalyst amount and time. From t = 0 to t = 7, conversion of 1-octene is increasing for all samples as shown in Figure 4.44.

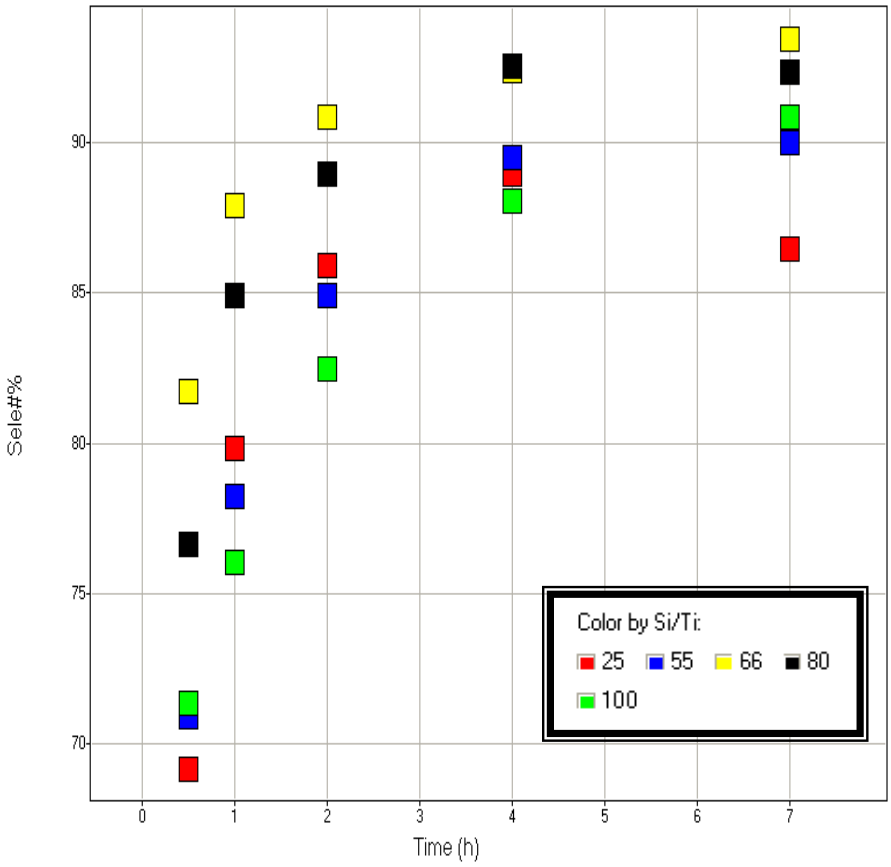

Figure 4.44: Effect of titanium contents towards selectivity to epoxide with time.

The same trend shows for selectivity of epoxides where the highest, 95% is obtained when higher amount of catalyst is being used. Figure 4.45 shows the rate of formation of 1,2-epoxyoctane over various Ti-MCM-41 samples. All reactions are carried out at 60 ^{o}C.

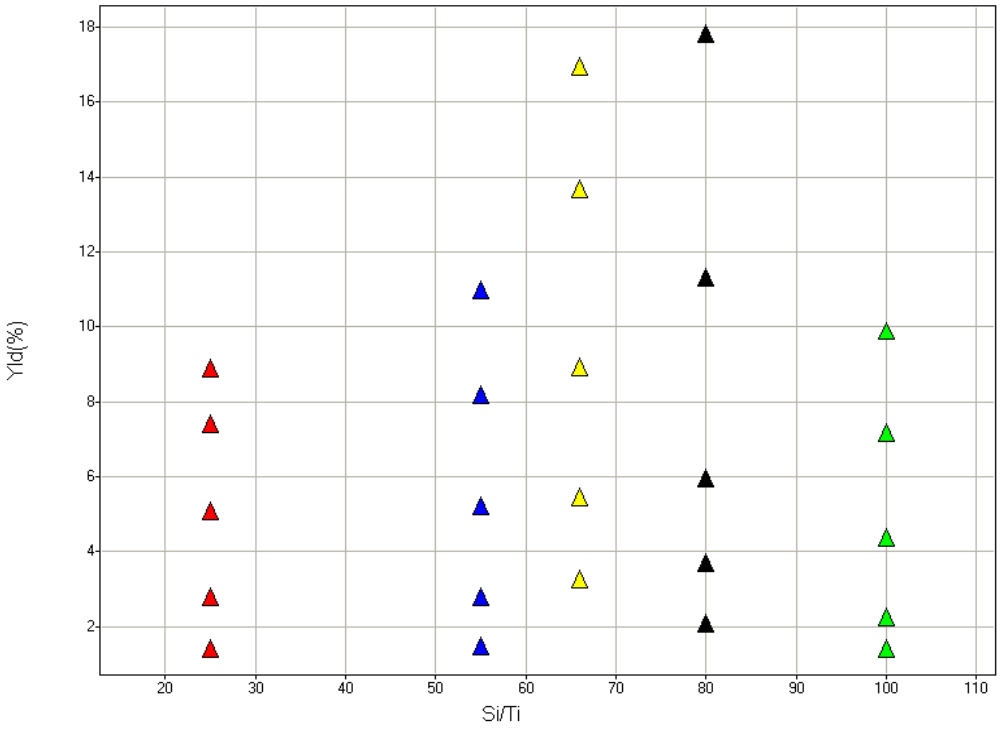

Figure 4.45: Effect of titanium content on 1,2-epoxyoctane yield.

As for the yield as shown in Figure 4.45, only maximum 18 % of epoxyoctane from sample 80Ti-MCM-41 is produced due to low conversion of 1-octene. It can be seen that sample with low titanium loading, 100-TiMCM41 does not shows any significant changes to the rate of reactions towards the formation of 1,2-epoxyoctane. However, remarkably higher activities are shown by samples at higher titanium loading, 66-TiMCM41 and 80-TiMCM41. In addition, 1,2-octanediol and 2-octanone are observed as by-products thus lowered the selectivity towards 1,2-epoxyoctane.

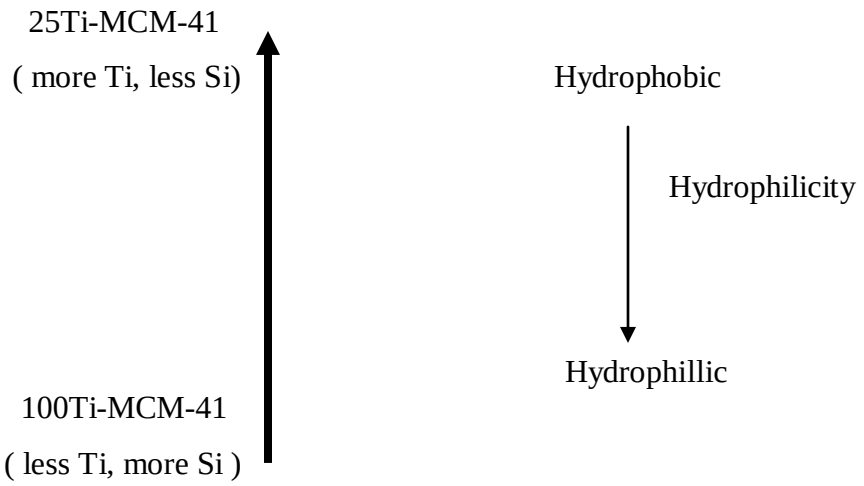

Figure 4.46: Influence of varying amount of titanium.

High concentration of silanol groups located at the external surface of the pores of Ti-MCM-41 as in sample 100Ti-MCM-41 gives a relatively hydrophilic character, hence lower the catalytic activity and turnover. On the other hand, at high titanium content (25Ti-MCM-41), although the hydrophobicity is improved, catalyst deactivation will occur due to high side compounds. Titanium sites in MCM-41 catalysts are buried on the silica walls, being non-accessible to the reactants, thus lower the catalytic activity and turnover. In other word, we cannot reject the possibility that in Ti-MCM-samples, some of this Ti is located in the "shielded" core of the wall and remains inaccessible from the channels. The best is to use catalysts with average amount of titanium (66Ti-MCM-41 with 1.68 % Ti or 80Ti-MCM-41 with 1.24 % Ti). This has been supported by the following data shown in Table 4.6.

Table 4.6: Varying Si/Ti ratio for the epoxidation of 1-octene using Ti-MCM-41 as catalyst and TBHP as oxidants.

Sample	C8 conversion (%)	Epoxide selectivity (%)	TBHP selectivity (%)
25Ti-MCM-41	10.3	86.5	28.5
55Ti-MCM-41	12.2	90.0	34.2
66Ti-MCM-41	18.1	93.5	41.4
80Ti-MCM-41	19.3	92.4	38.0
100Ti-MCM-41	10.9	90.9	27.5

In the case of 66-TiMCM41 and 80-TiMCM41, it is clear that if one takes into account the titanium loadings, one should expect similar intrinsic activity and selectivity towards epoxide in both cases, as it is observed experimentally. It is observed that the selectivity of 1,2-epoxyoctane for both samples are amongst the highest in comparison the rest titanium loadings.

80-TiMCM41, which contains 1.24 wt% titanium, exhibits the highest 1-octene and methyl oleate conversion in all five samples. The activities of 25Ti-MCM-41 and 100Ti-MCM-41 were similar. The activity of Ti-MCM-41 per unit weight of catalyst increases with titanium contents, meaning to say that high Ti content renders the catalysts more active, however does not present a linear relationship.

High concentration of silanol groups located at the external surface of the pores of Ti-MCM-41 as in sample 100T-iMCM41 gives a relatively hydrophilic character; hence lower the catalytic activity and turnover. On the other hand, at high Ti content (25Ti-MCM41), although the hydrophobicity is improved, catalyst deactivation will occur due to high side products.

Titanium sites in MCM-41 catalysts are buried on the silica walls, being non-accessible to the reactants, thus lower the catalytic activity and turnover. In other word, we cannot reject the possibility that in Ti-MCM-samples, some of this titanium is located in the "shielded" core of the wall and remains inaccessible from the channels.

For larger Ti contents, as in the order of Ti-MCM-41 sample, the turnover on the Ti-silica will be smaller, probably due to the formation of Ti-O-Ti bonds. The results given in Table 4.6 and Table 4.7 clearly show that the intrinsic activity (TON) is 80Ti-MCM-41 > 66Ti-MCM-41 > 55Ti-MCM-41 > 25Ti-MCM-41 > 100Ti-MCM-41.

It seems likely that the reaction using Si/Ti = 80 shown to be catalytically active towards epoxidation of 1-Octene in the viewpoint of silicon to titanium ratio used. On the basis of these results, 80Ti-MCM-41 and 66Ti-MCM-41 are applied for the optimization of 1-octene epoxidation reaction.

With these catalytic systems, hydrophobic/ hydrophilic properties of the surface are just as important as the number of active sites.

(b) Effect of Temperature

Reaction temperature plays an important role in the catalytic performance. Figure 4.47 depicts the effect of catalyst concentration on 1-octene epoxidation over Ti-MCM41. In the case of this system, the maximum conversión of 1-octene for reaction temperature 50 ˚C, 60 ˚C and 70 ˚C after 7 hours of reaction are 18.03%, 31.84% and 53.12% respectively.

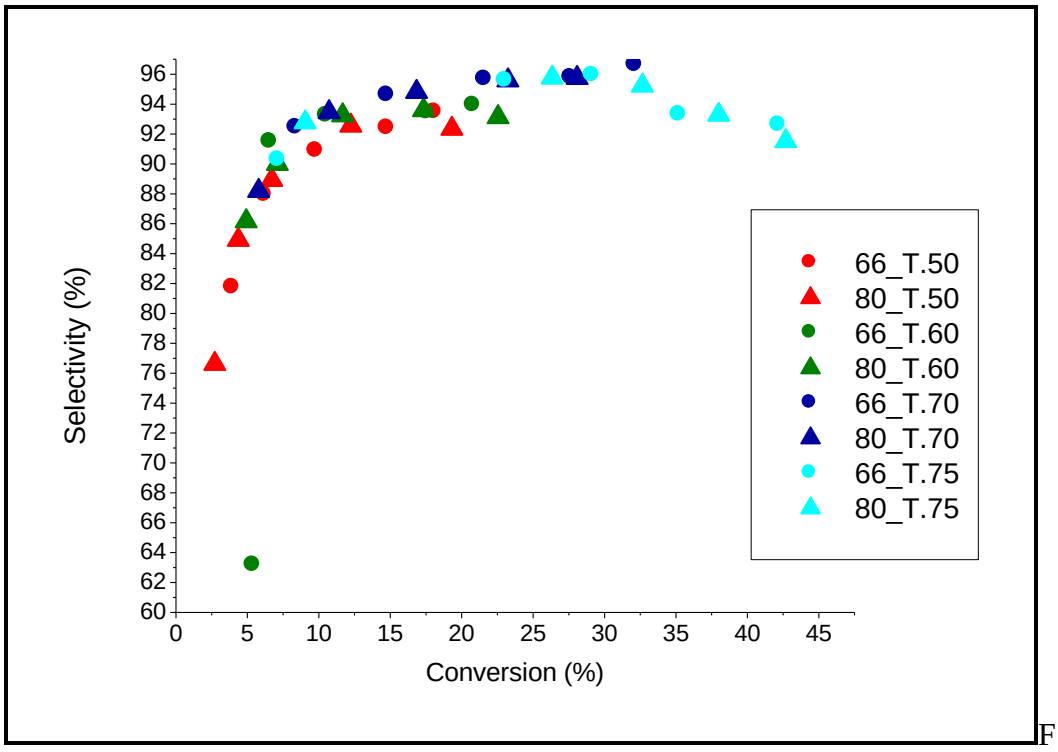

Figure 4.47: Effect of temperature on conversion and selectivity during the epoxidation of 1-octene with Ti-MCM-41 sample. C=C / TBHP = 4 : 1, catalyst = 0.5 g, wt. % of Ti = 1.68 % and 1.24 % , time = 7 hrs.

The highest conversion, 53.12% is obtained for reaction temperature 70 ˚C. Selectivity of epoxide is also the highest, 98.81% for reaction temperature 70 ˚C after an hour of reaction. At high temperature for example T=70 ˚C, the efficiency for the incorporation of titanium in the silicate matrix is higher compared to that at low temperature (T=50 ˚C) for a given Si/Ti mole ratio.

However, beyond a certain temperature (T=75 ˚C), depending upon the composition of the reactant mixture, the concentration of the anatase phase starts growing, thus lower the catalytic activity of the titanium sites. The selectivity is descending throughout the reaction; stating a decrease of 6.61% from 98.81% to 92.20%. Selectivity of epoxide are optimum for reaction temperature 60 ˚C, where the values lie within 97.91% to 98.48% from t = 0 till t = 7 hours.

From this experiment of determining optimum temperature of reaction, I can conclude that the best temperature is 60 ˚C. It is also observed that increase in the reaction time resulted in an increase in the 1-octene conversion initially before the reactant start to leveling off at 75 ˚C and above.

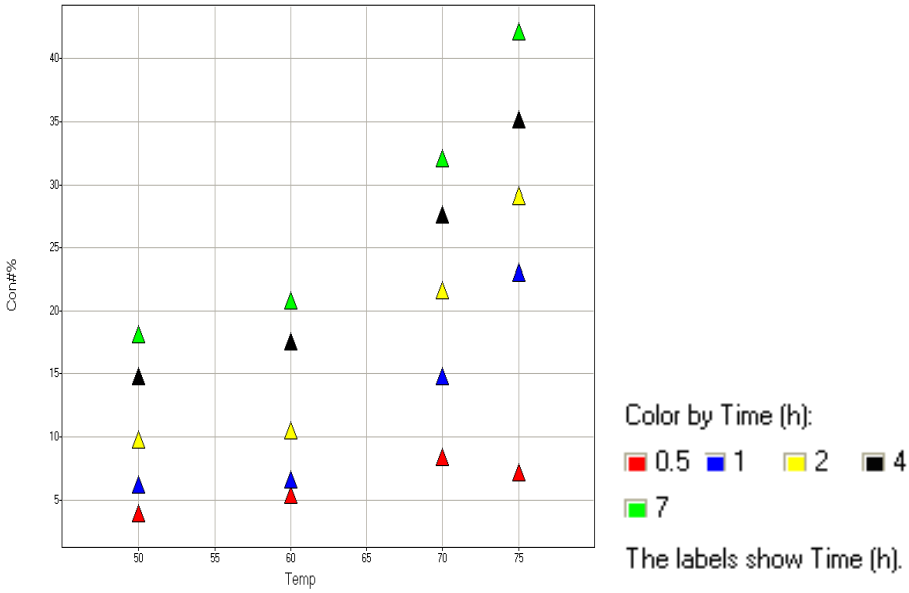

Figure 4.48: Effect of reaction temperature on the epoxidation of 1-octene. Reaction conditions: Catalyst 66Ti-MCM-41 (1.68 wt% of Ti with respect to 1-octene); C=C / TBHP = 4 : 1; reaction time = 7 hrs.

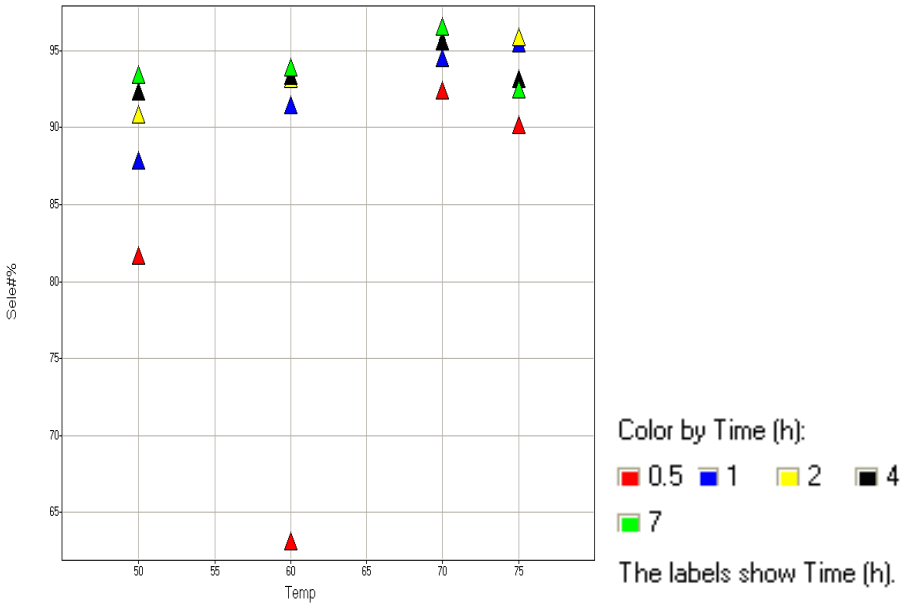

Figure 4.49: Effect of reaction temperature on the selectivity towards epoxide. Reaction conditions: Catalyst 66Ti-MCM-41 (1.68 wt% of Ti with respect to 1-octene); C=C / TBHP = 4 : 1; reaction time = 7 hrs.

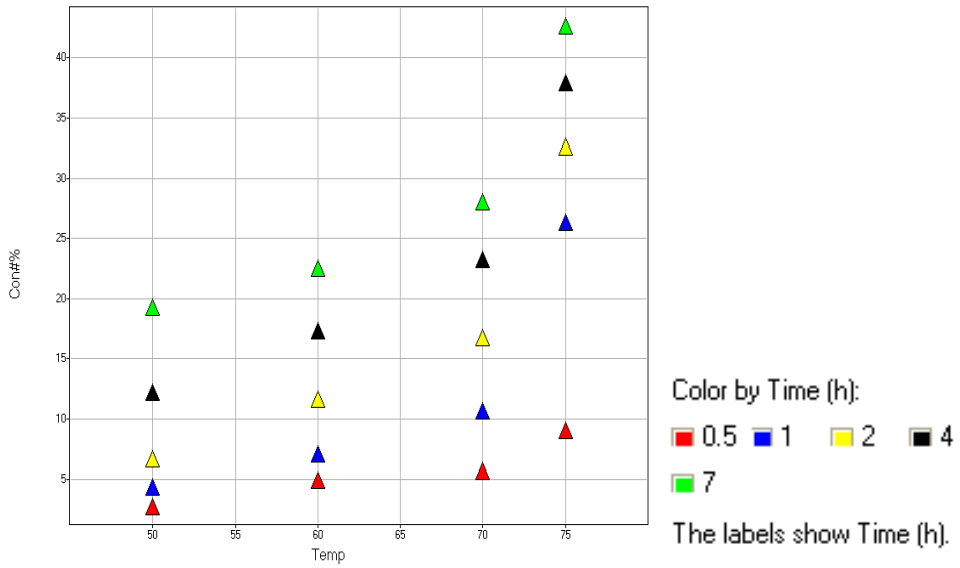

Figure 4.50: Effect of reaction temperature on the epoxidation of 1-octene. Reaction conditions: Catalyst 80Ti-MCM-41 (1.24 wt% of Ti with respect to 1-octene); C=C / TBHP = 4 : 1; reaction time = 7 hrs.

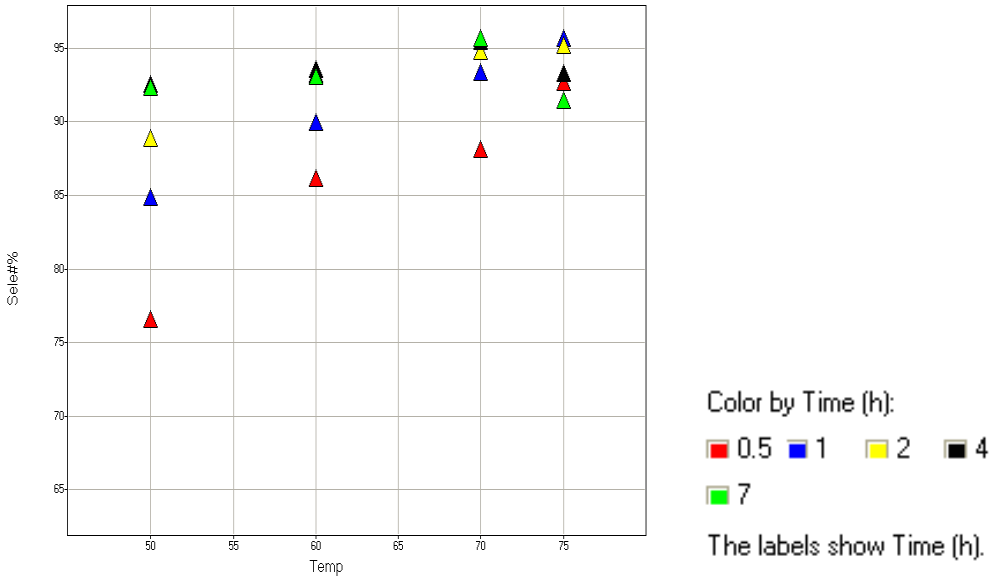

Figure 4.51: Effect of reaction temperature on the selectivity towards epoxide. Reaction conditions: Catalyst 80Ti-MCM-41 (1.24 wt% of Ti with respect to 1-octene); C=C / TBHP = 4 : 1; reaction time = 7 hrs.

It was observed that upon increasing the temperature, the reaction rate was slightly accelerated as shown in Figure 4.48 to Figure 4.51. However, the selectivity to epoxide decreased. Increasing temperature from 50 ^{o}C to 75 ^{o}C produces a drop in selectivity of 10% while the conversion increases from 10% to 90%. The lower selectivity to epoxidized products is attributed to the acid-catalyzed oxirane ring opening at higher temperature, hence favoured to the formation of glycol and ketone as by-products. It is clear that the temperature plays a crucial role on the by-products formation rate.

Making a compromise between conversion and selectivity, results in the selection of 60 ^{o}C as the optimal temperature for epoxidation of 1-octene while for methyl oleate, 70 ^{o}C is the optimal temperature to carry out reactions comparing the different Ti-MCM-41 catalysts.

This also implies that the reaction temperature should be kept below 70 ^{o}C to hinder diol and ketone formation as by-products; since they will result in a decrease to epoxide selectivity and yield as a consequence of alkene rearrangement and epoxide ring opening reaction.

(c) Effect of Molar Ratio (C=C / TBHP)

The effect of 1-octene / TBHP mole ratio on 1-octene conversion and the product selectivity over Ti-MCM-41 is shown in Figure 4.52. 1-octene conversion increases with the increase in 1-octene / TBHP mole ratio mainly due to reaction being pushed towards the right, which is towards the formation of 1,2-epoxyoctane. However, the selectivity of 1,2-epoxyocatane increases very slowly over the range.

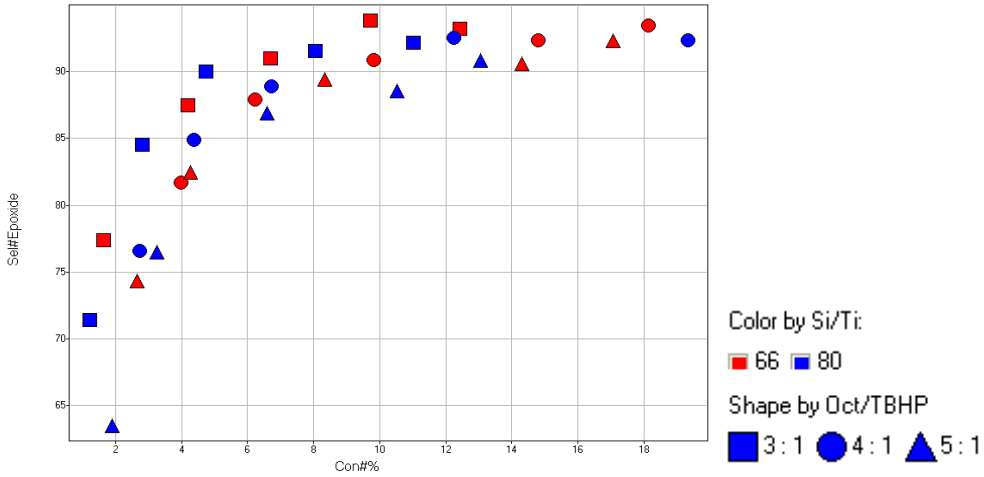

Figure 4.52: Effect of 1-octene to TBHP molar ratios on the epoxidation of 1-octene. Reaction conditions: Temperature = 60 ˚C; wt. % of Ti = 1.68 % and 1.24 %, time = 7 hrs.

Catalytic epoxidation with 80-TiMCM41 of 1-octene was optimized to 62% yield of epoxide obtained in 1.5 h (C=C / TBHP = 4 : 1, 1.24 wt % Ti, 60 ˚C) resulting in a TOF value (turnover frequency) of 20 mol.(mol Ti)$^{-1}$.h^{-1}. TOF is an indicator

that measures the reaction rate per active sites per time or the production capacity of a given apparatus. From Figure 4.52, the best alkene to oxidant ratio is 4:1.

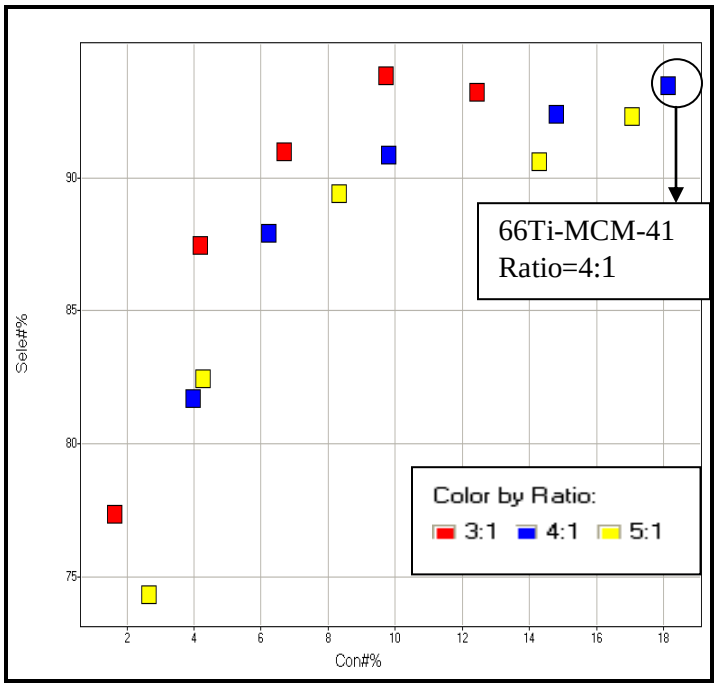

Figure 4.53: Selectivity to epoxide vs 1-octene conversion at 60 ˚C for different 1-C_8H_{16}: TBHP molar ratio of 3:1, 4:1& 5:1 on 66Ti-MCM-41.

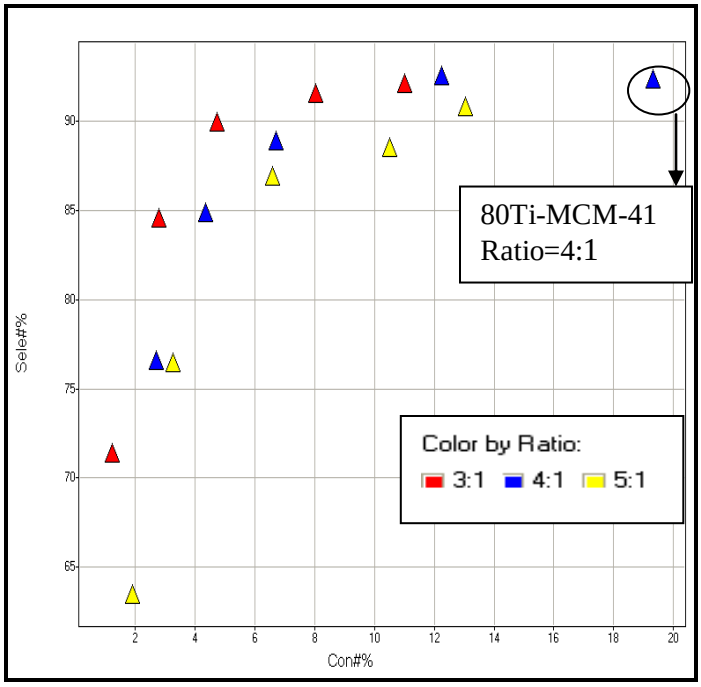

Figure 4.54: Selectivity to epoxide vs 1-octene conversion at 60 ˚C for different 1-C_8H_{16}: TBHP molar ratio of 3:1, 4:1& 5:1 on 80Ti-MCM-41.

It has been observed that the epoxide selectivity is dramatically improved by increasing the molar ratio of 1-octene to TBHP in the feed, because less water is introduced into the reaction system via TBHP. In general, the model catalysts shows good selectivity to 1,2-epoxyoctane based on the TBHP consumed. In other word, epoxide yields are based on the amount of peroxide used.

4.1.3 Process Optimization for Reaction with methyl oleate

After the characterization of Ti-MCM-41 catalysts, the activity of these materials on the epoxidation of methyl oleate and its correlation with all the previous analysis will be discussed here. The main objective of this section is to find out the optimal reaction conditions for epoxidation of methyl oleate that maximize both selectivity and yield of the product, *i.e.* epoxy methyl oleate [methyl-(9,10)-epoxyoctadecanoate].

Optimal reaction conditions mean temperature close to room temperature, atmospheric pressure, avoidance of solvents or use of "green" solvents if a solvent is required, use of stable and relatively cheap heterogeneous catalyst (Ti-MCM-41) and low reaction times to obtain high yields. These reaction conditions are necessary to undertake the epoxide production in bench and pilot plant to produce them in larger amounts.

Figure 4.55 below shows a proposed mechanism for epoxidation of methyl oleate towards epoxide.

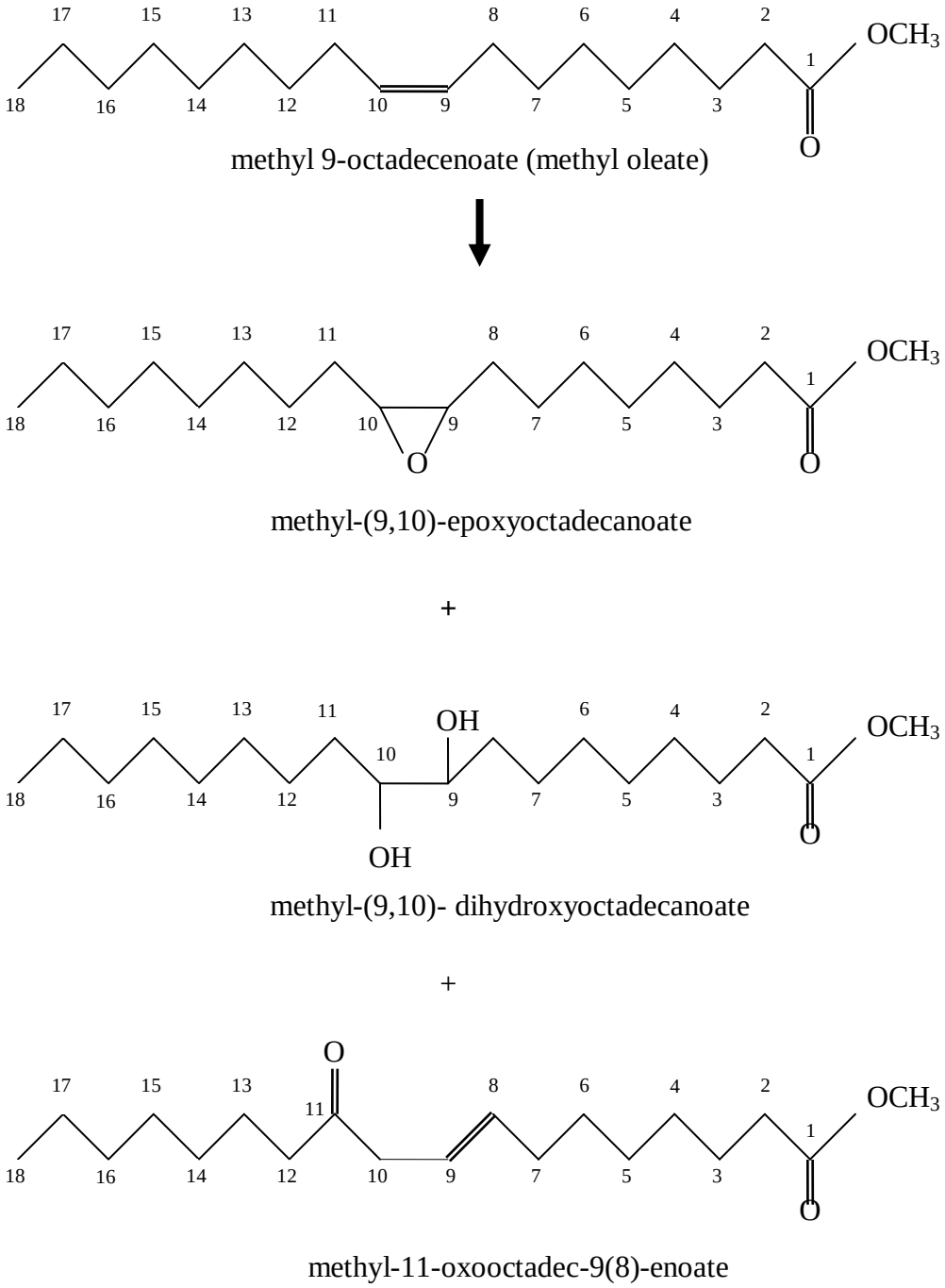

Figure 4.55: Proposed reaction scheme of epoxidation of methyl oleate to epoxide. Reaction condition: C=C / TBHP = 4 : 1, catalyst = 0.5 g, wt. % of Ti = 1.68 %, time = 7 hrs.

Table 4.7: Varying Si/Ti ratio for the epoxidation of methyl oleate using Ti-MCM-41 as catalyst and TBHP as oxidants. Conditions: TBHP/oleate = 1:1 mol/mol, temp. = 70 °C.

Sample	% of Ti	C18 conversion (%)	Epoxide selectivity (%)	TBHP selectivity (%)
25Ti-MCM-41	2.85	41.5	90.4	91.2
55Ti-MCM-41	2.29	43.6	91.7	92.5
66Ti-MCM-41	1.68	57.3	95.2	96.1
80Ti-MCM-41	1.24	48.5	93.3	93.8
100Ti-MCM-41	1.13	33.4	88.6	90.7

The different activities observed showed to be a function of the level of Ti dispersion (molecular) and textural properties of the supports such as the external surface area. 100Ti-MCM-41 is the least active catalyst due to its lowest Ti loading and most probably less dispersion of Ti than in all the other catalysts because. The absorption band in the UV spectra shows 100Ti-MCM-41 is the most shifted.

Based on data above, the superior activity of 66Ti-MCM-41 and 80Ti-MCM-41 are due to higher Ti loading and comparable surface are that is 905.03 m^2/g and 997.26 m^2/g respectively.

One parameter that is of extreme importance for the industrial application of epoxidation technologies is the efficiency in the hydroperoxide consumption, which has to be maximized. Table 4.7 shows the TBHP selectivities for the experiments. Clearly, all the experiments run with a very high efficiency in the use of the hydroperoxide. This high THBP selectivity results from the relatively fast diffusion of the olefin to the Ti-TBHP peroxo complex (see Figure 4.39) where it takes the oxygen before it is released as gas (peroxide decomposition).

In summary, these results suggest that for the epoxidation of oleic acid methyl ester with TBHP catalyzed by Ti-MCM-41, the two more important catalyst properties are Ti dispersion and external surface area, both must be high. After the important conclusion drawn from the epoxidation reactions with Ti-MCM-41 regarding the outstanding role of the external surface area, it was straight forward to reach the idea that a simple amorphous Ti-loaded silica could also do the job, provided the Ti is properly dispersed.

4.2 Process Based on Utilizing Silylated Ti-MCM-41

Catalytic activities for epoxidation of 1-octene and methyl oleate using *tert*-butyl hydroperoxide as oxidant as well as the selectivity to the desired epoxide strongly depend on the hydrophobic properties and on the number of free silanol groups of Ti-MCM-41 catalysts.

Ti-MCM-41 bears a serious shortcoming because of its hydrophilic surface character. The hydrophilic character induces side reactions of epoxidation and thus considerably decreases the efficiency of the catalyst in these catalytic reactions. H_2O when present will compete with the reactant which also has to be adsorbed on the Ti atom in the transition state. In other words, in terms of adsorption properties, the most hydrophobic catalysts exhibit highest catalytic activity.

In this case, a large number of silanol groups in Ti-MCM-41 have to be reduced by reaction with organosilanes [148-149] or by introducing organosilanes directly to the synthesis gel of mesoporous materials [150-152] and this modification is reflected in the final properties of the catalyst [153]. The alteration of these materials with the incorporation of different organosilane groups allows modifying the hydrofilic/hydrofobic properties of the surface, that it is a key parameter for obtaining a successful catalyst.

In this manner, it has recently been shown that this silylation technique for the modification of mesoporous molecular could overcome such drawback [107]. For this study, hexamethyldisilazane (HMDS) is used to modify the number or the nature of the organosilane groups bounded onto the walls of Ti-MCM-41 catalysts.

Figure 4.56 shows the replacement of Si-OH groups by hydrolytically stable Si-CH_3 ($SiMe_3$) groups which inhibits the adsorption of water and, therefore, increases hydrophobicity of catalyst, which will not be affected by moisture. The incorporation of organic groups with alkylsilanes over these materials is due to the high density of silanol groups on their surface, which act as anchorage for the silane groups as shown in Figure 4.56 below.

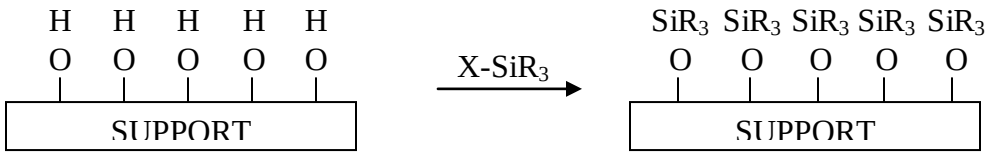

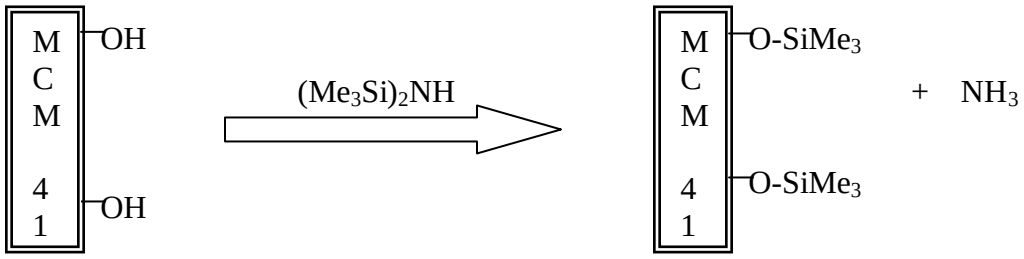

Figure 4.56: Proposed surface reaction to enhance hydrophobicity of MCM-41 by silylation of the surface silanols (Si-OH).

The internal silanols present in this mesoporous structure give rise to the hydrophilic nature, thus retarding a liquid phase reaction in the presence of water (being adsorbed more selectively on the catalyst surface rather than the organic reactant) as a diluent or as a product of consumption of TBHP.

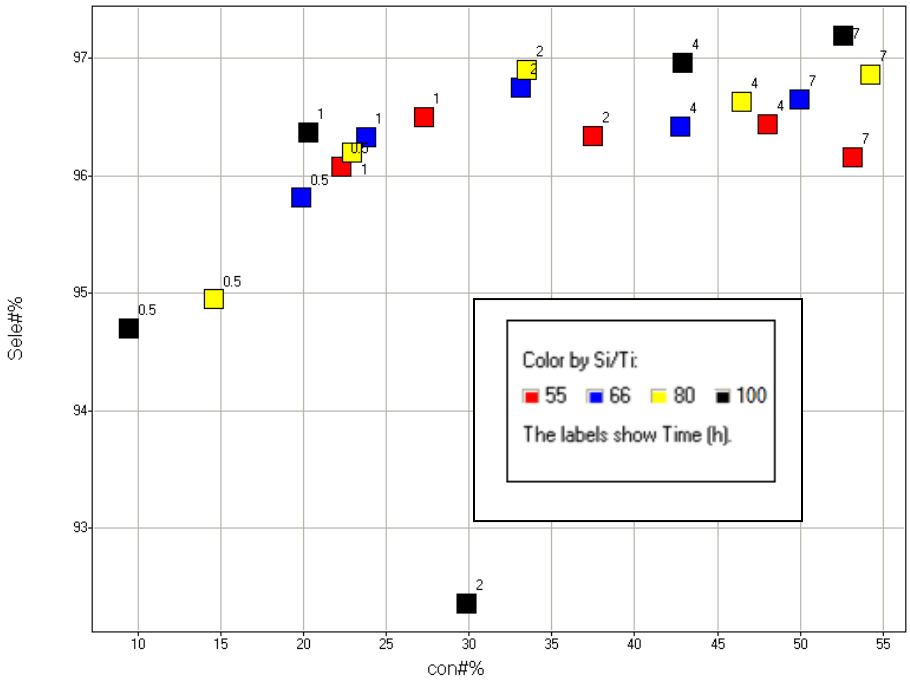

Figure 4.57: Catalytic Performance of various silylated Ti-MCM-41 towards epoxidation of methyl oleate at T=60 ^{o}C.

Under the experimental conditions employed in this work and on this bulky methyl oleate compound, Ti-MCM-41 catalyst displayed a high catalytic activity. In all cases, the methyl oleate conversion is above 50% after 7 hours of reaction with 80Ti-MCM-41 has the highest oleate conversion that is 54.9 %.

Good selectivities to epoxides were achieved. All samples show a selectivity of > 96% towards epoxide formation. Since the catalytic performance of Ti-MCM-41 not only were constant during the three repeated 7 hour-cycles, but rather improved, it is possible to conclude that this material is reasonably stable and reusable for this sort of reactions.

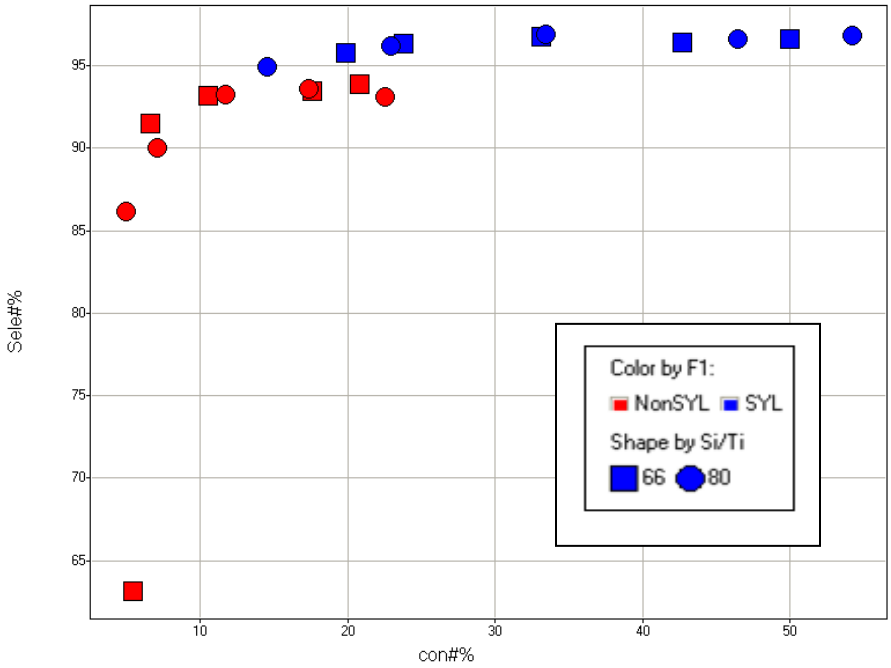

Figure 4.58: Selectivity to epoxide vs methyl oleate conversion using silyated and non-silyated 66Ti-MCM-41 and 80Ti-MCM-41.

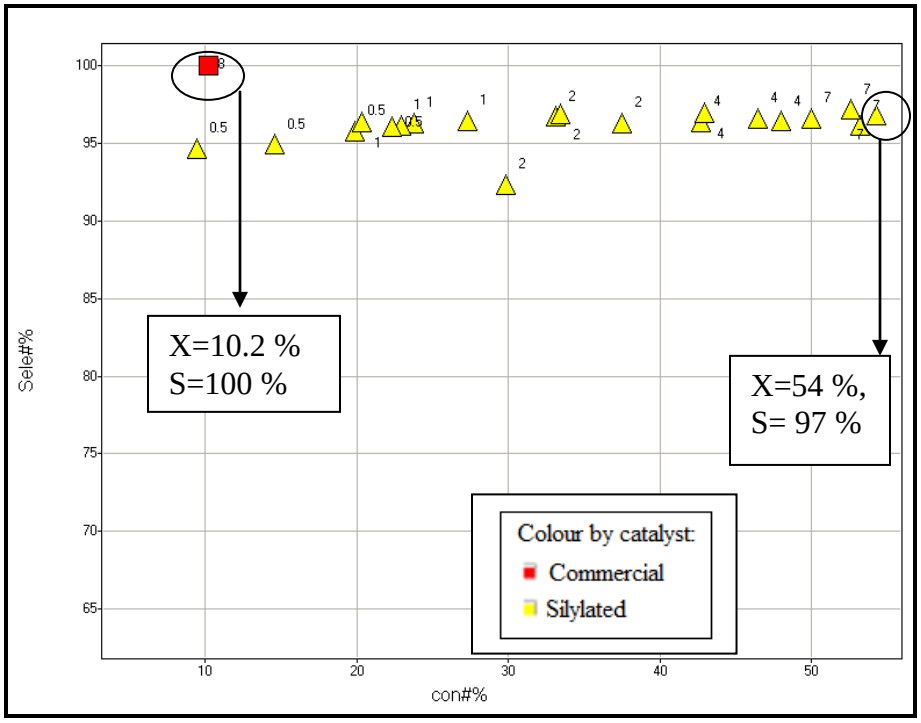

Figure 4.59: Commercial catalyst vs 80-Ti-MCM-41 silylated catalyst at T=60^{o}C. X is methyl oleate conversion; S is epoxide selectivity.

When comparing silylated and non-silylated samples as shown in Figure 4.61 and Figure 4.62, it's found that silylated samples exhibit higher catalyst activity, and the conversion and TON increased three times as compared to non-silylated samples. Silylation increases greatly the hydrophobicity of Ti-MCM-41 catalysts and therefore, water concentration on the surface is reduced, and the subsequent glycol formation is nearly avoided.

Formation of glycols poisons the catalytically active Ti sites of the mesoporous structure. Silylation also decreases the number of silanol groups (and very probable Ti-OH groups). These groups posses a weak acid character, but strong enough to catalyze the undesired reaction of oxirane ring opening.

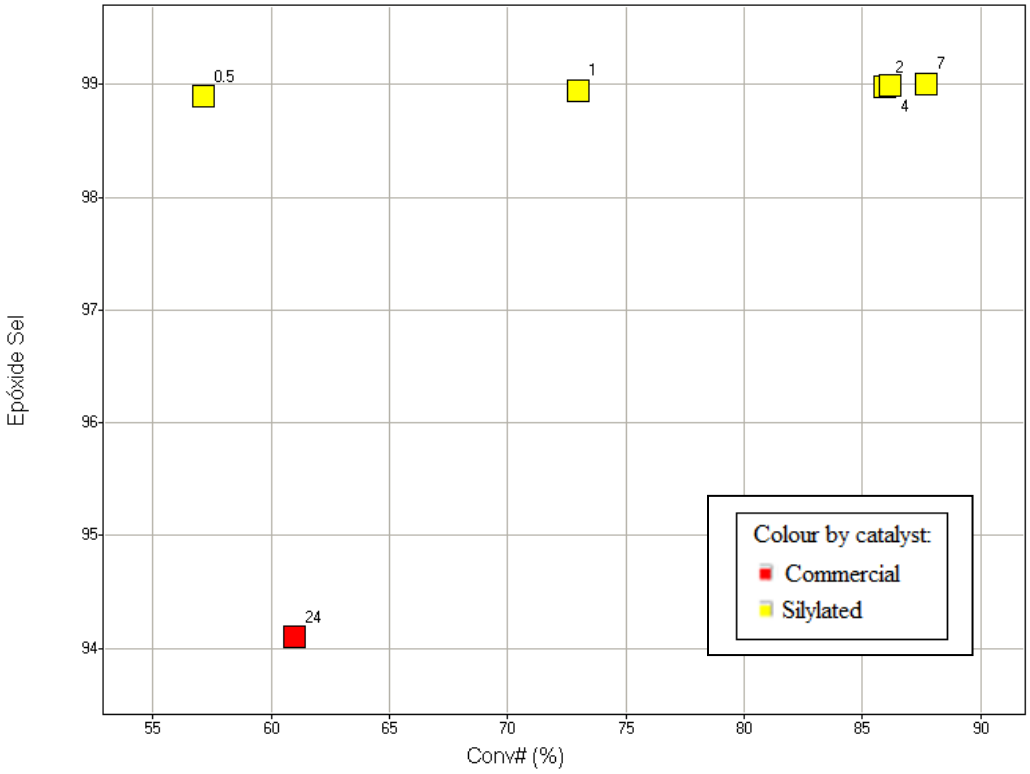

Figure 4.60: Commercial catalyst vs 80-Ti-MCM-41 silylated catalyst at T=70^{o}C.

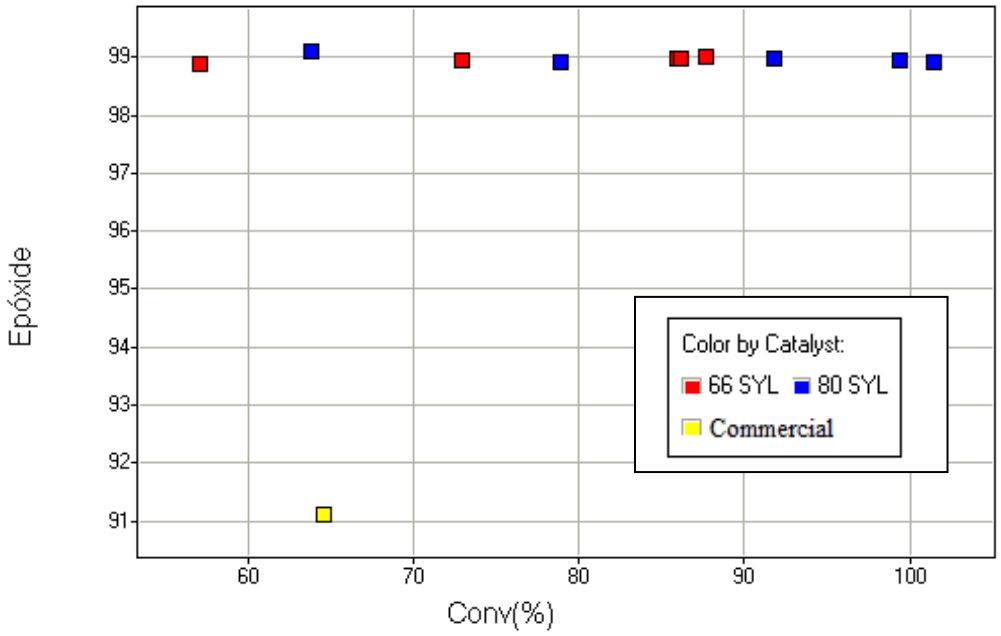

Figure 4.61: Commercial catalyst vs 66Ti-MCM-41 and 80-Ti-MCM-41 silylated catalyst at T=70^{o}C towards epoxidation of methyl oleate.

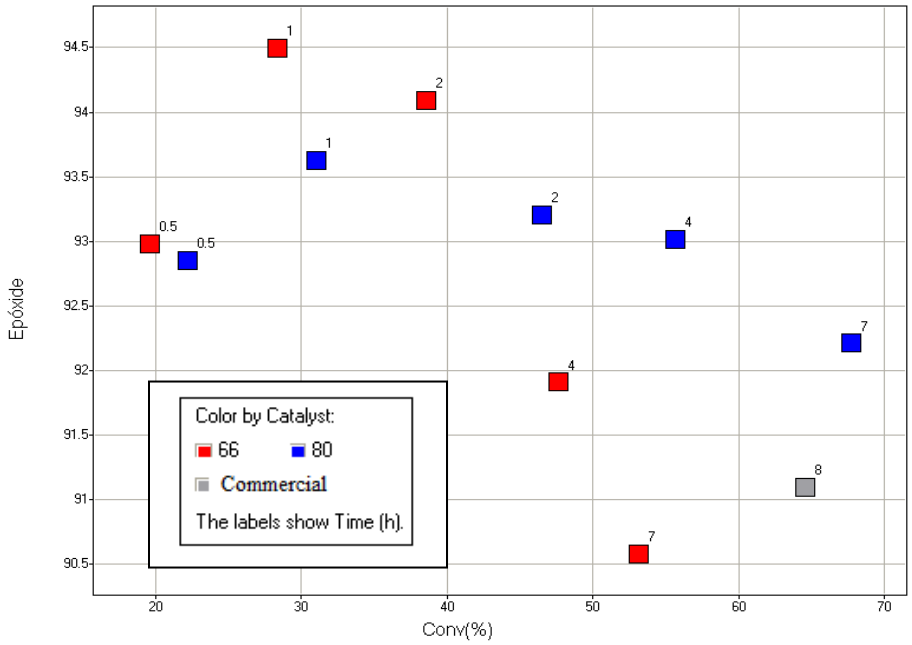

Figure 4.62: Commercial catalyst vs 66Ti-MCM-41 and 80-Ti-MCM-41 non-silylated catalyst at T=70^{o}C towards epoxidation of methyl oleate.

In conclusion, trimethylsilylation of Ti-MCM-41 resulted in an increase in hydrophobicity and thus a remarkable enhancement in their catalytic activity for epoxidation of methyl oleate with TBHP.

It is of interest to explore the effectiveness of trimethylsilylation as an attempt to optimise the catalysts with respect to the maximum surface coverage of trimethylsilyl groups bounded to the Ti-MCM-41 walls.

4.2.1 Effect of Degree of Silylation

For methyl oleate, reactions with different degree of silylation are also being done. HMDS [$(Me_3Si)_2NH$] is used as silylating agent. The three degrees are $SiMe_3/SiO_2$ = 0.05, 0.2 and 0.3.

The results in Figure 4.63 indicate that liquid-phase silylation with HMDS significantly improves both the activity and selectivity of Ti-MCM-41 catalysts in the epoxidation of methyl oleate with TBHP. The turnover frequency (TOF) is increased by 25-30% while selectivity, increase to 13.9% by silylation. Accordingly, it appears that increased hydrophobicity enhances the intraporous concentration of the methyl oleate substrate near the titanium active sites. The non-silylated Ti-MCM-41 catalysts demonstrated a total selectivity of 45.2% for the methyl oleate oxidation products and the increased epoxide selectivity after silylation is entirely obtained at the expense of these allylic oxidation products.

Therefore, the C=C double bond becomes much more localized (electron rich) and also accessible for the epoxidation which accounts for the increasing trend in the conversion. Similarly, the increase in the selectivity stands for the increased hydrophobic character of the catalyst.

The effect of degree of silylation on the epoxidation of Methyl Oleate is demonstrated below .

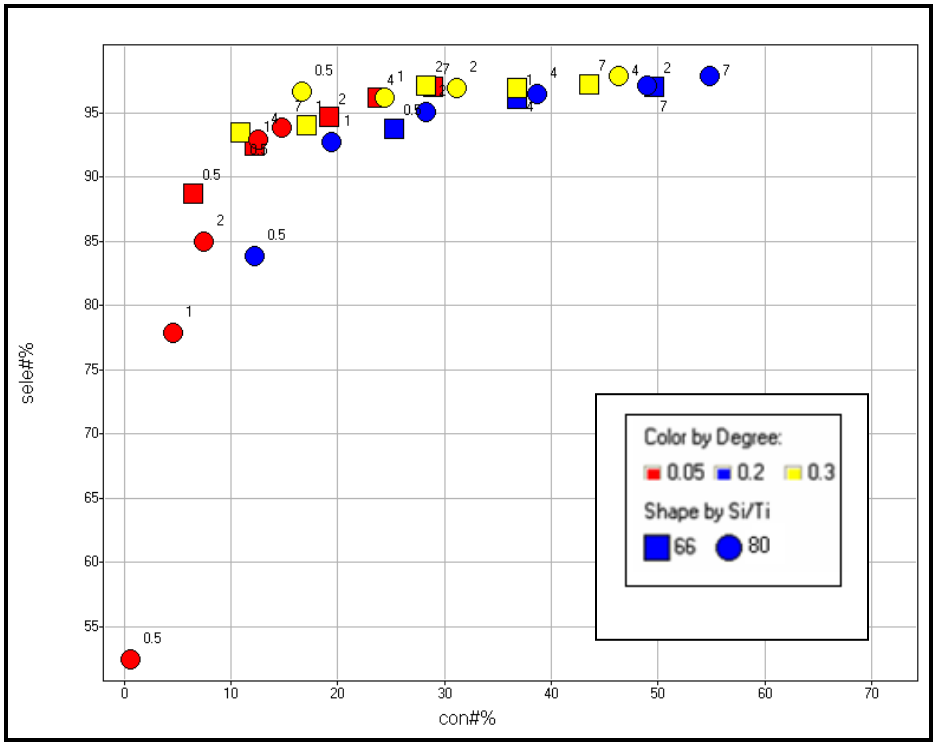

Table 4.63: Selectivity to epoxide vs methyl oleate conversion using various degree of silyated 66Ti-MCM-41 and 80Ti-MCM-41 samples.

It is of interest that relatively low levels of silylation ($SiMe_3/SiO_2$ = 0.2) significantly improve the catalyst selectivity to the epoxide, but that over the

range of silylation ($SiMe_3/SiO_2$ = 0.3), there is very little influence on the catalytic conversion. On the contrary, a significant improvement in catalytic activity is observed when the silylation gives rise to a surface coverage of > 40%. In this case, the selectivity to the epoxide is close to 100%.

The best silylated sample is 80 SYL 0.2, exhibit conversion as high as 52% within 2 hours. The effectiveness of trimethylsilylation is nearly 100% when $SiMe_3/SiO_2$ ratio is 0.2 in the silylating solution, while decreasing strongly when the ratio is upper this value, in this case is $SiMe_3/SiO_2$ ratio is 0.3. This result clearly indicates that the maximum coverage of trimethylsilyl groups bounded to the Ti-MCM-41 walls is close to $SiMe_3/SiO_2$ ratio of 0.2.